Development and Control of An Intelligent Social Robot

by

Mahmoud FARHAT

THESIS PRESENTED TO ÉCOLE DE TECHNOLOGIE SUPÉRIEURE
IN PARTIAL FULFILLMENT FOR THE DEGREE OF
DOCTOR OF PHILOSOPHY
Ph.D.

MONTREAL, OCTOBER 10, 2024

ÉCOLE DE TECHNOLOGIE SUPÉRIEURE
UNIVERSITÉ DU QUÉBEC

BOARD OF EXAMINERS

THIS THESIS HAS BEEN EVALUATED

BY THE FOLLOWING BOARD OF EXAMINERS

Mr. Maarouf Saad, Thesis supervisor
Department of Electrical Engineering at École de technologie supérieure

Mr. Mohammad H. Rahman, Thesis Co-Supervisor
Department of Mechanical Engineering at University of Wisconsin-Milwaukee

Mr. Roberto E. Lopez-Herrejon, Thesis Co-Supervisor
Department of Software Engineering and IT at École de technologie supérieure

Mr. Christian Belleau , Chair, Board of Examiners
Department of Mechanical Engineering at École de technologie supérieure

Mrs. Lyne Woodward , Member of the Jury
Department of Electrical Engineering at École de technologie supérieure

Mr. Yassine Kali, Member of the Jury
School of Engineering at Université du Québec en Abitibi-Témiscamingue (UQAT)

Mr. Nahi Kandil, External Independent Examiner
School of Engineering at Université du Québec en Abitibi-Témiscamingue (UQAT)

THIS THESIS WAS PRESENTED AND DEFENDED

IN THE PRESENCE OF A BOARD OF EXAMINERS AND THE PUBLIC

ON SEPTEMBER 18, 2024

AT ÉCOLE DE TECHNOLOGIE SUPÉRIEURE

ACKNOWLEDGEMENTS

I wish to convey my profound appreciation and heartfelt thanks to my esteemed mentors, Professor Marrouf Saad, Professor Mohammad H. Rahman, Roberto E. Lopez-Herrejonn, Dr. Ibrahim Brahmi, and Yassine Kali, for their guidance and encouragement. Their willingness to provide support at every turn has played a pivotal role in my academic endeavors. Being mentored by you all stands out as a significant highlight of my educational journey.

My sincere gratitude extends to the Institute for Comprehensive Professions, Azizia, as well as the Libyan government, for granting me the opportunity to pursue my studies overseas. I am indebted to my peers at the Institute Fathi Abu Qurain, particularly Tawfiq Al-Bouaishi and Ali Breem, along with all those who have cheered me on. My thanks are also due to Engineer Muhammad Abu Al-Houl, whose unwavering and substantial support has been a cornerstone of my academic journey in Canada.

Further, my gratitude goes out to my colleagues in the Electronic Engineering department at École de Technologie Supérieure for their amiable companionship and steadfast support. I extend special thanks to my examination committee, including our external member, Professor Nahi Kandil. It was an honor to have you on my Ph.D. committee, and I am thankful for the time and effort you have invested. A heartfelt tribute to my parents, whose encouragement in my pursuit of the highest academic qualifications has been unwavering, before their passing.

Additionally, I must acknowledge my brothers and sisters for their emotional support and unwavering support during challenging times. My wife deserves a special mention for her enduring encouragement and moral support throughout our time here. Her kindness, patience, and tranquility during our toughest days have been an invaluable pillar of strength that I will forever cherish. And to my beloved children, Islam, Aws, Areen, and my little girl Elaph—words fail to encapsulate my gratitude for your sacrifices, which have allowed me to concentrate fully on my work. Your understanding means more to me than any algorithm or solution; my love for you transcends all everything.

Développement et Contrôle d'un Robot Social Intelligent

Mahmoud FARHAT

RÉSUMÉ

Les robots humanoïdes rencontrent un défi majeur pour obtenir des mouvements stables en raison des mouvements complexes des jambes et de la puissance de traitement limitée. Le robot NAO, développé par Aldebaran Robotics, met en évidence ces difficultés avec son système de marche rigide, qui restreint les améliorations en matière de contrôle et de vitesse. Ces restrictions entraînent des mouvements non naturels, une efficacité énergétique réduite et une probabilité accrue de chutes, en particulier dans des circonstances imprévisibles. L'importance de la stabilité dynamique et du contrôle de l'équilibre pour un mouvement efficace des robots sur différentes surfaces a conduit à un intérêt croissant pour le contrôle du mouvement humain-robot. De nombreuses recherches se sont concentrées sur la découverte de modèles de marche permettant aux robots humanoïdes de maintenir une stabilité dynamique et de s'adapter à différentes surfaces, y compris la création de démarches statiques pour la stabilité et l'adaptabilité.

L'étude de la stabilité dynamique a été cruciale pour comprendre la marche des robots, en mettant l'accent sur le contrôle de l'équilibre comme essentiel pour la locomotion bipède. Cette connaissance est directement appliquée aux robots humanoïdes, soulignant la nécessité d'une réponse rapide, du maintien de l'équilibre et de la marche rapide pour une interaction efficace dans le monde réel. Ainsi, les avancées en matière de stabilité améliorent la compréhension théorique et soutiennent la fonctionnalité pratique des robots humanoïdes dans des environnements dynamiques. Malgré ces avancées, plusieurs défis persistent, notamment l'adaptation aux dynamiques inconnues, l'efficacité énergétique, la complexité du contrôle, l'adaptabilité au terrain et l'intégration d'interactions réactives avec des environnements changeants. La première étape de cette thèse a consisté à effectuer des simulations approfondies pour analyser les modèles dynamiques du robot NAO. De plus, notre méthodologie a été mise à l'épreuve dans divers scénarios réels, montrant la capacité du robot NAO à atteindre une locomotion stable à haute vitesse et sur des surfaces inclinées. En outre, le système convertit le couple en commandes positionnelles exécutables, permettant un contrôle précis et efficace des mouvements du robot NAO. Cela garantit que le robot peut effectuer des tâches complexes avec précision et fiabilité, améliorant ainsi son efficacité opérationnelle.

Cette thèse améliore la stabilité de la marche du robot NAO avec trois stratégies de contrôle innovantes. Tout d'abord, la combinaison des Techniques de Fonction d'Approximation Modifiée (MFAT) avec le contrôle adaptatif par mode glissant permet un contrôle précis des moteurs du robot NAO virtuel. Deuxièmement, l'approche basée sur le Mode Glissant Terminal à Temps Fixe avec Observateur de Perturbation Non Linéaire (NDO-FTSM) gère efficacement les entrées de couple et réduit les erreurs de suivi à zéro dans des conditions incertaines. Enfin, le contrôle par Mode Glissant Terminal à Temps Fixe avec Estimation du Délai de Temps (TDE) améliore la stabilité en cas de perturbations et de ressources computationnelles limitées du robot NAO.

Mots-clés: Équilibre et Stabilité- Marche Dynamique- Dynamiques Non Linéaires- Contrôle en Mode Glissant- Temps Fixe- Délai Temporel

Development and Control of An Intelligent Social Robot

Mahmoud FARHAT

ABSTRACT

Humanoid robots face a significant challenge in achieving stable movement due to complex leg movements and limited processing power. The NAO robot developed by Aldebaran Robotics, highlights these difficulties with its rigid walking system, which restricts improvements in control and speed. These restrictions result in unnatural movements, decreased energy efficiency, and a higher possibility of falls, particularly in unpredictable circumstances. The importance of dynamic stability and balance control for effective robot movement on different surfaces has led to a growing interest in the control of human-robot movement. Extensive research has focused on discovering walking patterns that enable humanoid robots to maintain dynamic stability and adapt to different surfaces, including creating static gaits for stability and adaptability.

The study of dynamic stability has been crucial for understanding robot walking, emphasizing balance control as essential for bipedal locomotion. This knowledge is directly applied to humanoid robots, highlighting the necessity of fast response, balance maintenance, and rapidly walking for effective real-world interaction. Thus, stability advances theoretical comprehension and underpins practical humanoid robot functionality in dynamic environments. Despite these advancements, several challenges persist, including addressing unknown dynamics, energy efficiency, control complexity, terrain adaptability, and integrating responsive interactions with changing environments. The first step of this thesis involved conducting extensive simulations to analyze the dynamic models of the NAO robot. Moreover, our methodology was put to the test in various real-life scenarios, showcasing the NAO robot's ability to achieve stable locomotion at high velocities and on inclined surfaces. In addition, the system converts torque into executable positional commands, allowing for precise and efficient control of the NAO robot's movements. This ensures that the robot can perform complex tasks accurately and reliably, enhancing its operational effectiveness.

This thesis improves the NAO robot's walking stability with three innovative control strategies. First, introducing Modified Function Approximation Techniques (MFAT) with adaptive sliding mode control allows for precise motor control of the vritual NAO robot . Second, the Nonlinear Disturbance Observer-based Fixed-Time Terminal Sliding Mode (NDO-FTSM) approach effectively manages torque inputs and converge tracking errors to zero under uncertain conditions. Finally, Fixed-Time Terminal Sliding Mode control with Fixed Time Observer (FTO) enhances stability amid disturbances and limited computational resources of the NAO robot.

Keywords: Balance and Stability, Dynamic Walking, Non-linear Dynamics, Sliding Mode Control, Fixed-time, Time Delay

TABLE OF CONTENTS

Page

INTRODUCTION 1

CHAPTER 1 LITERATURE REVIEW AND RESEARCH PROBLEM 5
1.1 Problems of bipedal locomotion 6
1.1.1 Effect of an uncertain dynamic model on stability walking 6
1.1.2 High non-linearity of the system 8
1.1.3 Apply control strategies for uncertain nonlinear systems 8
1.2 NAO Robot Overview 10
1.2.1 Coordinate Definitions for NAO Robot 11
1.3 Motivation and Objectives 13
1.4 Methodology 14
1.5 Originality of the research and contribution 15
1.6 List of publications 16

CHAPTER 2 NOVEL ADAPTIVE BALANCED CONTROL OF HUMANOID ROBOT TYPE NAO ROBOT 19
2.1 Abstract 19
2.2 Introduction 20
2.3 Kinematic and Dynamic modeling of NAO robot 23
2.3.1 Kinematic model of the right leg of biped robot 23
2.3.2 Dynamic modeling of the right leg of NAO robot 24
2.3.3 Control Goals 26
2.4 Control Design 27
2.4.1 Model-based control scheme 27
2.4.2 Adaptive function approximation approach 28
2.5 Simulation and Comparative Study 32
2.5.1 Adaptive control based modified function approximation technique Simulation Implementation 34
2.6 Conclusion 38

CHAPTER 3 WALKING POSITION COMMANDED NAO ROBOT USING NONLINEAR DISTURBANCE OBSERVER-BASED FIXED-TIME TERMINAL SLIDING MODE 39
3.1 Abstract 39
3.2 Introduction 40
3.2.1 Context and Motivation 40
3.3 Preliminaries 43
3.3.1 NAO Robot's Legs Model 43
3.3.2 Problem Formulation 46
3.4 NDO-based FTSM Controller 46

3.5 Experimental results 54
3.6 Conclusion 64

CHAPTER 4 NEW FIXED-TIME OBSERVER-BASED MODEL-FREE FIXED-TIME SLIDING MODE OF JOINT ANGLE COMMANDED NAO HUMANOID ROBOT 67
4.1 Abstract 67
4.2 Introduction 68
4.3 Preliminaries 71
4.3.1 Modeling the Lower Body of the NAO Robot 71
4.3.2 Problem Formulation 74
4.4 Control Design 74
4.4.1 Dynamics and Disturbances Estimation 74
4.4.2 Fixed-Time TDE Error Observer 75
4.4.3 Fixed-time controller 80
4.5 Experimental results 85
4.6 Conclusion 92

CONCLUSION AND RECOMMENDATIONS 93

BIBLIOGRAPHY 99

LIST OF TABLES

Page

Table 2.1 Modified Denavit Hartenberg parameters corresponding to the link frames attachment in Figure 2.1 23

Table 2.2 Controller performance 38

Table 3.1 MD-H right leg parameters corresponding to the link frames attachment Taken from (Ding et al., 2016) 45

Table 3.2 Gains of the proposed controller 54

Table 3.3 Comparison of control performance 66

Table 4.1 Modified DH Parameters Taken from (Hashemi and Jadidi, 2012a) 71

Table 4.2 Parameters of the Proposed Controller 88

Table 4.3 Numerical comparison in terms of the IAE 88

Table 4.4 Numerical comparison in terms of the ECI 90

LIST OF FIGURES

Page

Figure 1.1 Bipedal humanoid hardware design of Atlas robot, NAO robot, Cassie bipedal robot, and human-robot Lola 11

Figure 1.2 Dimension and structure of the NAO robot 12

Figure 1.3 All lower joints in NAO robot and initial position 13

Figure 2.1 Link frames assignment on NAO robot's right leg 24

Figure 2.2 Schematic view of NAO robot's right leg (single support phase) 25

Figure 2.3 Block diagram shows swinging between feet using time delay 26

Figure 2.4 Model adaptive sliding mode control diagram using MFAT 33

Figure 2.5 Model adaptive sliding mode control diagram using MFAT 34

Figure 2.6 The measured trajectory under state-feedback based adaptive modified function approximation controller 35

Figure 2.7 Tracking errors under state-feedback based adaptive modified function approximation controller 35

Figure 2.8 Control input based adaptive modified function approximation controller of right leg 36

Figure 2.9 Estimation of inertia matrix 36

Figure 2.10 Estimation of Coriolis and centrifugal matrix 37

Figure 2.11 Estimation of gravitational forces, ... 37

Figure 3.1 Kinematic model of NAO humanoid robot joints and its coordinate frames 44

Figure 3.2 The structure of the proposed NDO-based FTSM control scheme 53

Figure 3.3 Right leg joint tracking during the 1^{st} scenario 56

Figure 3.4 Left leg joint tracking during the 1^{st} scenario 57

Figure 3.5 Right leg joint tracking error during the 1^{st} scenario 58

Figure 3.6 Right leg torque inputs during the 1^{st} scenario via the proposed controller 58

Figure 3.7 The NAO robot walks on an uphill sloped surface (second scenario) 59

Figure 3.8 Right leg torque inputs during the 1^{st} scenario via the proposed controller 60

Figure 3.9 Right leg torque inputs during the 1^{st} scenario via the proposed controller 61

Figure 3.10 Right leg joint tracking error during the 2^{nd} scenario via the proposed controller 62

Figure 3.11 Right leg torque inputs during the 2^{nd} scenario via the proposed controller 62

Figure 3.12 Comparative trajectory tracking experiment results of right leg 63

Figure 3.13 Comparative trajectory tracking experiment results of left leg 64

Figure 3.14 Uncertainties in experiment results of right and left legs 65

Figure 4.1 The coordinate frames and joints of the NAO humanoid robot kinematic model 72

Figure 4.2 Control scheme diagram 85

Figure 4.3 Experiment of walking using the developed controller. 86

Figure 4.4 Experiment: trajectory tracking the performance of the proposed controller on right and left legs 87

Figure 4.5 Experiment: trajectory tracking error signals using a proposed controller on right and left legs. 89

Figure 4.6 Experiment: Comparison of the tracking performance of joints under the proposed control and the reference 91

Figure 4.7 Experiment: right and left legs torque inputs 92

LIST OF ABBREVIATIONS

AI	Artificial Intelligence
ASD	Autism Spectrum Disorder
BCS	Body Coordinate System
ETS	École de Technologie Supérieure
DC	Direct Current
DoF	Degree of Freedom
DH	Denavit-Hartenberg parameters
FTSMC	Fixed Time Sliding Mode Control
FTDE	Fixed Time Delay Estimation
FK	Forward kinematics (FK)
JCS	Joint Coordinate System
MFAT	Modified Function Approximation Technique
PID	Proportional-Integral-Derivative
TDE	Time Delay Estimation
SMC	Sliding Mode Control
WCS	World Coordinate System
ZMP	Zero-Moment Point

LIST OF SYMBOLS AND UNITS OF MEASUREMENTS

α_{i-1}	angle from $\hat{Z}_{i-1}$ to $\hat{Z}_i$ measured about $\hat{X}_{i-1}$ (rad)
a_{i-1}	distance from $\hat{Z}_{i-1}$ to $\hat{Z}_i$ measured along $\hat{X}_{i-1}$ (cm)
d_{i-1}	distance from X_{i-1} to X_i measured about Z_i (cm)
μ_i, θ_i	joint's position (rad)
$\dot{\mu}_i, \dot{\theta}_i$	joint's velocity (rad/s)
η_d, θ_d	desired's position
$\theta_j(t)$	measured position
$\dot{\theta}_j(t)$	measured velocity
$\theta_j^d(t)$	measured desired position
$\dot{\theta}_j^d(t)$	measured desired velocity
X Y Z	Cartesian coordinate system main axes
$\circ$	degree
V_i	Lyapunov function candidate
τ, u	control torque (Nm)
$\Gamma_m(t)$	motor torque (Nm)
$\overline{D}_i(t)$	matched uncertain functions
S	sliding manifold
$e, \dot{e}$	position error and velocity error
$\boldsymbol{q}_j, \dot{\boldsymbol{q}}_{m,j}, \ddot{\boldsymbol{q}}_{m,j}$	angular position, velocity and acceleration vectors, respectively

$\hat{D}$	estimation of external disturbances,
D	external disturbances
$d(t)$	external disturbances caused by the force contact pressure
$\tilde{D}$	estimation error of external disturbances
$T_{i,max}^{slid}$	convergence time
P_{fc}	force contact pressure (N/m2)
M	inertia matrix
C	Coriolis and centrifugal matrix terms
G	gravitational vector terms
$\varepsilon(t)$	time delay error vector
$\hat{\varepsilon}(t)$	estimated time delay error vector
rad	radian
S, sec	second
Nm	Newton meter
cm	centimeter

INTRODUCTION

The continuous progression in humanoid robots' walking capabilities continues to garner interest from academic researchers, primarily due to the efficiency and enhanced task execution these advancements bring.

Humanoid robots, generally designed with a structure similar to the human form, including a torso, head, arms, and legs, have seen significant evolution over the last thirty years. The field of robotics has shifted from focusing on traditional industrial manipulators to embracing autonomous, wheeled, and legged machines (Kemp et al., 2008). Specifically, bipedal humanoid robots stand out from other robotic forms, such as industrial robots, due to their ability to emulate human movement using a two-legged gait. A primary objective in the development of humanoid robots is to achieve self-sufficient and dependable bipedal movement. Bipedal locomotion covers a range of activities, including walking, running, and hopping, with a particular emphasis on walking due to its relevance in understanding and replicating human motion (Meng et al., 2018).

The main challenges in achieving stable bipedal locomotion involve handling the robot's complex range of motion, dealing with its non-linear dynamics, and the effective processing of data for operational control. Environmental variables, such as terrain gradient and unexpected external disturbances, also play a significant role in sustaining stability during bipedal movement. To overcome these obstacles, it is essential to create a variety of theoretically sound walking patterns and to develop suitable control mechanisms that can ensure steady and balanced bipedal movement.

This thesis is centered on developing and managing a bipedal walking motion for humanoid robots, inspired by human gait patterns. The primary objective of this study is to achieve stable and dynamic locomotion in biped humanoid robots through the integration of effective locomotion and control strategies.

The organization of this thesis is given as follows:

Chapter 1 of this thesis is structured as follows. The first section addresses the problems associated with bipedal locomotion, including the effects of an uncertain dynamic model on walking stability, the challenges posed by the system's high non-linearity, and the application of control strategies to uncertain nonlinear systems and their solutions. Following this, Section 2 outlines the motivation and objectives of the thesis, encompassing enhancements in NAO robot locomotion, the achievement of walking stability in humanoid robots, and the pursuit of model-free joint angle tracking. The methodology employed in the research is detailed in Section 3 followed by a discussion on the originality of the research and its contributions to the field in Section 4. Finally, Section 5 presents a list of publications related to the thesis, providing a comprehensive overview of the academic contributions resulting from the research efforts. This introductory chapter sets the stage for the subsequent chapters, establishing the context, objectives, and significance of the research conducted in this thesis.

Chapter 2 presents a comprehensive exploration of critical aspects related to the control of the NAO robot's legs. The chapter begins with a detailed examination of the kinematic model and the dynamic modeling of the right leg of a biped robot, providing the foundational framework necessary for subsequent analyses. The control goals are then elucidated, outlining the specific objectives that the proposed approach aims to achieve. The chapter introduces the innovative Adaptive Function Approximation approach, emphasizing its role in efficiently capturing and adapting to the unknown dynamics of the NAO robot. To assess the performance of the proposed approach, simulations, and a comparative study are conducted using Matlab code and V-REP simulation to implement the novel adaptive tracking controller based on the Modified Function Approximation Technique (MFAT). These discussions collectively contribute to a comprehensive understanding of the proposed control strategy and its potential implications for enhancing the locomotion capabilities of the NAO robot.

Chapter 3 provides a comprehensive exploration of the proposed Nonlinear Disturbance Observer-based Fixed-Time Sliding Mode controller for the NAO robot. It begins by establishing the context and motivation behind the development of this controller. The section on problems delves into the intricate details of the NAO robot's legs, and proceeds with a thorough Problem Formulation, articulating the specific issues targeted by the NDO-based FTSM controller. Subsequently, the development and implementation of the controller are detailed using Microsoft Visual C++ alongside NAOqi 2.5, running on a Linux platform. NAOqi, the middleware developed by SoftBank Robotics, facilitates communication and control of the NAO robot. These tools facilitate real-time communication with the NAO robot, enabling the transmission of instructions. The chapter includes an exploration of Experimental Results, emphasizing the practical implementation and performance of the proposed controller. Comparative results with other controllers are presented, offering a robust evaluation framework. Overall, Chapter 3 encapsulates a holistic view of the development, implementation, and experimental validation of the NDO-based FTSM controller, shedding light on its efficacy in addressing the complexities of the NAO robot's locomotion.

Chapter 4 focuses on introducing a new fixed-time observer-based model-free fixed-time sliding mode tailored for controlling the joint angle of the NAO robot. The motivation behind adopting this approach is its ability to address challenges related to uncertainties in the model and the limited computational capabilities of processing. The chapter begins with a careful examination of the leg model, presenting a detailed problem formulation that uncovers the complexities in this specific aspect. It then delves into the control design, exploring elements such as Dynamics and Disturbances Estimation, the design of a Fixed-Time Disturbance Estimator to assess uncertainties, and Error Approximation, ultimately leading to the implementation of a Fixed-Time Controller. The chapter crucially validates the proposed controller in real-time through experimental results, confirming its effectiveness on the NAO robot. In conclusion, the

chapter provides valuable insights into the overall performance of the introduced controller and suggests potential directions for future research and improvements.

Conclusion

This thesis has comprehensively examined the challenges and solutions associated with bipedal locomotion in humanoid robots, with a specific focus on the NAO robot. Through a systematic exploration spread across five chapters, this work has detailed the intricacies of dynamic modeling, control mechanism design, and practical implementation of various innovative control strategies. Each chapter has built upon the previous, detailing sophisticated theoretical models, developing advanced control strategies, and validating these through simulations and experimental setups.

The results validate the efficiency of the implemented control strategies, showing significant improvements in the NAO robot's balancing and motion performance. Additionally, the research highlights enhanced stability and efficiency in the robot's movements, contributing to a deeper understanding of humanoid locomotion dynamics and control methodologies.

CHAPTER 1

LITERATURE REVIEW AND RESEARCH PROBLEM

The increasing deployment of humanoid robots across a variety of sectors showcases the broad potential and adaptability of contemporary robotic technology in improving both service delivery and operational efficiency. These advanced robots find applications in numerous areas, including healthcare, where they contribute to patient care and medical procedures; in industrial settings, where they perform tasks requiring high precision; and within the aerospace sector, assisting in complex operations and interactions with humans (Araujo et al., 2023),(Chien et al., 2024), and (Graf and Eckstein, 2023). The wide-ranging adoption of humanoid robots is propelled by their capability to execute tasks with remarkable accuracy and to engage in intricate interactions. For instance, humanoid robots can adapt to various settings by learning and adjusting to new tasks, such as assisting the elderly with daily activities (Boudjedir et al., 2023) or supporting surgeons in medical procedures (Su et al., 2022). This integration of humanoid robots into daily environments, like homes and schools, and professional environments, such as hospitals and offices, opens up new prospects for innovation and elevates service quality (Hou et al., 2024). Their ability to offer consistent and reliable support is especially beneficial for tasks that are repetitive or require exactitude. Moreover, the versatility of robots, adaptable to diverse tasks and contexts, emphasizes their role in enhancing operational effectiveness and improving the quality of life in various fields. This trend towards the utilization of robotic assistance is indicative of the evolving application of technology, forecasting substantial benefits for efficiency, productivity, and service personalization.

However, humanoid robots are vulnerable to external disturbances that can disrupt their stability, potentially causing them to lose equilibrium and topple. Therefore, the integration of propulsion and recovery control is vital in the context of humanoid robots. This problem is commonly known as the bipedal locomotion issue in literature (Stephens and Atkeson, 2010), and (Hosseinmemar et al., 2019). A comprehensive review encompassing gait, drive mechanisms, sensors, and control systems for bipedal walking robots has been conducted (Kuniyoshi et al., 2000). The review establishes a foundation by examining the scientific analysis of human gait, particularly

emphasizing its relevance to bipedal robot design. It was conducted a comprehensive analysis of the complete human gait cycle, highlighting the critical issues of balance and stability, especially during the single support phase where bipedal movement is inherently unstable. Additionally, the review explores the impacts of passive and active gait on energy demand, providing valuable insights into the efficiency of different locomotion strategies. Another study (Parra-Moreno et al., 2023) focuses on motion imitation techniques for bipedal locomotion in humanoid robots. This study contributes to understanding how robots can effectively mimic human-like walking patterns, thereby enhancing the adaptability and naturalness of bipedal robotic movements.
In addition, (Vadakkepat and Walker, 2002) provides a thorough analysis of stability, and control in bipedal locomotion. The authors explore various techniques and meticulously assess their energy costs, offering valuable insights for the practical implementation of bipedal robots. In summary, the reviews collectively cover essential aspects of the bipedal locomotion problem, providing valuable perspectives on gait analysis, motion imitation, and stability/control considerations.

1.1 Problems of bipedal locomotion

In this section, we delve into the fundamental challenges associated with the bipedal locomotion problem. Most research work in this type of robotic system has so far focused on the following three points: uncertain dynamics under external disturbances impact, high non-linearity of the system, and control strategies to improve the walking stability of bipedal walking robots.

1.1.1 Effect of an uncertain dynamic model on stability walking

Bipedal robots face major challenges in maintaining stable walking, especially when their dynamic models involve both known and unknown uncertainties. These uncertainties can come from various sources, such as variations in joint mechanics, inaccuracies in physical properties like mass and center of gravity, and complex environments. To manage these challenges, various control strategies are used. Some strategies are designed for systems with known models, while others are suited to handle unknown dynamics, ensuring stability even in unpredictable conditions.

Additionally, external disturbances like uneven terrain or sudden impacts further complicate the accurate prediction and control of robot locomotion, amplifying the uncertainty in the dynamic models. Also, the system's performance needs to be unaffected by external disruptions, uncertainties dynamics, and internal parameter variations. The effects of an uncertain dynamic model on stability are multiple impacting various aspects of the robot's locomotion. At the core of these challenges is the potential for balance instability. The uncertainties in the dynamic model introduce discrepancies between predicted and actual robot behavior, making it difficult to maintain an upright posture during walking. This imbalance can manifest as gait variability, disrupting the consistency of the walking motion and hindering the robot's ability to achieve a stable and predictable gait (Castillo et al., 2020), (Donca et al., 2022), and (Slotine et al., 1991a).

Moreover, bipedal robots with uncertain dynamic models tend to exhibit heightened sensitivity to external disturbances. Small perturbations or changes in the environment can disproportionately affect the robot's stability, posing challenges in maintaining equilibrium and increasing the risk of falls (Castillo et al., 2020).

Adaptation becomes a central concern as well. The lack of accurate information about the system dynamics hampers the robot's ability to adjust control parameters in real-time to optimize stability. This limitation in adaptability can be particularly pronounced when the robot encounters changes in walking conditions or its surroundings (Grizzle et al., 2010).

Energy efficiency also comes into play. The instabilities induced by uncertain dynamic models may necessitate greater energy expenditure as the robot works to correct deviations from the desired walking trajectory. This increased energy consumption can undermine the overall efficiency of the walking process (Castillo et al., 2020).

Traditional control strategies may face limitations in compensating for uncertainties effectively. In response, advanced control techniques, including adaptive control, robust control, or a combination of both, are often employed. These strategies aim to enhance the robot's stability by enabling it to adjust control parameters (Gu and Yuan, 2021), and (Yedavalli, 2014).

1.1.2 High non-linearity of the system

The high non-linearity of a system can significantly impact the stability of biped robots. Complex dynamic behaviors can emerge from nonlinear systems, including bifurcation, chaos, etc. (Coron et al., 1995). Among these, linear systems are predictable, with proportional input-output relationships and typically a single equilibrium, making them easier to control. Nonlinear systems, however, can have multiple equilibria and complex, unpredictable behavior, requiring advanced control methods. (Added et al., 2021), and (Grizzle et al., 2001a).

Illustrating the concept of equilibrium points is fundamental in the study of dynamical systems. An equilibrium point is a state where the system remains unchanged over time. The number of equilibrium points in a dynamic system is of general theoretical interest because it provides insight into the system's behavior. For example, if a system has only one equilibrium point, it will typically converge to it. However, nonlinear systems can have multiple equilibrium points, and depending on the initial conditions, the system may oscillate between them or converge to one. (McBride and Del Vecchio, 2020), and (Wei, 2023). In brief, the number of equilibrium points in a dynamic system is an important characteristic that helps us understand the system's behavior over time.

Most recent studies have examined Lyapunov stability analysis for analyzing nonlinear feedback systems (Vidyasagar, 2002), (Khalil, 2009), and (Bouzaouache and Braiek, 2008). The Lyapunov candidate is a powerful tool in the analysis of dynamic systems. It serves as a key method for assessing stability and providing valuable insights into the behavior of nonlinear feedback systems. By carefully choosing a suitable Lyapunov candidate, researchers can effectively demonstrate the stability of a system and gain a deeper understanding of its dynamics.

1.1.3 Apply control strategies for uncertain nonlinear systems

The control of uncertain nonlinear dynamics is one of the challenging topics of nonlinear control engineering problems. Nonlinear control theory and application have made great progress in recent years, but there are still many new and challenging problems in the areas of theory

analysis and applications, which cover the fields of multiobjective control, design of regulating and tracking systems, fault estimation, nonlinear robust control and filtering, stability and stabilization, etc (Xie et al., 2019), (Yao and Deng, 2017), and (Chen et al., 2016).

Nonlinear control is a technique used to control systems that are nonlinear in nature. It is a powerful tool that can be used to control a wide range of systems, including those that are uncertain or have unknown dynamics. The application of nonlinear control on an uncertain dynamic model is an active area of research. One approach is to use adaptive robust model predictive control (MPC) techniques designed to address system uncertainties and external disturbances while maintaining high control performance (Kellett and Braun, 2023). Another approach is adaptive control, which is not just a single control method but a family of methods used to control systems with unknown parameters or dynamics (Qi et al., 2019). It is a type of control method used by a controller which must adapt to a controlled system with parameters that vary or are initially uncertain. As a NAO robot moves, its effective mass can change if it interacts with objects, like carrying items, or due to internal shifts, such as battery depletion or component adjustments, affecting its dynamics and control (Shimkin, 2009).

Adaptive control is different from robust control in that it does not need a priori information about the bounds on these uncertain or time-varying parameters; robust control guarantees that If the changes remain within specified limits, there is no need to modify the control law, whereas adaptive control involves the control law adjusting itself in response to system changes. The foundation of adaptive control is parameter estimation, which is a branch of system identification (Kellett and Braun, 2023).

A nonsingular fixed-time terminal sliding mode controller is indeed a promising solution to eliminate singularity system compared to conventional SMC (Ai and Wang, 2023). This fixed-time convergence is a significant advantage in applications requiring precise timing and rapid response. Considering essential benefits such as fast fixed-time nonsingular terminal sliding mode control method overcomes the singularity problem, achieves faster convergence,

and ensures system states reach equilibrium within a fixed time(Qin et al., 2023a), and (Chen et al., 2024).

One common approach to controlling an uncertain dynamic model is the use of robust MPC methods to guarantee stability in the presence of disturbances and model uncertainties (Chen et al., 2021). Another approach to controlling an uncertain dynamic model involves the use of robust model predictive control with sliding mode. This technique is capable of handling nonlinear systems with input constraints and uncertainties, optimizing the tracking of reference trajectories even in the presence of uncertainty (Li et al., 2021)). However, due to the complexity of the model's regression matrix, these controllers are often computationally intensive and challenging to implement. The regression matrix reflects the relationship between system variables, and its complexity can increase significantly in systems with high nonlinearity or multiple uncertainties, making real-time application more difficult.

As a solution, a time delay estimation (TDE) technique is proposed in (Wang et al., 2018) to estimate the unknown uncertainties in the dynamic model of biped robots. TDE is a method used to predict and compensate for time delays in a system by estimating the difference between the current state and a previous state affected by unknown dynamics and disturbances. However, TDE is prone to errors in estimating the exact time delay, especially in the presence of external disturbances and the strong nonlinear behavior of the robot's model. These time delay errors can reduce the accuracy of the estimation, making the technique less effective in approximating the system's true dynamics.

These control approaches have been applied to several versions of biped robots, as shown in Figure 1.1

1.2 NAO Robot Overview

The NAO robot, developed by Softbank Robotics (Aldebaran Robotics, 2024), is a humanoid robot designed for various applications, including research, education, and entertainment. The NAO robot stands approximately 33.3 centimeters tall from the center of mass, typically located

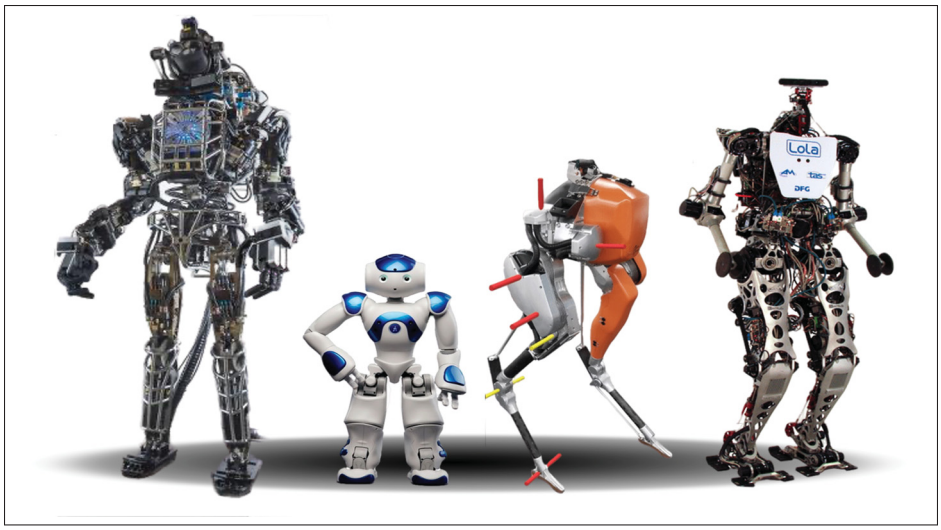

Figure 1.1 Bipedal humanoid hardware design of Atlas robot , NAO robot , Cassie bipedal robot, and human-robot Lola
Taken from ((ExtremeTech, 2013),(Source, 2024), (Technical University of Munich, 2024), and (Xiong et al., 2021), respectively)

near the hip area, to the end of the leg, as shown in Figure 1.2. The lower body of the NAO robot has 12 degrees of freedom (DoF). Figure 1.3 demonstrates that there are 6 joints in each leg, granting complete mobility for both legs. Its compact size and versatile capabilities make it an ideal platform for exploring advanced robotics and artificial intelligence (AI) concepts (Aldebaran Robotics, 2024).

The robot is equipped with various sensors, including cameras, microphones, sonars, and tactile sensors, enabling it to perceive and interact with its environment. Additionally, the NAO robot features powerful computing capabilities, facilitating real-time processing and decision-making.

1.2.1 Coordinate Definitions for NAO Robot

To precisely control the movements and interactions of the NAO robot, a well-defined coordinate system is crucial. The NAO robot typically utilizes a standard set of coordinate frames to represent its various components (Chen et al., 2018), and (Said et al., 2015d). The robot's spatial

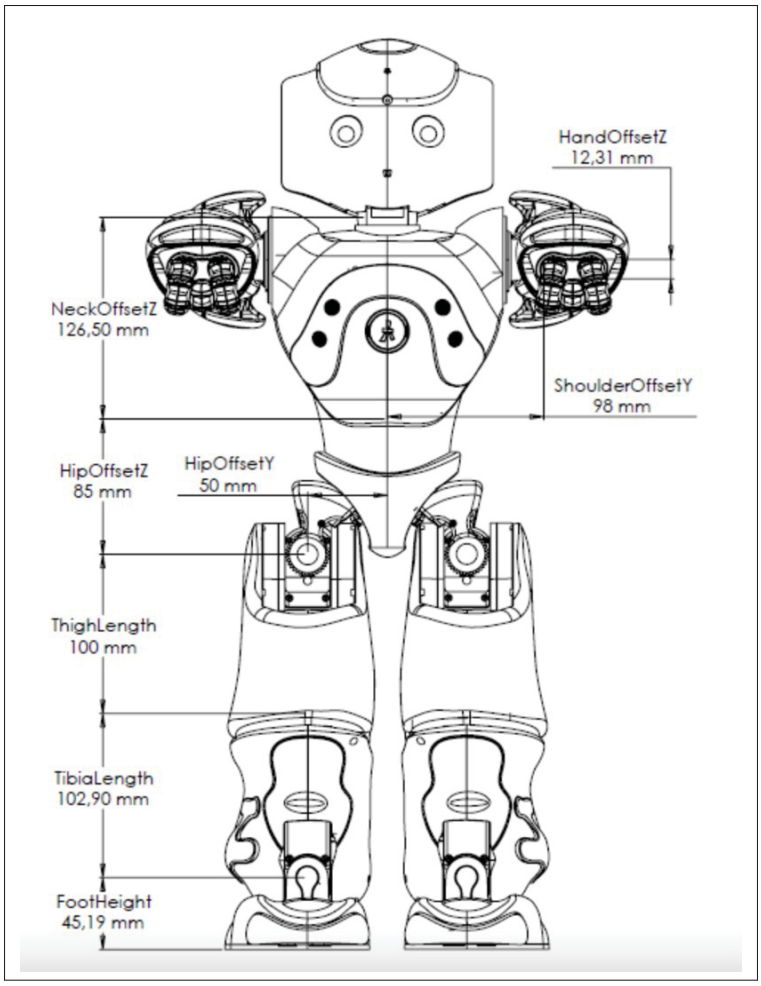

Figure 1.2 Dimension and structure of the NAO robot
Taken from (Dong et al., 2018)

awareness, movement, and interaction with the environment are facilitated by these coordinate systems. Here's how they function as a collective:

- World Coordinate System (WCS): The absolute reference frame representing the global environment in which the robot operates. It remains fixed and provides a consistent reference for spatial positioning.
- Body Coordinate System (BCS): The coordinate frame attached to the robot's body, typically located at its center of mass. Movements and orientations are defined relative to this frame, offering a local reference for body-centric operations.

- Joint Coordinate System (JCS): Each joint of the NAO robot has its own coordinate system, which defines the rotational axes and orientations of the joints for both the right and left legs. Joint angles are measured with respect to these coordinate frames, making them crucial for controlling the robot's articulated limbs.
- Sensor Coordinate Systems: Different sensors on the NAO robot, such as cameras and sonars, have their own coordinate systems. These systems are used to interpret sensory input and integrate it into the overall control framework.

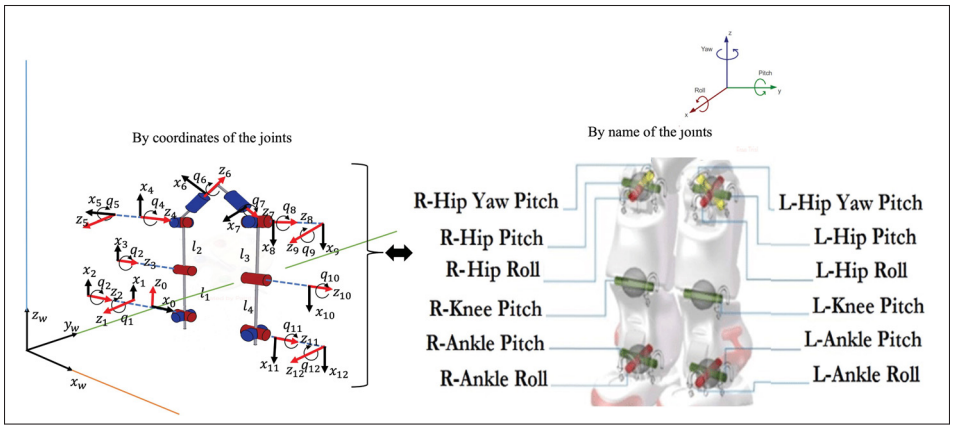

Figure 1.3 All lower joints in NAO robot and initial position
Taken from (Farhat et al., 2024), and (Cerón et al., 2023)

Understanding and accurately defining these coordinate systems are fundamental for developing control algorithms, kinematic models, and dynamic simulations for the NAO robot. This ensures precise control and coordination of its movements in various applications, ranging from basic locomotion to more complex tasks such as object manipulation and interaction with the surrounding environment.

1.3 Motivation and Objectives

Controlling and stabilizing bipedal robot locomotion, particularly with constrained dynamic characteristics and walking gait trajectories, presents a significant challenge due to the complexity of balancing, dynamic stability, and coordination of multiple joints in real time. Identifying and addressing issues such as external disturbances, ground reaction forces, and the nonlinear nature

of human-like walking is crucial for achieving smooth and stable movement. The motivation and objectives of this research are outlined as follows:

1. **Enhancing NAO Robot Locomotion:**
   - *Motivation:* Addressing the impact control strategies that influence how the robot adjusts its movements in response to environmental factors and unknown dynamics on the NAO robot's locomotion.
   - *Objective:* Improve robot locomotion by implementing sliding mode control based on the Modified Function Approximation Technique (MFAT).

2. **Walking Stability in Humanoid Robots:**
   - *Motivation:* Tackling the fundamental problem of walking stability, focusing on the nonlinear dynamic model of the NAO robot's legs.
   - *Objective:* Propose a control strategy employing a Nonlinear Disturbance Observer (NDO) based Fixed-time Terminal Sliding Mode (FTSM) to achieve performance tracking control in two scenarios (High speed and slope surface).

3. **Model-Free Joint Angle Tracking:**
   - *Motivation:* The focus on stabilizing NAO's walking dynamics is driven by its high value in both practical use and control strategy development, making the effort worthwhile.
   - *Objective:* Introduce a model-free control approach, integrating Fixed Time Delay Estimation (FTDE) with Fixed Time Sliding Mode Control (FTSMC) for accurate estimation and error counterbalancing.

1.4 Methodology

A bipedal robot often necessitates both balance control and motion planning to function. Humanoid robots vary in design, particularly in their leg mechanisms; however, they share certain common features. These include the integration of sensors in the robot's feet to monitor contact points and forces on the walking surface, the implementation of a complex motion control system, and the presence of a minimum of six fully rotating and position-controlled

joints for each leg.

To obtain a dynamic model equation, Lagrange formulation is used to obtain the dynamics based on kinetic and potential energies. The approach taken in this research involves applying three types of control approaches with online feed-forward to process future data, thereby enhancing a control signal. This is achieved by minimizing energy consumption and converging tracking errors to zero, ensuring the stability of the robot's walking despite uncertainties and external disturbances. Furthermore, the walking gait of the robot is refined through online sensing of environmental conditions, incorporating sensory feedback, and fine-tuning its motion parameters.

The focus of this research includes:

- Developing a kinematic model of the joints of the lower limbs of the right and left legs for the NAO robot to determine joint angles, link positions, velocities, and acceleration.
- Estimating dynamic behavior of the links and related joint torques.
- Transforming computed torques generated by the controller into position commands for the interface.
- Implementing a control approach for dynamic walking.

1.5 Originality of the research and contribution

The thesis aims to develop the motion stability of a lower limbs of robot called the NAO in various environments to ensure better stability walking. The stability of a robot's dynamic model is influenced by its complex mechanical structure, nonlinearities, dynamic uncertainties, external disturbances, sensor limitations, and control system dynamics. Addressing these factors is crucial for developing effective control strategies and ensuring stable robot behavior in real-world environments. Hence, the focus of the development lies in two aspects. The primary objective is to achieve natural, human-inspired movement in the NAO robot's lower limbs through comprehensive kinematic and dynamic analysis. Additionally, the aim is to develop robust nonlinear control laws that ensure the lower limbs maintain desired stability, even in the presence of uncertainties and external disturbances. Although there are many research papers on

controlling these robots, only a few of them address the challenges posed by high nonlinearity and dynamic uncertainties. Most studies that assume the dynamic model of the robot is already known typically rely on rigid body dynamic models, with the Lagrange dynamic model being a common approach. The robot's complex mechanical structure and hard nonlinearities pose a challenge in determining its overall dynamic model, impacting its behavior. Various control approaches have been suggested by researchers to address the uncertainty problem, such as adaptive control, sliding mode control, and time delay estimation techniques. In this work, we propose novel control strategies that differ from what appears in the previous research. The main contributions of thesis are:

1. The Modified Function Approximation Technique (MFAT): the proposed solution, completely eliminates the need to use basis functions in dynamic parameter approximation. The approach involves utilizing a new adaptive sliding mode controller based on MFAT to address the unknown dynamics of the NAO robot.
2. Introducing a novel nonlinear disturbance observer-based fixed-time terminal sliding mode control technique. This approach achieves a robust walking control objective within a fixed-time without taking into account initial conditions and the presence of uncertainties and disturbances. A new fixed-time observer is proposed to estimate uncertainties in the model and reduce the impact of errors caused by time delays in the system, enhancing the robustness of the control system when integrated with fixed-time sliding mode control. Consequently, Time Delay Estimation (TDE) emerges as an approach unaffected by the size of the estimated dynamic parameters, particularly in scenarios involving high Degrees of Freedom (DOFs).

1.6 List of publications

1. Farhat M, Brahmi B, Saad M, Rahman MH. Novel adaptive balanced control of humanoid robot type NAO robot. International Journal of Modelling, Identification and Control. 2021;39(3):211-20.

2. Farhat M, Kali Y, Saad M, Rahman MH, Lopez-Herrejon RE. Walking position commanded NAO robot using nonlinear disturbance observer-based fixed-time terminal sliding mode. ISA transactions. 2023 Dec 23.
3. M. Farhat, Y. Kali, M. Saad, M. H. Rahman and R. E. Lopez-Herrejon, "New Fixed-Time Observer-Based Model-Free Fixed-Time Sliding Mode of Joint Angle Commanded NAO Humanoid Robot," in IEEE Transactions on Control Systems Technology, doi: 10.1109/TCST.2024.3469051. 2024 Oct 4.

CHAPTER 2

NOVEL ADAPTIVE BALANCED CONTROL OF HUMANOID ROBOT TYPE NAO ROBOT

Mahmoud Farhat[1] , Brahim Brahmi[2] , Maarouf Saad[1] , Mohammad H Rahman[2]

[1] Département de Génie Mécanique, École de Technologie Supérieure,
1100 Notre-Dame Ouest, Montréal, Québec, Canada H3C 1K3

[2] Mechanical Engineering Department, McGill university, Montreal,
1100 Notre-Dame Ouest, Montréal, Québec, Canada H3C 1K3

[3] Mechanical/Biomedical Engineering Department,University of Wisconsin-Milwaukee,
Milwaukee, WI 53211, United States

Article published in "International Journal of Modelling, Identification and Control", June 2022

2.1 Abstract

This paper presents a novel adaptive tracking controller based on the Modified Function Approximation Technique (MFAT). The proposed approach includes a sliding mode with MFAT to approximate the unknown dynamic model of the NAO robot on which it mainly relies. The impact policy and unknown dynamics of the system are considered when implementing the control approach to improve the NAO's robot locomotion. Unlike conventional FAT, the basis functions in the dynamic parameters approximation updated law are avoided in the proposed MFAT. The Lyapunov function is presented a stability analysis according to which all error signals are uniformly ultimately bounded in a closed loop. Simulations were performed to validate the design MFAT approach for the NAO robot by carrying out a comparative study with a conventional model-based controller.

keyword: Adaptive control, Humanoid robots, Function Approximation Technique, NAO robot, biped locomotion

2.2 Introduction

Recent advancement in the development and control of humanoid robots have drawn significant interest to the scientific community, which has led to their integration in several fields such as the military (Meng et al., 2018) and public services Sadeque and Balachandran (2020), for example, NAO robot (Graf and Eckstein, 2023), DURUS robot (Reher et al., 2016), and HRP-2 robot (Dalibard et al., 2013). However, the ability to balance and walk in a real environment still has challenges and needs to be improved. In current research, biped locomotion and dynamic walking are considered to be the most important challenges in developing this type of robot (Chien et al.; Hou et al., 2024; 2024). Other issues that effect the stability locomotion of the robot is the non-linear dynamics model with number Degrees of Freedom (DoF) such as hips, arms, knees and ankles (Goswami and Vadakkepat; Zhao and Gu, 2019; 2020). Extensive research has been conducted to overcome the problems of the robot's leg stability, locomotion, and dynamic walking caused by the effect of unknown dynamics and external forces in real-time (Wu et al.; Wang et al.; Mendez-Monroy; Liu et al., 2018; 2017a; 2017; 2018a). However, these problems are still unresolved and require major improvements.

Different approaches have been applied to the walking improvement of a biped robot, using a linear biped model (Ding et al.; Wang et al.; Liu et al., 2016; 2013; 2018a). These control schemes try to maintain the robot's center of mass inside supports polygon to achieve balancing.. However, due to the complex mechanical structure of these robots, these control approaches cannot ensure the balance and dynamic walking in the presence of even small external forces in the real environment. Other control approaches have been proposed to overcome the loss of balance during walking motion, by focusing on linear control that does not need the dynamic model of the robot, such as traditional PID control (Herzog et al., 2014) and optimal linear control (Lee and Goswami, 2012)

However, these approaches utilize a two-dimensional or three-dimensional linear inverted pendulum model (LIPM) to simplify the dynamic modelling. (Hauser et al.; Ryoo, 2011; 2016). Other studies have introduced a Model Predictive Control (MPC) to minimize errors due to the acceleration constraints in order to control the footsteps position (Herdt et al.; Castano et al.;

Brahmi et al., 2010a; 2016a; 2019a). The MPC controller was used with the ACO (ant colony optimization) technique (Kashyap and Parhi, 2021a) to achieve stability during locomotion on an uneven surface to achieve stability in a short time and to stabilize itself. However, the effects of swing-leg constraints were not included in the control model. A fuzzy optimized Q-Learning (FOQL) algorithm was proposed to avoid fixed obstacles. This algorithm demonstrated the ability to optimize the path planning for the static environment without any collision (Wen et al., 2019a). The authors in (Kashyap et al., 2020a) proposed a novel technique that depends on the hybridization of the dynamic window approach with learning-based optimization. Using this approach can avoid collision and obstacles during navigation in both static and dynamic terrain. Another control strategy to maintain footstep locations uses a Linear Quadratic Regulator (LQR) that adapts the foot locations. However, although LQR is applied to a robot, its resistance to large external forces is considered weak (Faraji et al., 2019). Furthermore, several studies have shown that the unknown dynamics and external disturbances of the robot have a major impact on keeping the robot stable in different situations. Some research has suggested using control foot swing to reduce energy consumption (Gao and Wu, 2018), and other research has proposed an optimal closed-loop controller using a linearization model for robust walking (Kim and Collins; Liu et al., 2017; 2018b). A Zero-Moment Point (ZMP) method used in (Kashyap and Kumar, 2020) on the NAO humanoid robot shows the torque behavior at each joint. This approach simplifies the locomotion of the NAO robot by simulation and experiment.

In reality, simplifying the biped robot's dynamic model is impractical and inconvenient due to the non-linear system associated with walking, uneven ground, and disturbances. To overcome the problems mentioned above, an advanced adaptive approach is a promising solution for these kinds of robots. Contrary to the regressor-based control technique (He et al.; Al-Shuka and Song, 2018; 2018), several control approaches have been designed, for example, the Function Approximation Technique (FAT) to withhold the regression (Huang and Chien; Chien and Huang, 2010; 2004) that is considered as a regressor-free control method. This approach has been employed successfully on a rigid robot manipulator to approximate its unknown dynamics (Huang and Chien; Chien and Huang, 2010; 2004). The philosophy of this approach is based on the estimation of the robot's dynamic model utilizing a limited linear combination of orthonormal

basis functions. Its major problem, however, is that it only performs perfectly when using the basis function.

This paper presents a new adaptive sliding mode controller that has been applied to an NAO robot having unknown dynamics. Contrary to the conventional FAT control, the Modified Function Approximation Technique (MFAT) completely eliminates the need to use basis functions in dynamic parameter approximation. The MFAT is able to consider unmatched perturbation by using sliding mode control to compensate for uncertainties, which is considered as a robust control. This combination makes the control scheme more effective against unknown undesirable disturbances with an uncertain dynamic model of the NAO robot. It can be shown through the Lyapunov function theory that all signals are uniformly ultimately bounded in a closed loop. The simulation results and comparative study with model-based torque control prove the effectiveness of the proposed control approach performed on the NAO robot locomotion. The results of the simulation and the comparative analysis to show the viability of the proposed technique are presented. The contribution of this work is summarized as follows:

- A new adaptive MFAT augmented with sliding mode control is developed to approximate the NAO's dynamic robot model in order to track the desired trajectories (to achieve robust and dynamic locomotion), even if its dynamics are completely uncertain.
- The adaptive MFAT approach requires only the robot's dynamic model to provide online approximate of the inertia matrix, the Coriolis and centrifugal matrix and the gravitational forces of the robot.

The remainder of the paper is organized as follows: In Section 2.3, a description of the dynamic model of an NAO robot is presented, the main characteristics of the right leg and problem formulation; Section 2.4 gives the details of the control system; Section 2.5 illustrates the simulation and comparative analysis; In Section 2.6, the conclusion is drawn and future work is discussed.

2.3 Kinematic and Dynamic modeling of NAO robot

2.3.1 Kinematic model of the right leg of biped robot

Some research has utilized Modified Denavit-Hartenberg (MDH) parameters as described in Table 2.1, which gives the main characteristics of the right leg of the NOA robot (Fierro et al.; Hashemi and Jadidi, 2017a; 2012b). The right leg contains 6 Degrees of Freedom (DoFs) that includes ($\boldsymbol{\eta}_{AnkleRoll}, \boldsymbol{\eta}_{AnklePitch}, \boldsymbol{\eta}_{KneePitch}, \boldsymbol{\eta}_{HippPitch}, \boldsymbol{\eta}_{HipRoll}$ and $\boldsymbol{\eta}_{HipYaw-Pitch}$) as presented in Figure 2.1. Following to (Hashemi and Jadidi, 2012b), the forward kinematic chain was used by analyzing the position and orientation of the humanoid right leg to obtain the homogeneous transformation matrices $T_i^{i-1} \in \mathbb{R}^{4\times4}$.

$$T_i^{i-1} = \begin{bmatrix} C\eta_i & -S\eta_i & 0 & a_{i-1} \\ S\eta_i C\alpha_{i-1} & C\eta_i C\alpha_{i-1} & -S\alpha_{i-1} & -S\alpha_{i-1}d_i \\ S\eta_i S\alpha_{i-1} & C\eta_i S\alpha_{i-1} & C\alpha_{i-1} & C\alpha_{i-1}d_i \\ 0 & 0 & 0 & 1 \end{bmatrix} \tag{2.1}$$

The forward kinematics equation is obtained by multiplication of individual homogeneous transformation matrices ($T_i^{i-1} \in \mathbb{R}^{4\times4}$) which is composed of a rotation matrix ($R_{4\times4}$), and a transnational vector ($P_{3\times1}$), as given in Eq.(2.1).

Table 2.1 Modified Denavit Hartenberg parameters corresponding to the link frames attachment in Figure 2.1

joint (i)	$\boldsymbol{\alpha}_{i-1}$	$\boldsymbol{a}_{i-1}$	$\boldsymbol{\eta}_i$	$\mathbf{d_i}$
1	$\frac{\pi}{2}$	0	η_1	0
2	$\frac{\pi}{2}$	0	η_2	0
3	0	l_3	η_3	0
4	0	l_4	η_4	0
5	$-\frac{\pi}{2}$	0	η_5	0
6	$\frac{\pi}{4}$	0	η_6	d_6

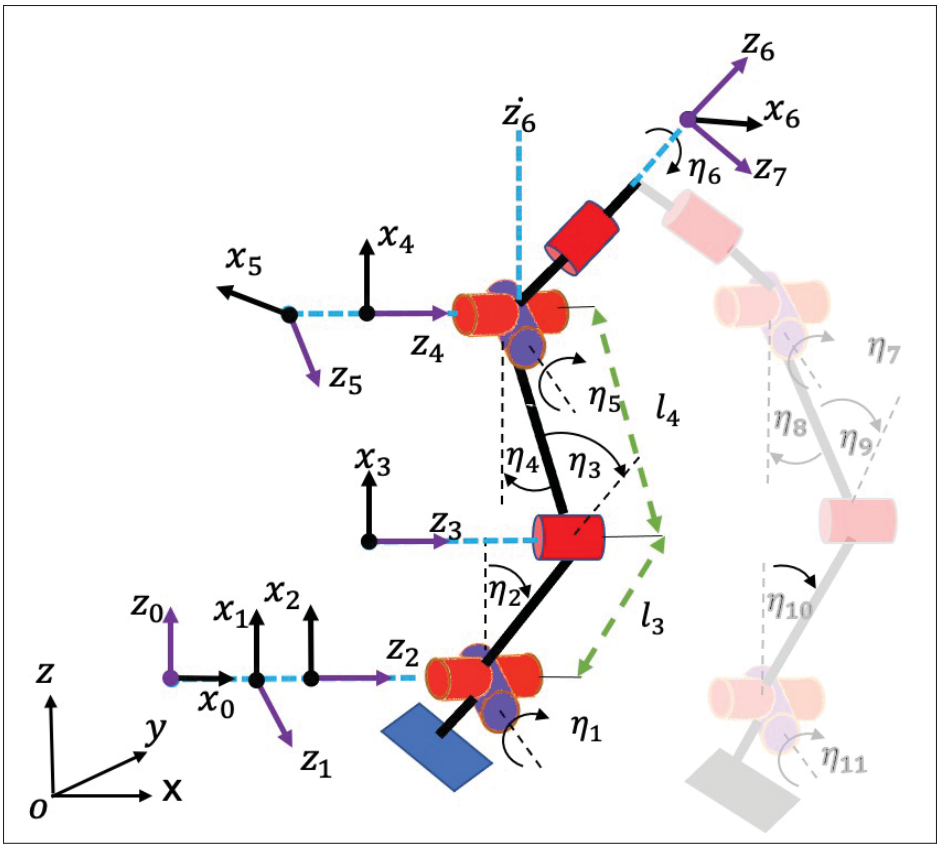

Figure 2.1 Link frames assignment on NAO robot's right leg
Taken from (Fierro et al., 2017a)

where $T_6^0 = T(\frac{0}{1})T(\frac{1}{2})T(\frac{2}{3})T(\frac{3}{4})T(\frac{4}{5})T(\frac{5}{6})$ are multiplication of the individual homogeneous transformation matrices to determine one single transformation (Said et al.; Niku, 2015a; 2020).

2.3.2 Dynamic modeling of the right leg of NAO robot

NAO robot contains 11 DoFs for two legs and including the waist as depicted in Figure 2.1 (Seleem and Assal; Janardhan and Kumar, 2017; 2019). It should be noted that the angles for 6 and 7 are actuated by only one motor. That means the angles of systems ($\eta_6 = \eta_7$) shown in Figure 2.1 are the same joint. Only one actuator control these 2 angles.Using the Lagrange method, we have developed NAO robot's right leg's dynamic model with constraints f_{ex} as expressed by the Eq.(2.2) (Grizzle et al., 2001b). Time delay ($\Delta(t)$) between the right leg and left leg is used to implement the trajectory on the robot as shown in Figure 2.2. Dynamic walking

assumes that the walking movements take place in the sagittal plane and on a horizontal surface without obstacles. The schematic diagram given below shows the angles of the NAO robot during the single support phase (SSP) (Fierro et al., 2017a); only one foot is in contact with the ground as shown in Figure 2.2. Using the Lagrange method, one can obtain the dynamic modeling equation as follows (Westervelt et al., 2018):

$$M(\eta)\ddot{\eta} + C(\eta, \dot{\eta})\dot{\eta} + G(\eta) + f_{ex} = \tau \tag{2.2}$$

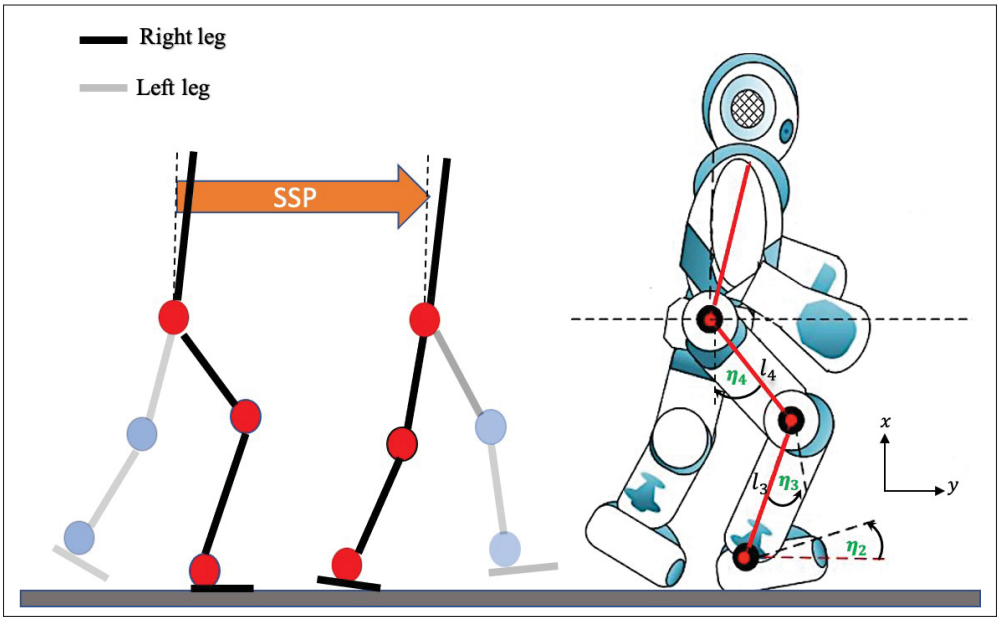

Figure 2.2 Schematic view of NAO robot's right leg (single support phase) Taken from (Liu et al.; Westervelt et al., 2017; 2018)

where $\eta, \dot{\eta}$ and $\ddot{\eta} \in \mathbb{R}^{6\times1}$ indicate the vector of the rotation angle, velocity and acceleration vector of each joint, respectively. $M(\eta) \in \mathbb{R}^{6\times6}$ indicates the positive definite mass/inertia matrix. $C(\eta, \dot{\eta}) \in \mathbb{R}^{6\times6}$ denotes the Coriolis and centrifugal matrix. $G(\eta) \in \mathbb{R}^{6\times1}$ denotes the gravitational forces, $f_{ex} \in \mathbb{R}^{6\times1}$ is the contact force vector, $\tau \in \mathbb{R}^{6\times1}$ is the control torque vector. Time delay applied between the legs is defined as:

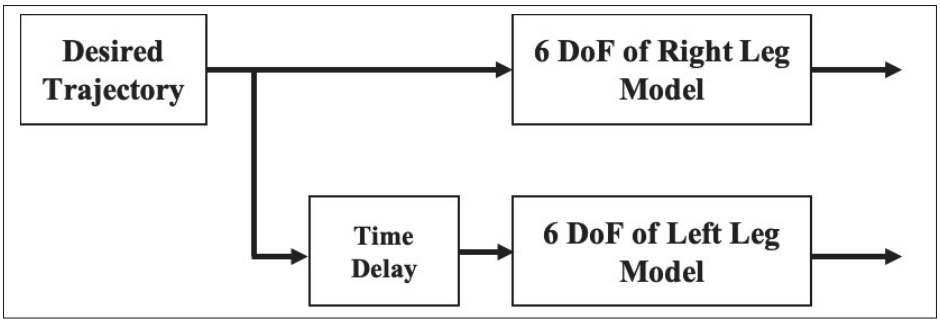

Figure 2.3 Block diagram shows swinging between feet using time delay

$$\Delta(t) = t - \frac{\Xi}{2} \tag{2.3}$$

where t is the execution time of the walking task, Ξ is a step's period time between the left and right leg and will be determined later in the simulation section.

Remark 2.1 The NAO robot's external force (f_{ex}) is a contact force (reaction force) generated when walking on flat ground without obstacles, which is measured with four sensors mounted under the foot (Zhong and Chen, 2016).

2.3.3 Control Goals

The objective of this paper is first, designing an adaptive control scheme to ensure converging the tracking error to zero in case the modeling uncertainty of the NAO robot. Secondly, closed-loop dynamics of tracking errors (e) remain Uniformly Ultimately Bounded (UUB).

Assumption 2.1 The reference Trajectories $\eta_d, \dot{\eta}_d$ and $\ddot{\eta}_d$ are known, smooth, continuous and bounded.

Property 2.1 : $\dot{M} - 2C$ is a skew-symmetric matrix. $\forall \eta, \dot{\eta} \in \mathbb{R}^n,\ \eta^T(\dot{M} - 2C)\eta = 0$ (Craig; Huang et al., 2005; 2006).

Lemma 2.1 Let $V(y)$ the Lyapunov function be continuous and positive definite, realizing $\gamma_1(\|y\|) \leq V(y) \leq \gamma_2(\|y\|)$, where γ_1 and γ_2 are respectively, the lower and upper bounds of

$V(y)$, which derivative $\dot{V}(y) = dV(y)/dt$ satisfies $\dot{V}(y) \leq -k_i V(y) + C_i$, where k_i and C_i are positive constants. Hence, the solution y is also bounded (Li et al., 2012).

2.4 Control Design

2.4.1 Model-based control scheme

The steps below can define errors in both position and velocity for the robot system as follows:

$$e = \eta - \eta_d \tag{2.4}$$

$$\omega = \dot{\eta}_d - \Lambda e \tag{2.5}$$

$$\varpi = \dot{\omega} \tag{2.6}$$

$$\sigma = \dot{\eta} - \omega \tag{2.7}$$

where $\eta \in \mathbb{R}^6$ and $\eta_d \in \mathbb{R}^6$ represent the actual and desired trajectory, respectively. $e \in \mathbb{R}^6$ describes tracking error, and $\Lambda \in \mathbb{R}^{6\times6}$ is a positive-definite, diagonal matrix. $\omega \in \mathbb{R}^6$ and $\varpi \in \mathbb{R}^6$ represent the required trajectory and its derivative, respectively, while $\sigma \in \mathbb{R}^6$ represents the selected sliding surface of sliding mode control, taking into consideration Eqs.(2.4,2.5,2.6,2.7). Hence, we can express Eq.(2.2) as follows:

$$M\dot{\sigma} + C\sigma + M\varpi + C\omega + G = \tau + f_{ex} \tag{2.8}$$

Then, the model-based control τ can be designed as:

$$\tau = -Ksign(\sigma) + \mu \tag{2.9}$$

where

$$\mu = (M\varpi + C\omega + G - f_{ex})$$

If the matrices M, C, and G of Eq.(2.8) are known, it is easy to design control law τ to ensure controlling the locomotion of the NAO robot, and $K \in \mathbb{R}^{6\times6}$ is a positive-definite, diagonal matrix.

Theorem 2.1 By designing a model-based torque control (2.9) for the NAO robot system (2.2), the whole system and error signals are asymptotically stable.

Proof: Define the following positive definite Lyapunov function:

$$V_1 = \frac{1}{2}\sigma^T M\sigma \tag{2.10}$$

Differentiating V_1, we get

$$\dot{V}_1 = \sigma^T M\dot{\sigma} + \frac{1}{2}\sigma^T \dot{M}\sigma \tag{2.11}$$

substituting $(M\dot{\sigma})$ from (2.8) and using **Property 3.1** gives

$$\dot{V}_1 = -\sigma^T K sign(\sigma) \tag{2.12}$$

It is clear that $\dot{V}_1$ is a negative semi-definite. Consequently, we can easily prove that σ is uniformly bounded and square-integrable, and $\dot{\sigma}$ is also uniformly bounded. Hence $\sigma \to 0$ as $t \to \infty$ or we may say that $e \to 0$ as $t \to \infty$. By using Barbalat's lemma, we can conclude that e and σ will converge to zero. Therefore, the system represented by the Eq.(2.2) will be asymptotically stable. The proof is complete.

2.4.2 Adaptive function approximation approach

Since the dynamic model of the robot is not always available in real-time due to the NAO's robot complex dynamic structure, unavailabilities of some measurements, and its contact with the external environment, MFAT will be used to overcome these issues. This section begins with the

following assumption: Since the dynamic model of the robot is not always available in real-time due to the NAO's robot complex dynamic structure, unavailabilities of some measurements, and its contact with the external environment, MFAT will be used to overcome these issues. This section begins with the following assumption:

Assumption 2.2 Matrices and vectors system $M(\eta)$, $C(\eta, \dot{\eta})$, and $G(\eta)$ is uncertain.

Based on **Assumption 2.2**, the system matrices and vectors $M(\eta)$, $C(\eta, \dot{\eta})$, $G(\eta)$ are unknown. Therefore, the model-based control (2.9) is unavailable in practice. A new modified function approximation technique is employed to approximate all unknown dynamics. In this context, the adaptive control ensures the stability of the NAO's robot locomotion (2.2) and guarantees uniformly ultimately bounded tracking errors in a closed-loop. Hence, to achieve adaptive control, let us change (the FAT) approach referred to in Eq. (2.2) by excluding the basis function used in (Huang and Chien; Chien and Huang, 2010; 2004) as follows:

$$\begin{cases} M_e &= M - \varepsilon_M \\ C_e &= C - \varepsilon_C \\ G_e &= G - \varepsilon_G \end{cases} \tag{2.13}$$

where $M_e \in \mathbb{R}^{6\times6}$ is an approximation of inertia matrix, $C_e \in \mathbb{R}^{6\times6}$ is the Coriolis with the centrifugal matrix, and $G_e \in \mathbb{R}^6$ is the gravitational vector. $\varepsilon_M \in \mathbb{R}^{6\times6}$ is error approximation of inertia matrix, $\varepsilon_C \in \mathbb{R}^{6\times6}$ is the error approximation of Coriolis and centrifugal matrix, and $\varepsilon_G \in \mathbb{R}^6$ is error approximation of the gravitational vector.

Employing Eq.2.13, the closed-loop dynamics (2.8) becomes:

$$M\dot{\sigma} + C\sigma + M_e\varpi + C_e\omega + G_e - \varepsilon = \tau + f_{ex} \tag{2.14}$$

Hence, the compound approximation error vector is expressed by $\varepsilon = (\varepsilon_M\varpi + \varepsilon_C\omega + \varepsilon_G) \in \mathbb{R}^6$. The stability of the NAO robot's locomotion is ensured by introducing an adaptive sliding mode

control during walking as follows:

$$\tau = \hat{M}_e \varpi + \hat{C}_e \omega + \hat{G}_e - f_{ex} - K_1 sign(\sigma) \tag{2.15}$$

replacing the control input (2.15) into (2.14). Hence, the closed-loop of the exoskeleton robot system can be described as follows:

$$M\dot{\sigma} + C\sigma + K_1 sign(\sigma) = -\tilde{M}_e \varpi - \tilde{C}_e \omega - \tilde{G}_e + \varepsilon \tag{2.16}$$

where $\tilde{M}_e = M_e - \hat{M}_e$, $\tilde{C}_e = C_e - \hat{C}_e$ and $\tilde{G}_e = G_e - \hat{G}_e$ are the estimation error of M_e, C_e, and G_e respectively. Through selecting an appropriate update law $\hat{M}_e$, $\hat{C}_e$ and $\hat{G}_e$, we can easily ensure $\tilde{M}_e \to 0$, $\tilde{C}_e \to 0$ and $\tilde{G}_e \to 0$. Hence, the control input Eq.2.15 can achieve the required efficiency and preserve the system's stability.

Remark 2.2 It is necessary to mention that ε_M, ε_C, and ε_G can not be disregarded. Nevertheless, their variations are bounded and described by the compound approximation error ε, where this lumped error satisfies $\|\varepsilon\| \leq \gamma$.

Theorem 2.2 For the NAO robot system represented by the Eq.(2.2), by using the designed adaptive approximation technique (2.15), we can ensure that the system is stable via the control where all error signals in the closed-loop system are considered Uniformly Ultimately Bounded (UUB).

Proof: Consider the Lyapunov function candidate as follows:

$$V_2 = \frac{1}{2}\sigma^T M \sigma + \frac{1}{2} Tr\left(\tilde{M}_e^T \Lambda_{M_e} \tilde{M}_e + \tilde{C}_e^T \Lambda_{C_e} \tilde{C}_e + \tilde{G}_e^T \Lambda_{G_e} \tilde{G}_e\right) \tag{2.17}$$

where $\Lambda_{M_e} \in \mathbb{R}^{6\times6}$, $\Lambda_{C_e} \in \mathbb{R}^{6\times6}$ and $\Lambda_{G_e} \in \mathbb{R}^{6\times6}$ are diagonal positive-definite matrices, and $Tr(.)$ indicates the trace of the matrix. The time derivative of Eq.2.17 is described below:

$$\dot{V}_2 = \sigma^T M \dot{\sigma} + \frac{1}{2}\sigma^T \dot{M} \sigma + Tr\left(\dot{\tilde{M}}_e^T \Lambda_{M_e} \tilde{M}_e + \dot{\tilde{C}}_e^T \Lambda_{C_e} \tilde{C}_e + \dot{\tilde{G}}_e^T \Lambda_{G_e} \tilde{G}_e\right) \tag{2.18}$$

Replacing $M\dot{\sigma}$ from Eq.2.16, the Eq. 2.18 can be written as follows:

$$\dot{V}_2 = \sigma^T \left(\frac{1}{2}\dot{M} - C\right)\sigma - \sigma^T K_1 sign(\sigma) - \sigma^T \tilde{M}_e \varpi - \sigma^T \tilde{C}_e \omega - \sigma^T \tilde{G}_e + \sigma^T \varepsilon$$
$$+Tr\left(\dot{\tilde{M}}_e^T \Lambda_{M_e} \tilde{M}_e + \dot{\tilde{C}}_e^T \Lambda_{C_e} \tilde{C}_e + \dot{\tilde{G}}_e^T \Lambda_{G_e} \tilde{G}_e\right) \tag{2.19}$$

Using **Property 2.2**, one can obtain:

$$\begin{aligned}\dot{V}_2 &= -\sigma^T K_1 sign(\sigma) + \sigma^T \varepsilon - Tr\left(\varpi\sigma^T \tilde{M}_e + \omega\sigma^T \tilde{C}_e + \tilde{G}_e \sigma^T\right) \\ &\quad +Tr\left(\dot{\tilde{M}}_e^T \Lambda_{M_e} \tilde{M}_e + \dot{\tilde{C}}_e^T \Lambda_{C_e} \tilde{C}_e + \dot{\tilde{G}}_e^T \Lambda_{G_e} \tilde{G}_e\right) \\ &= -\sigma^T K_1 sign(\sigma) + \sigma^T \varepsilon \\ &\quad +Tr\left(\left(\dot{\tilde{M}}_e^T \Lambda_{M_e} - \varpi\sigma^T\right)\tilde{M}_e + \left(\dot{\tilde{C}}_e^T \Lambda_{C_e} - \omega\sigma^T\right)\tilde{C}_e + \left(\dot{\tilde{G}}_e^T \Lambda_{G_e} - \sigma^T\right)\tilde{G}_e\right)\end{aligned} \tag{2.20}$$

In order to achieve stability of the robot system in Eq.2.20, we can use the fact that $\tilde{(.)}_e = (.)_e - \hat{(.)}_e$ and choosing the update laws as follows:

$$\begin{cases} \dot{\hat{M}}_e^T &= -\left(\varpi\sigma^T + \mu_{M_e}\hat{M}_e{}^T\right)\Lambda_{M_e}^{-1} \\ \dot{\hat{C}}_e^T &= -\left(\omega\sigma^T + \mu_{C_e}\hat{C}_e^T\right)\Lambda_{C_e}^{-1} \\ \dot{\hat{G}}_e^T &= -\left(\sigma^T + \mu_{G_e}\hat{G}_e^T\right)\Lambda_{G_e}^{-}1 \end{cases} \tag{2.21}$$

where $\mu_{(.)_e}$ is determined as $\lim_{t\to\infty}\mu_{(.)_e} = 0$ and $\int_0^t \mu_{(.)_e} dw = Q_{(.)s} < \infty$. In practice, we then choose $\mu_{(.)_e}$ as: $\mu_{(.)_e} = \dfrac{1}{1+t^2}$. Substituting update laws Eq. 2.21 in Eq. 2.20, we find

$$\dot{V}_2 = -\sigma^T K_1 sign(\sigma) + \sigma^T \varepsilon + \mu_{M_e} Tr\left(\hat{M}_e^T \tilde{M}_e\right) + \mu_{C_e} Tr\left(\hat{C}_e^T \tilde{C}_e\right) + \mu_{G_e} Tr\left(\hat{G}_e{}^T \tilde{G}_e\right) \tag{2.22}$$

Using **Remark 2.2** and the following inequalities

$$\sigma^T \varepsilon \leq \frac{\sigma^T \sigma}{2} + \frac{\gamma^2}{2}$$

$$Tr\left((\hat{.}_e)^T(\tilde{.}_e)\right) \leq \frac{1}{2}Tr\left((._e)^T(._e)\right) - \frac{1}{2}Tr\left((\tilde{.}_e)^T(\tilde{.}_e)\right)$$

where $(\tilde{.}_e) = (._e) - (\hat{.}_e)$

Eq. 2.22 becomes:

$$\begin{aligned}
\dot{V}_2 \leqslant & -\sigma^T\left(K_1 - \frac{1}{2}I_{6\times6}\right)sign(\sigma) - \frac{\mu_{M_e}}{2}Tr\left((\tilde{M}_e)^T(\tilde{M}_e)\right) \\
& -\frac{\mu_{C_e}}{2}Tr\left((\tilde{C}_e)^T(\tilde{C}_e)\right) - \frac{\mu_{G_e}}{2}Tr\left((\tilde{G}_e)^T(\tilde{G}_e)\right) \\
& +\frac{\mu_{M_e}}{2}Tr\left((M_e)^T(M_e)\right) + \frac{\mu_{C_e}}{2}Tr\left((C_e)^T(C_e)\right) \\
& +\frac{\mu_{G_e}}{2}Tr\left((G_e)^T(G_e)\right) + \frac{\gamma^2}{2} \\
\dot{V}_2 \leqslant & -\alpha_1 V_2 + \alpha_2
\end{aligned} \tag{2.23}$$

where $\alpha_1 = min\left(\gamma_{min}\left(K_1 - \frac{1}{2}I_{6\times6}\right), \frac{\mu_{M_e}}{2}, \frac{\mu_{C_e}}{2}, \frac{\mu_{G_e}}{2}\right)$ and $\alpha_2 = \left(\frac{\gamma^2}{2}\right)$, with γ_{min} the minimum eigenvalues of $\left(K_1 - \frac{1}{2}I_{6\times6}\right)$ matrix, while
$\frac{\mu_{M_e}}{2}Tr\left((M_e)^T(M_e)\right) + \frac{\mu_{C_e}}{2}Tr\left((C_e)^T(C_e)\right) + \frac{\mu_{G_e}}{2}Tr\left((G_e)^T(G_e)\right) \rightarrow 0$ due to the definition of $\mu_{(.)_e}$ in Eq 2.21. Achieving the condition $(K_1 - \frac{1}{2}I_{6\times6}) > 0$ implies that $\dot{V}_2 \leq 0$. According to **Lemma 2.1**, all closed-loop error signals have proven to be fully UUB. ■

Figure 2.4 presents the architecture of the proposed adaptive sliding mode control diagram using MFAT.

2.5 Simulation and Comparative Study

In this section, the controller's efficiency is verified in using Simulink (Matlab 2019a) and *V-rep* environments, the platform to implement the numerical simulation. *V-rep* is the

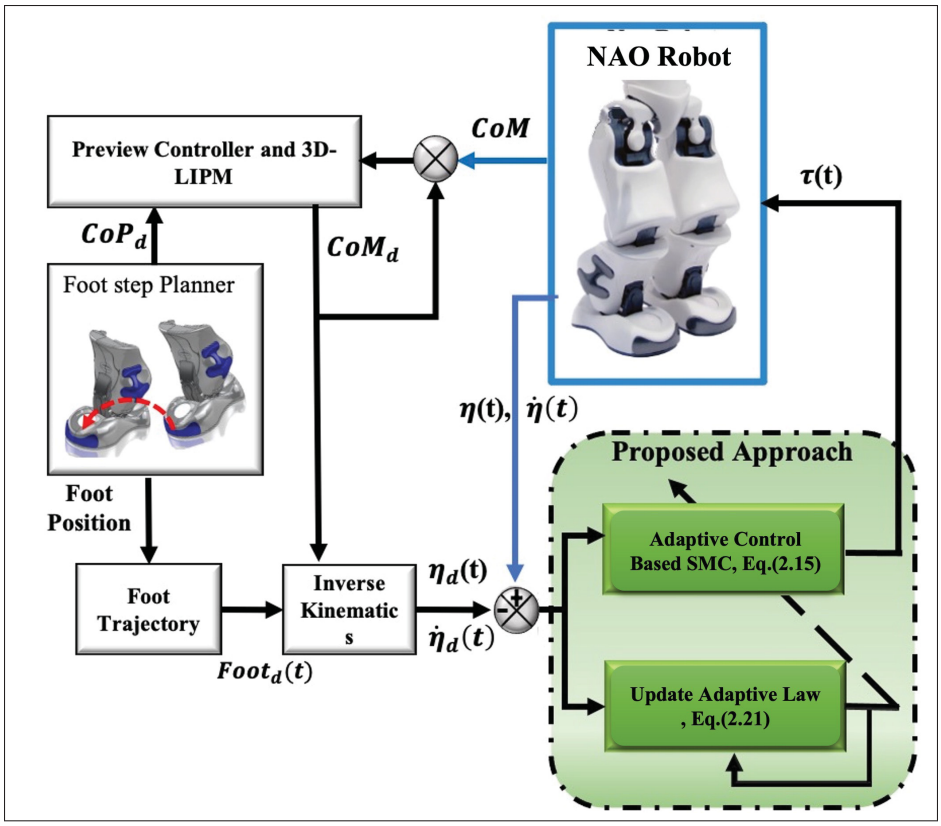

Figure 2.4 Model adaptive sliding mode control diagram using MFAT

Virtual Robot Experimentation Platform used to implement the proposed control as a virtual environment (Freese et al., 2010). Communication between the Simulink software developed in Matlab® and V-rep is done by ROS (Robot Operating System) as shown in Figure 2.5. The ROS platform is an operating system for robots considered as a middleware. Indeed, this software runs in parallel and coordinates several executable (algorithms, components or sensors) called "nodes". In our case, ROS will mainly allow us to establish communication between Matlab, Simulink and the NAO robot. ROS primarily allows executables to exchange information synchronously via topic or asynchronously via a service. A topic carries information based on subscription/publication (subscribe/publish). In this case, one or more nodes are able to publish information on a topic, and one or more nodes will be able to read this information. On the other hand, the service allows synchronous communication between two nodes.

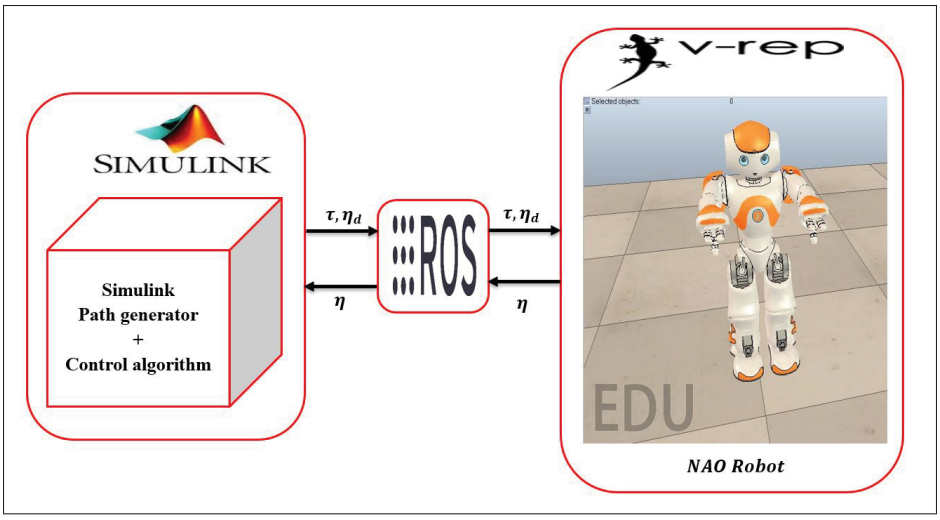

Figure 2.5 Model adaptive sliding mode control diagram using MFAT

2.5.1 Adaptive control based modified function approximation technique Simulation Implementation

In this part, the effectiveness of the designed controller (2.15) is verified by simulation. All initial values are set as $(\hat{M}_{eii} = 1)$, $(\hat{C}_{eii} = 1)$ and $(\hat{G}_{ei} = 1)$. The updating-law parameters provided in (2.21) are set as $\Lambda_{M_e} = 10I_{6\times6}$, $\Lambda_{C_e} = 10I_{6\times6}$, and $\Lambda_{G_e} = 10I_{6\times1}$. Controller parameters are selected manually as follows: $K_1 = diag[30, 80, 30, 80, 80, 30]$, $\Lambda = diag[2, 2, 2, 2, 2, 2]$ and $\Xi = 0.75\ sec$.

The detailed results are shown in Figures (2.6-2.8). In the first column of Figure 2.6, the measured η and desired trajectory η_d are plotted to show that η and η_d quickly converge in small neighbourhood, demonstrating that the NAO robot tracking is efficient. In the second column of Figure 2.7, tracking error (e) is plotted, showing that e converges to the desired error and measured error are close to zero. In Figure 2.8, control input τ shows, that the control input based adaptive modified function approximation controller (2.15) is smaller than the control input generated under the model-based controller (2.9) shown in Table 2.2 below. Figures (2.9-2.11) show the estimation of the dynamic system $\hat{M}$, $\hat{C}$, and $\hat{G}$ under state-feedback based adaptive modified function approximation controller. Although M, C, and G are unknown dynamics, the adaptive modified function approximation controller (2.15) achieves good tracking execution

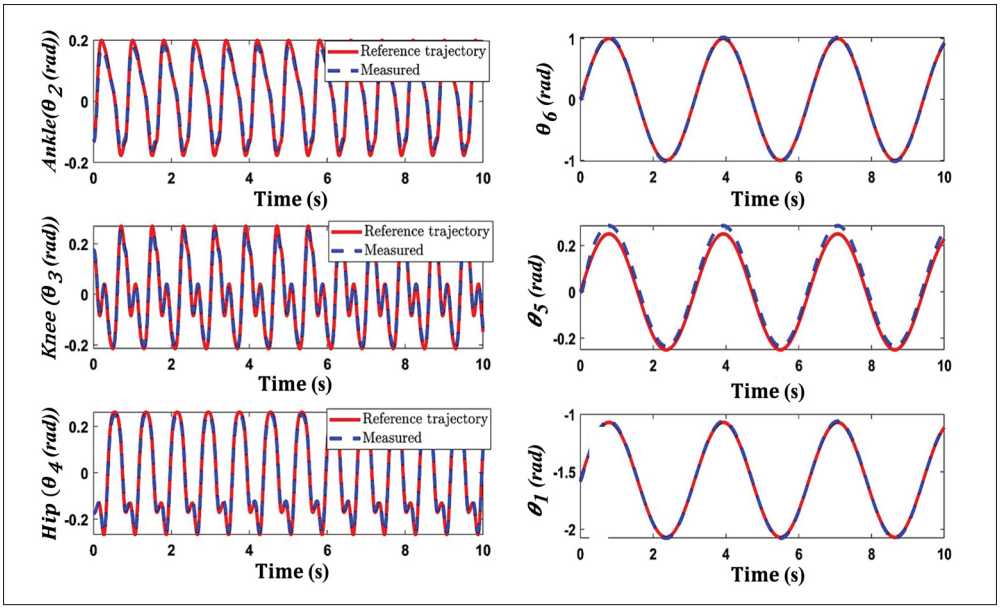

Figure 2.6 The measured trajectory η and desired trajectory η_d under state-feedback based adaptive modified function approximation controller (2.15)

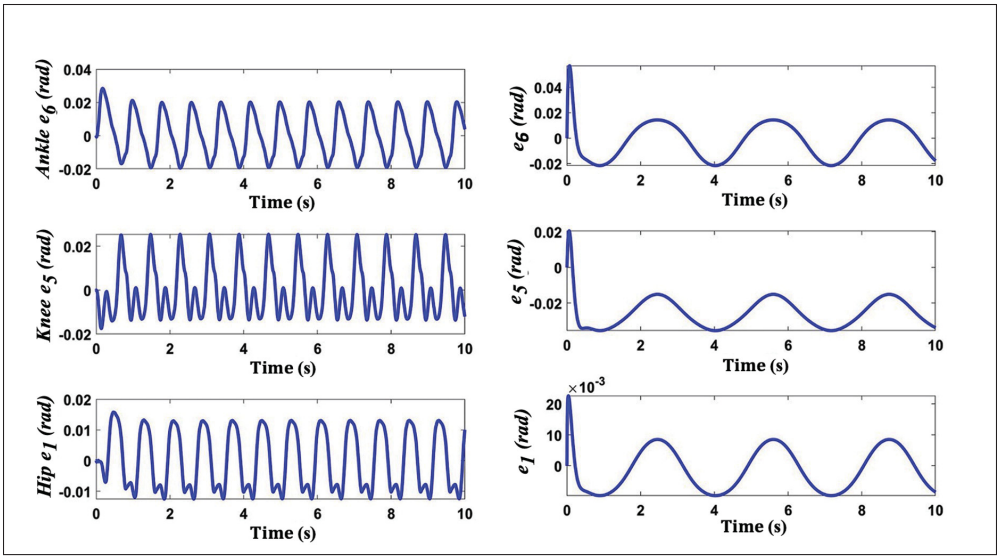

Figure 2.7 Tracking errors under state-feedback based adaptive modified function approximation controller (2.15)

by the NAO robot, as shown by our simulation results. Table 2.2 presents a summarized performance of the designed control techniques: the model-based controller (2.9) and the

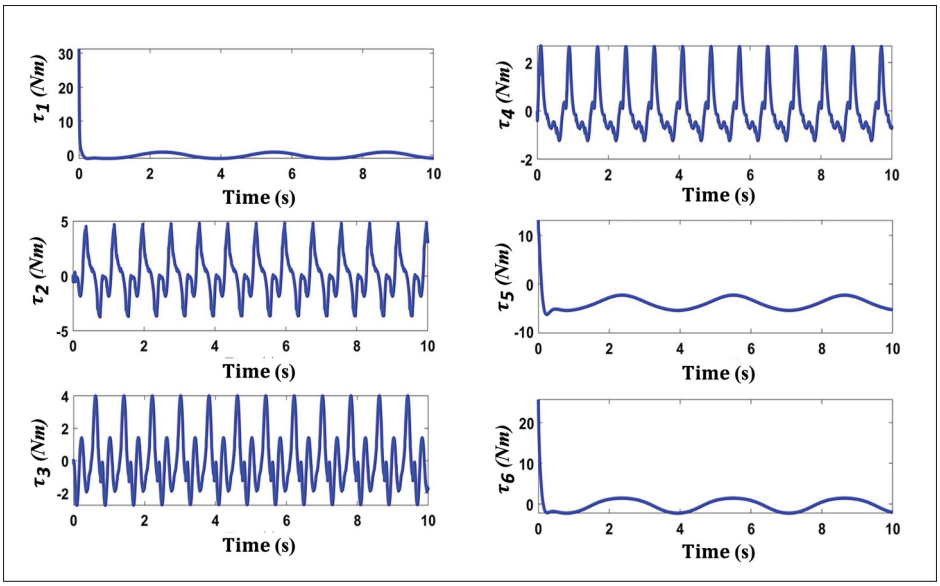

Figure 2.8 Control input τ based adaptive modified function approximation controller of right leg (2.15)

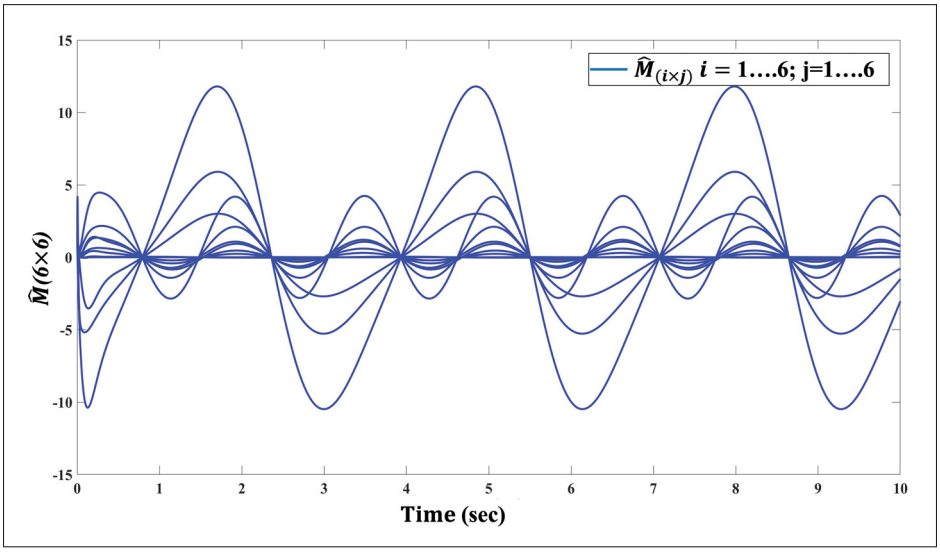

Figure 2.9 Estimation of (M) Matrix under state-feedback based adaptive modified function approximation controller (2.15)

adaptive modified function approximation controller (2.15) investigated in this paper. It is observed in Table 2.2 that the adaptive modified function approximation controller (2.15) was

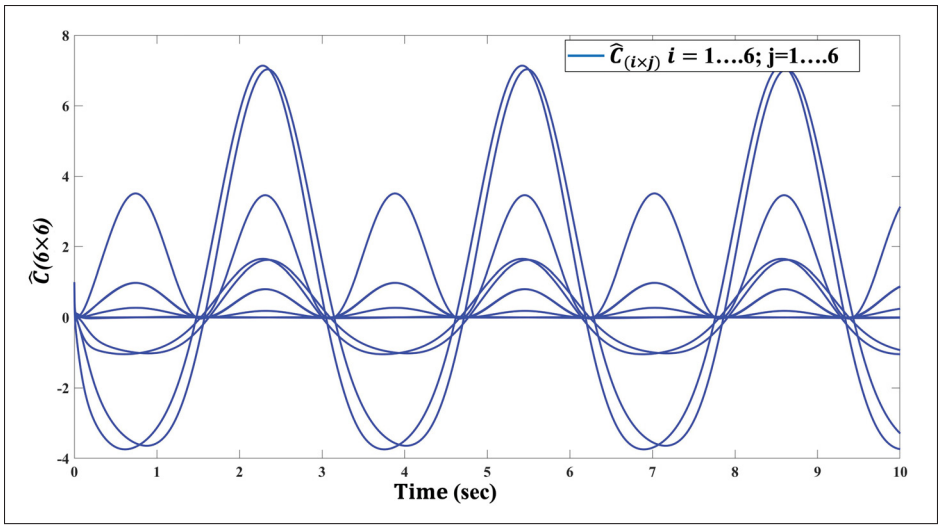

Figure 2.10 Estimation of (C) Matrix under state-feedback based adaptive modified function approximation controller (2.15)

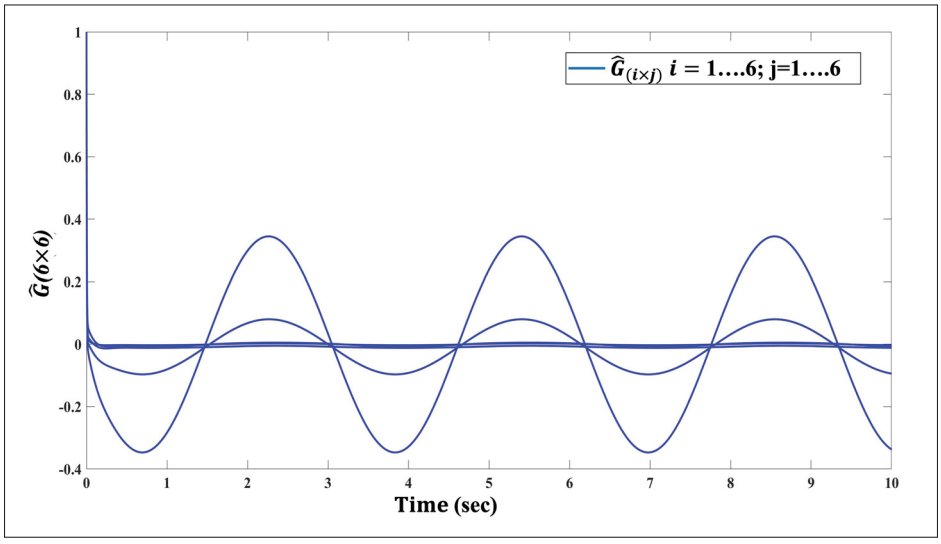

Figure 2.11 Estimation of (G) vector under state-feedback based adaptive modified function approximation controller (2.15)

able to provide good tracking with the control input although the dynamic model of the robot M, C, and G was completely unknown. Therefore, our results prove the feasibility of the proposed adaptive method.

Table 2.2 Controller performance

Parameters	**Control input (2.9)**	**Control input (2.15)**
$Ankle\ RMS(e_2)$	0.0619	0.0501
$Knee\ RMS(e_3)$	0.0036	0.0013
$Hip\ RMS(e_4)$	0.0394	0.0266
$max(\tau_2)$	5.879	4.145
$max(\tau_3)$	8.864	4.259
$max(\tau_4)$	4.468	3.326

2.6 Conclusion

In this paper, an adaptive control based on Modified Approximation Technique (MFAT) is developed to control the NAO robot with unknown dynamics in combination with a sliding mode control. A walking NAO robot is used to implement the proposed control technique. Unlike a conventional FAT, the proposed updated FAT completely eliminates the use of base functions in dynamic model estimation law. The combination of MFAT with the adaptive control is developed to approximate the dynamic modeling of the NAO robot to guide the motors' drive to track the desired trajectories. The effectiveness of the proposed scheme has been proved through ROS and MATLAB simulation results. Finally, the comparative study of the model-based controller and sliding mode-based adaptive modified function approximation controller validates the advantage and disadvantage of these different control schemes.

CHAPTER 3

WALKING POSITION COMMANDED NAO ROBOT USING NONLINEAR DISTURBANCE OBSERVER-BASED FIXED-TIME TERMINAL SLIDING MODE

Mahmoud Farhat[1] , Yassine Kali [2] , Maarouf Saad[1] , Mohammad H Rahman[3] , Roberto E. Lopez-Herrejon [1]

[1] Département de Génie Mécanique, École de Technologie Supérieure,
1100 Notre-Dame Ouest, Montréal, Québec, Canada H3C 1K3

[2] School of Engineering, Université du Québec en Abitibi-Témiscamingue,
Rouyn-Noranda, QC J9X 5E4 Canada

[3] Mechanical/Biomedical Engineering Department,University of Wisconsin-Milwaukee,
Milwaukee, WI 53211, United States

Article published in the journal "ISA Transactions", December 2023

3.1 Abstract

The walking stability of a humanoid robot is a fundamental problem due to the complex nonlinear dynamic model of the robot's legs. This work introduces the performance tracking control for the humanoid NAO robot by using a Nonlinear Disturbance Observer (NDO)-based Fixed-time Terminal Sliding Mode (FTSM). The influence of uncertain external disturbance is considered while implementing the control strategy to improve the walking motion of the NAO robot. An NDO is adapted to estimate the uncertainties and external disturbances. A novel FTSM surface is proposed to drive the tracking errors to zero in fixed-time. The designed NDO-based FTSM control law achieves robustness while reducing the chattering phenomenon. The Lyapunov's stability theory is used to establish the fixed-time stability of the sliding surface and system states under the proposed control method. To validate the performance of the proposed NDO-based FTSM control, a real-time experiment was conducted on a humanoid NAO robot to demonstrate the improved tracking performance in the presence of the uncertain perturbation effect. The effectiveness of the proposed controller design is validated on a flat, upward inclined surface, and compared to another controller.

keyword: Humanoid robots, Uncertain Disturbance, Fixed-time convergence, Lyapunov function, Sliding mode, Chattering, Walking control.

3.2 Introduction

3.2.1 Context and Motivation

Humanoid robot movement includes a variety of control design challenges because of the large number of Degrees of Freedom (DoFs), highly nonlinear dynamics, and the swing leg's persistent influence on the ground (Koptev et al.; Kashyap and Parhi, 2021; 2021c). Bipedal systems are unable to adapt to environmental changes to create an accurate model of the system dynamics, represent uncertainty, and ensure stability in the locomotion of bipedal robot (Farhat et al., 2021a). Several researchers have used various methods to solve these problems, such as Optimization Aided PID, to improve the stability of the humanoid robot and the predictive controller (Brahmi et al.; Herdt et al.; Castano et al.; Kashyap and Parhi, 2019b; 2010b; 2016b; 2021c). Other studies have focused on dynamic walking to counteract balance loss during motion caused by environmental factors like uneven ground and external disturbances (He et al.; Wang et al., 2014; 2017b). Therefore, achieving balanced walking in real-time with a humanoid robot requires building an outstanding control system to achieve balance performance and accommodate to ground conditions.

In the literature, the stability of walking has been the focus of extensive studies on the walking stability of a biped robot in a complex environment (Liu et al.; Song et al., 2018c; 2022a). To address the issues of stability and low accuracy of the tracking trajectory, kinematic modeling has been analyzed to track the robot's trajectory planning and walking robustness (Li et al., 2008). Dynamic walking has been a key issue in research on humanoid robots walking to perform tasks and maintain stability. Dynamic modeling has been used to design control laws to achieve zero tracking errors. Furthermore, several control methods have overcome the challenges of nonlinear systems (e.g., backstepping control, adaptive control, Fuzzy Logic and neural networks) (Khoi and Nguyen Xuan; Li et al., 2021; 2019). Other studies have used the linear inverted pendulum

to formulate a dynamic system to overcome the complex system (Kashyap and Parhi; Wang et al., 2021b; 2012). However, previous studies have not considered applying the simulation results to a real biped robot and tested under speed walking situations with several DoFs.

One of the techniques most frequently used with nonlinear systems is Sliding Mode Control (SMC). It is a reliable method for bringing nonlinear systems around the sliding manifold before reaching an equilibrium point. When designing the control, it is important to take into account the uncertainties and the external disturbances. This allows for a more robust and reliable control system that can effectively handle varying conditions and unexpected factors (He et al.; Zhang and Yang, 2014; 2013). The SMC approach is widely used in fields such as power systems, robotics, and aircraft (Komurcugil et al.; Wang et al.; Mechali et al., 2020; 2016; 2021). Compared to other control methods, SMC has attracted the attention of many researchers for its efficiency, and robustness against model uncertainties (Wang et al.; Li et al.; Lu et al., 2020b; 2019; 2015).

To enable the state trajectories of the system to reach the sliding surface in a given time, a finite-time control design is essential. A general design approach for the finite-time sliding mode control has been used to maintain the balancing of the robot gait (Ren et al.; Mahyuddin et al., 2019; 2014). The SMC is also employed to increase transient reaction speed and improve the steady-state accuracy of the robot's dynamic walking (Park and Kim; Nguyen et al., 2001; 2020). The sliding mode based on zero moment point (ZMP) controller was proposed to ensure the walking stability of the bipedal (Kim et al., 2019). However, only simulation results are presented. This methodology for designing sliding mode controllers shows the effectiveness of the proposed algorithm to drive the state trajectory onto the surface in finite-time. The SMC is also an effective method to reduce the influence of disturbances on the controlled system (Amirkhani et al.; Rahmani et al., 2019; 2018). However, conventional SMC suffers from the chattering phenomenon that might lead to system instability and ensure asymptotic convergence during the sliding phase.

To address the problem of chattering reduction and finite-time convergence during both reaching and sliding phase, a Terminal SMC (TSMC) that consists of nonlinear sliding manifolds has been developed (Yu et al.; Wang et al.; Sanchez-Magos et al., 2005; 2003; 2020). The robustness, stability, and convergence time of the closed loop system have been demonstrated using Lyapunov theory (Wang et al.; Farid and Ruggiero, 2020a; 2021). Two main weaknesses remain: the convergence that depends mainly on the initial conditions and the slow convergence when the system states are far away from the desired equilibrium (Yu and Zhihong, 2002). To enhance the convergence rate during the sliding phase, a Fast TSMC (FTSMC) has been proposed in (Vo et al.; Yu et al., 2020; 2005). It was demonstrated that faster convergence performance is obtained (Amirkhani et al.; Zheng et al.; Han et al., 2019; 2015; 2018). However, the conducted practical works indicate that the chattering is still present. Moreover, once again, the convergence time relies on the initial conditions which make it challenging to ensure a desired consistent behavior across several case studies.

Motivated by previous observations, this paper proposes a nonlinear disturbance observer-based fixed-time terminal sliding mode control technique that aims to achieve a desired robust walking control objective within a fixed time without taking into account the initial conditions and even in the presence of the uncertainties and the disturbances. Unlike the methods that ensure asymptotic of finite-time convergence, the proposed method can guarantee safety in the applications where time is very crucial. Another interesting feature of the proposed controller relies on the tuning of three gains only for the reaching phase and three others for the sliding phase while other proposed fixed-time controllers require more parameters. This is thanks to a designed exponent that switches between two values according to the tracking error variable for the sliding phase and according to the terminal sliding surface variable for the reaching phase. In addition, the uncertainties and the disturbances are estimated using a nonlinear disturbance observer (Bu et al.; Guoyuan et al.; Shi and Hou, 2015; 2004; 2008) that consists of an arctan-based tracking differentiator and is able to estimate accurately a wide range of matched uncertainties and to cancel the effect of unmatched measurement noise. Furthermore, this observer does not require the upper bounds of the uncertainties and allows the choice of small switching gains.

This implies a chattering reduction and an acceptable control effort. All the above-mentioned features are demonstrated using Lyapunov theory. Finally, in order to control the NAO robot effectively, the computed torques generated by the controller need to be transformed into a position command, as proposed in (Kali et al., 2021). This transformation step is crucial to ensure compatibility between the controller's output and the NAO robot's actuators and control interface. The main contributions of this paper are as follows:

- Regardless of initial conditions, a fixed-time terminal sliding mode controller is proposed to ensure convergence within a fixed-time during both the reaching and the sliding phase. For each phase, a new convergence time is demonstrated in terms of three controller gains only. Moreover, the adopted reaching law ensures robustness such as the effect of the estimation errors are rejected.
- Experimental results are conducted to assess and compare the effectiveness of the proposed fixed-time technique with recent proposed fixed-time controller. An image of the implemented PD control is used to make the implementation possible.

The remainder of the paper is organized as follows: Section 3.3 describes the lower body dynamic model for the NAO robot and formulates the control objective. Section 3.4 presents the design of the used arctan-based nonlinear disturbance observer as well as the new FTSM method while Section 3.4 shows the experimental results conducted on the real NAO humanoid robot.

3.3 Preliminaries

3.3.1 NAO Robot's Legs Model

The dynamic model of the lower body of the NAO robot has been developed using the Lagrange formulation, which was investigated and analyzed. The modified Denavit-Hartenberg (MD-H) approach is used to obtain the main characteristics of each leg (right and left) of the NAO robot as described in Table 3.1. The NAO robot has 12 DoFs of the lower body, 6 DoFs for each leg (Chang et al., 2017) as shown in Figure 3.1. Each leg contains three hip joints, one knee joint and two ankle joints (Bayraktaroğlu et al.; Hashemi and Khajepour; Niku, 2018; 2017; 2020).

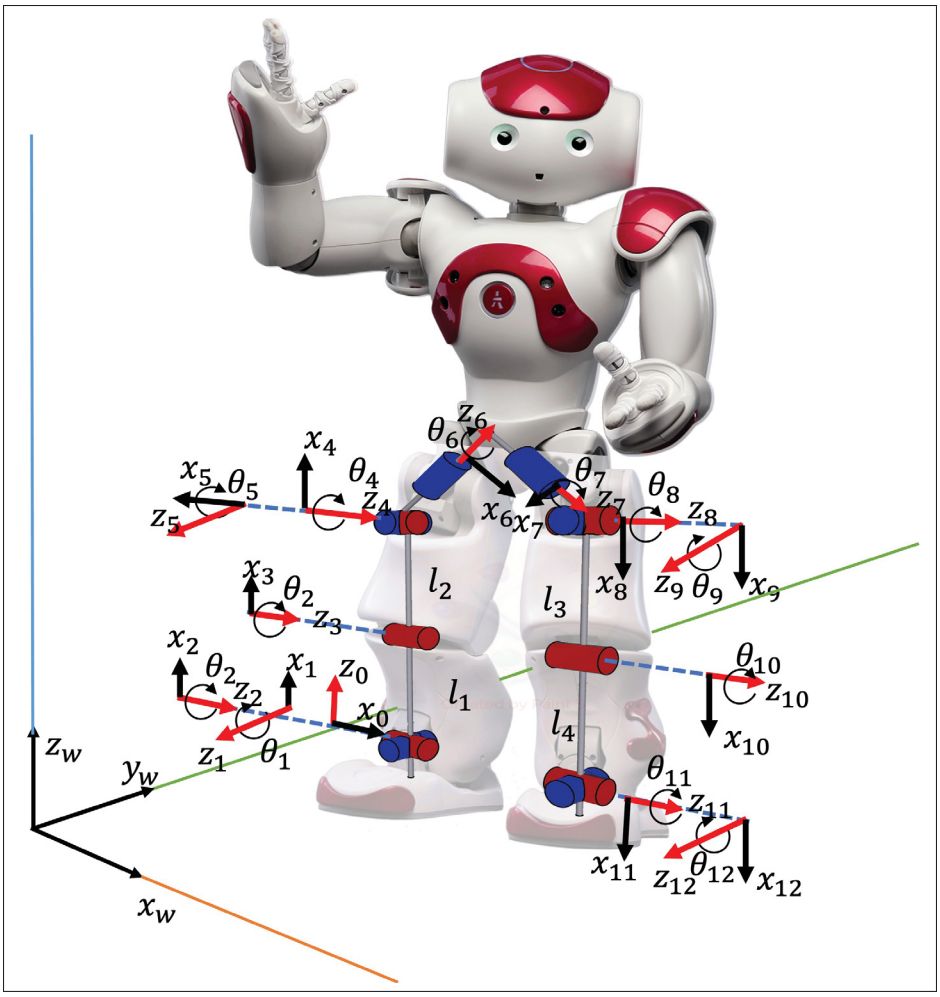

Figure 3.1 Kinematic model of NAO humanoid robot joints and its coordinate frames

The rotation matrix ($\boldsymbol{R}_{3\times3}$), and transnational vector ($\boldsymbol{P}_{3\times1}$) are described by the homogeneous transformation matrices ($\boldsymbol{T}_i^{i-1} \in \mathbb{R}^{4\times4}$), as given in Eq.(3.1).

$$\boldsymbol{T}_i^{i-1} = \begin{bmatrix} \cos(q_i) & -\sin(q_i) & 0 & a_{i-1} \\ \sin(q_i)\cos(\alpha_{i-1}) & \cos(q_i)\cos(\alpha_{i-1}) & -\sin(\alpha_{i-1}) & -\sin(\alpha_{i-1})d_i \\ \sin(q_i)\sin(\alpha_{i-1}) & \cos(q_i)\sin(\alpha_{i-1}) & \cos(\alpha_{i-1}) & \cos(\alpha_{i-1})d_i \\ 0 & 0 & 0 & 1 \end{bmatrix} \tag{3.1}$$

Table 3.1 MD-H right leg parameters corresponding to the link frames attachment
Taken from (Ding et al., 2016)

	Right Leg				Left leg			
link i	α_{i-1}	$\mathbf{a_{i-1}}$	$\mathbf{d_i}$	$\mathbf{q_j}$	α_{i-1}	$\mathbf{a_{i-1}}$	$\mathbf{d_i}$	$\mathbf{q_j}$
1	$\frac{\pi}{2}$	0	0	q_{1r}	$-\frac{\pi}{2}$	0	d_7	q_{7l}
2	$\frac{\pi}{2}$	0	0	q_{2r}	$\frac{\pi}{2}$	0	0	q_{8l}
3	0	l_1	0	q_{3r}	0	l_3	0	q_{9l}
4	0	l_2	0	q_{4r}	0	l_4	0	q_{10l}
5	$-\frac{\pi}{2}$	0	0	q_{5r}	$\frac{\pi}{2}$	0	0	q_{11l}
6	$\frac{\pi}{2}$	0	d_6	q_{6r}	$\frac{\pi}{2}$	0	0	q_{12l}

where

$$\begin{cases} \boldsymbol{T}^0_{6_R} = \boldsymbol{T}^0_1 \boldsymbol{T}^1_2 \boldsymbol{T}^2_3 \boldsymbol{T}^3_4 \boldsymbol{T}^4_5 \boldsymbol{T}^5_6 \\ \boldsymbol{T}^6_{12_L} = \boldsymbol{T}^6_7 \boldsymbol{T}^7_8 \boldsymbol{T}^8_9 \boldsymbol{T}^9_{10} \boldsymbol{T}^{10}_{11} \boldsymbol{T}^{11}_{12} \end{cases}$$

$\boldsymbol{T}^0_{6_R}$ and $\boldsymbol{T}^6_{12_L}$ are homogeneous transformation matrices for right and left legs, respectively (Said et al.; Siciliano et al., 2015b; 2009a). In this specific case, the dynamic model of the right and left legs is similar as described in Table 3.1. It should be noted that the joints for 6 and 7 are actuated by the same motor. Since it is considered that the dynamic model of right and left legs are similar, then, the model can be formulated by the Lagrangian dynamic equation as follows (Craig; Mokhtari et al.; González-Mejía et al., 2018a; 2021a; 2020a):

$$\ddot{\boldsymbol{q}}_j = \boldsymbol{M}(\boldsymbol{q}_j)^{-1}[\boldsymbol{\tau}_j - \boldsymbol{C}(\boldsymbol{q}_j, \dot{\boldsymbol{q}}_j)\dot{\boldsymbol{q}}_j - \boldsymbol{G}(\boldsymbol{q}_j) - \boldsymbol{P}_{fc}] \tag{3.2}$$

where $j = \{r, l\}$ with r and l stand respectively for right and left, $\boldsymbol{q}_j, \dot{\boldsymbol{q}}_j, \ddot{\boldsymbol{q}}_j \in \mathbb{R}^6$ are the vector of the rotation angle, velocity and acceleration vectors of each joint, respectively. $\boldsymbol{M}(q_j) \in \mathbb{R}^{6\times6}$ indicates the positive-definite inertia matrix. $\boldsymbol{C}(q_j, \dot{q}_j) \in \mathbb{R}^{6\times6}$ denotes the Coriolis and centrifugal matrix. $\boldsymbol{G}(q_j) \in \mathbb{R}^6$ denotes the gravitational forces, $\boldsymbol{P}_{fc} \in \mathbb{R}^6$ is the force contact pressure of the foot vector. $\boldsymbol{\tau_j} \in \mathbb{R}^6$ is the control torque vector. Moreover, each actuated joint is driven by the same DC servomotor whose dynamic model is described by:

$$\ddot{\boldsymbol{q}}_{m,j} = \boldsymbol{J}^{-1}_{m,j}\left[\boldsymbol{\tau}_{m,j} - \boldsymbol{\tau}_{L,j} - \boldsymbol{B}_{m,j}\dot{\boldsymbol{q}}_{m,j}\right] \tag{3.3}$$

where $\boldsymbol{q}_{m,j} = \boldsymbol{R}_j^{-1}\boldsymbol{q}_j$, $\dot{\boldsymbol{q}}_{m,j}$ and $\ddot{\boldsymbol{q}}_{m,j}$ are respectively the (6×1) angular position, velocity and acceleration vectors of the motor shaft with $\boldsymbol{R}_j = \text{diag}(r_{1j}, ..., r_{6l})$ is the gear reduction ratio constant, $\boldsymbol{J}_{m,j} = \text{diag}(J_{m1j}, ..., J_{m6j})$ is the moment of inertia matrix and $\boldsymbol{B}_{m,j} = \text{diag}(B_{m1j}, \cdots, B_{m6j})$ is the viscous friction matrix, $\boldsymbol{\tau}_{m,j} \in \mathbb{R}^6$ is the vector of the motor torques, $\boldsymbol{\tau}_{L,j} = \boldsymbol{R}_j\boldsymbol{\tau}_j \in \mathbb{R}^6$ is the load torque vector at the motor shaft (Buschmann et al., 2009). Hence, the combined NAO-motor dynamics can be obtained by combining Eqs. (3.2) and (3.3) as follows:

$$\ddot{\boldsymbol{q}}_j = \hat{\boldsymbol{M}}^{-1}(\boldsymbol{q}_j)\left[\boldsymbol{\tau}_{m,j} - \boldsymbol{H}(\boldsymbol{q}_j, \dot{\boldsymbol{q}}_j) - \boldsymbol{R}_j\boldsymbol{P}_{fc}\right] \tag{3.4}$$

where:

$$\hat{\boldsymbol{M}}^{-1}(\boldsymbol{q}_j) = \left(\boldsymbol{R}_j\boldsymbol{M}(\boldsymbol{q}_j) + \boldsymbol{R}_j^{-1}\boldsymbol{J}_{m,j}\right)^{-1}$$

$$\boldsymbol{H}(\boldsymbol{q}_j, \dot{\boldsymbol{q}}_j) = \boldsymbol{R}_j\boldsymbol{C}(\boldsymbol{q}_j, \dot{\boldsymbol{q}}_j)\dot{\boldsymbol{q}}_j + \boldsymbol{R}_j\boldsymbol{G}(\boldsymbol{q}_j) + \boldsymbol{R}_j^{-1}\boldsymbol{B}_{m,j}\dot{\boldsymbol{q}}_j.$$

3.3.2 Problem Formulation

The key challenge addressed in this study involves the design of an FTSM control strategy, incorporating the NDO, to achieve robust and precise walking position control for the NAO robot. This entails considering the uncertainties and disturbances inherent to real-world scenarios.

3.4 NDO-based FTSM Controller

Consider the robot leg dynamics which can be rewritten as:

$$\begin{cases} \dot{z}_1 = z_2 \\ \dot{z}_2 = \boldsymbol{F}(z) + \boldsymbol{B}(z_1)\boldsymbol{u} + \boldsymbol{D} \\ \boldsymbol{y} = z \end{cases} \tag{3.5}$$

where $z = [z_1^T, z_2^T]^T \in \mathbb{R}^{12}$ is the state variable vector in which $z_1 = \boldsymbol{q}_j$ and $z_2 = \dot{\boldsymbol{q}}_j$, $\boldsymbol{u} = \boldsymbol{\tau}_m \in \mathbb{R}^6$ is the control input vector,$\boldsymbol{B}(z_1) = \hat{\boldsymbol{M}}^{-1}(\boldsymbol{q}_j)$, $\boldsymbol{F}(z) = -\hat{\boldsymbol{M}}^{-1}(\boldsymbol{q}_j)\boldsymbol{H}(\boldsymbol{q}_j, \dot{\boldsymbol{q}}_j)$ and $\boldsymbol{D} = -\hat{\boldsymbol{M}}^{-1}(\boldsymbol{q}_j)\boldsymbol{R}_j\boldsymbol{P}_{fc}$ represents the vector of disturbances. The elements of the disturbance vector

$\boldsymbol{D}$ are assumed to be bounded by positive constants δ_i such as for $i = 1, \cdots, 6$:

$$|D_i| \leq \delta_i \tag{3.6}$$

The considered NDO is reported in (Bu et al.; Guoyuan et al.; Shi and Hou, 2015; 2004; 2008), its dynamics to estimate the disturbances of the studied system Eq. (3.5) is given by:

$$\begin{cases} \dot{\hat{z}} = \boldsymbol{F}(z) + \boldsymbol{B}(z_1)\boldsymbol{u} + \hat{\boldsymbol{D}} \\ \dot{\hat{\boldsymbol{D}}} = -\boldsymbol{R}^2 \left[\boldsymbol{L}_1 \boldsymbol{N}_1(z_2, \hat{z}_2) + \boldsymbol{L}_2 \boldsymbol{N}_2(\hat{\boldsymbol{D}}) \right] \end{cases} \tag{3.7}$$

where $\hat{z} = [\hat{z}_1^T, \hat{z}_2^T]^T = [\hat{\boldsymbol{q}}^T, \dot{\hat{\boldsymbol{q}}}]^T$ is the estimation of the state variable vector z, $\hat{\boldsymbol{D}}$ is the estimation of external disturbances, $\boldsymbol{R} = \text{diag}(R_1, \cdots, R_6)$, $\boldsymbol{L}_1 = \text{diag}(L_{11}, \cdots, L_{16})$ and $\boldsymbol{L}_2 = \text{diag}(L_{21}, \cdots, L_{26})$ are diagonal positive-definite matrices.
$\boldsymbol{N}_1(z_2, \hat{z}_2) = [\arctan(\delta_{11}(\hat{z}_{21} - z_{21})), \cdots, \arctan(\delta_{16}(\hat{z}_{26} - z_{26}))]$
and $\boldsymbol{N}_2(\hat{\boldsymbol{D}}) = \left[\arctan\left(\delta_{21}\frac{\hat{D}_1}{R_1}\right), \cdots, \arctan\left(\delta_{26}\frac{\hat{D}_6}{R_6}\right) \right]$ with δ_{1i} and δ_{2i} are positive design parameters for $i = 1, \cdots, 6$. By adjusting the gains of the observer, one can obtain accurate estimation of $\boldsymbol{D}$.

Now, for the fixed-time controller design, let us propose the following nonlinear sliding manifold:

$$\boldsymbol{S} = \boldsymbol{e}_2 + \boldsymbol{\Phi}_1 \boldsymbol{e}_1 + \boldsymbol{\Phi}_2 \text{sign}^{\varepsilon}(\boldsymbol{e}_1) \tag{3.8}$$

where $\boldsymbol{e}_1 = \boldsymbol{z}_1 - \boldsymbol{z}_{1d} \in \mathbb{R}^6$ and $\boldsymbol{e}_2 = \boldsymbol{z}_2 - \boldsymbol{z}_{2d} \in \mathbb{R}^6$ are respectively the position and the velocity tracking error vectors, $\boldsymbol{\Phi}_1$ and $\boldsymbol{\Phi}_2$ are (6×6) diagonal positive-definite matrices, $\text{sign}^{\boldsymbol{\varepsilon}}(\boldsymbol{e}_1) = \left[|e_{11}|^{\varepsilon_1} \text{sign}(e_{11}), \ldots, |e_{16}|^{\varepsilon_6} \text{sign}(e_{16}) \right]^T$ with $\boldsymbol{\varepsilon}_i$ is defined for $i = 1, \cdots, 6$ by:

$$\boldsymbol{\varepsilon}_i = \begin{cases} 1 + \boldsymbol{\varepsilon}_i^{\star}, & \text{if } |\boldsymbol{e}_{1i}| > 1 \\ 1 - \boldsymbol{\varepsilon}_i^{\star}, & \text{if } |\boldsymbol{e}_{1i}| \leq 1 \end{cases} \tag{3.9}$$

such as $\boldsymbol{\varepsilon}_i^{\star} \in (0, \frac{1}{2})$ $(1 < (1 + \boldsymbol{\varepsilon}_i^{\star}) < 1.5$ and $0.5 < (1 - \boldsymbol{\varepsilon}_i^{\star}) < 1)$ and $\text{sign}(\boldsymbol{e}_{1i})$ is defined as follows:

$$\text{sign}(\boldsymbol{e}_{1i}) = \begin{cases} -1, & \text{if} \quad e_{1i} < 0 \\ 0, & \text{if} \quad e_{1i} = 0 \\ 1, & \text{if} \quad e_{1i} > 0 \end{cases} \tag{3.10}$$

It is worth to mention that the switch of $\boldsymbol{\varepsilon}_i$ occurs when the error is equal to one to avoid any discontinuity on the sliding surface.

Theorem 3.1 Consider the proposed sliding manifold Eq. (3.8). The tracking error $\boldsymbol{e}_1$ converges to zero in a fixed-time smaller than:

$$T_{i,max}^{slid} = T_{i,max}^{reach} + \frac{2}{\boldsymbol{\varepsilon}_i^{\star} \boldsymbol{\phi}_{1i}} \ln\left(1 + \frac{\boldsymbol{\phi}_{1i}}{\boldsymbol{\phi_{2i}}}\right) \tag{3.11}$$

where $T_{i,max}^{slid}$ is the maximal time required for the tracking error $\boldsymbol{e}_1$ to reach zero during the sliding phase while $T_{i,max}^{reach}$ is the maximal time required for the system trajectories to reach the proposed sliding manifold. ***Proof.*** Consider the positive-definite Lyapunov function $\boldsymbol{V}_1 = 0.5\, \boldsymbol{e}_1^T \boldsymbol{e}_1$, where its derivative is computed as:

$$\boldsymbol{V}_1 = \boldsymbol{e}_1^T \boldsymbol{e}_2 \tag{3.12}$$

During the sliding phase ($\boldsymbol{S} = 0$), we have:

$$\boldsymbol{e}_2 = -\boldsymbol{\Phi}_1 \boldsymbol{e}_1 - \boldsymbol{\Phi}_2 \text{sign}^{\boldsymbol{\varepsilon}}(\boldsymbol{e}_1) \tag{3.13}$$

Substituting the above equation into Eq. (3.12) yields to:

$$\begin{aligned} \boldsymbol{V}_1 &= -\boldsymbol{e}_1^T \left(\boldsymbol{\Phi}_1 \boldsymbol{e}_1 + \boldsymbol{\Phi}_2 \text{sign}^{\boldsymbol{\varepsilon}}(\boldsymbol{e}_1)\right) \\ &= -\sum_{i=1}^{6} \phi_{1i} e_{1i}^2 + \phi_{2i} |e_{1i}|^{1+\varepsilon_i} \\ &= -\sum_{i=1}^{6} 2\phi_{1i} V_{1i} + \phi_{2i} (2V_{1i})^{0.5(1+\varepsilon_i)} < 0 \end{aligned} \tag{3.14}$$

Therefore, the origin is a globally stable equilibrium point. Now, let us rewrite Eq. (3.13) for $i = 1, \cdots, 6$ as follows:

$$e_{2i} = \begin{cases} -\phi_{1i} e_{1i} - \phi_{2i} |e_{1i}|^{1+\varepsilon_i^\star} \text{sign}(e_{1i}), & \text{if } |e_{1i}| > 1 \\ -\phi_{1i} \boldsymbol{e}_{1i} - \boldsymbol{\phi}_{2i} |e_{1i}|^{1-\varepsilon_i^\star} \text{sign}(e_{1i}), & \text{if } |e_{1i}| \leq 1 \end{cases} \tag{3.15}$$

Introducing new variable η_i given by:

$$\eta_i = \begin{cases} \ln(|e_{1i}|) + 1, & \text{if } |e_{1i}| > 1 \\ |e_{1i}|^{\varepsilon_i^\star}, & \text{if } |\boldsymbol{e}_{1i}| \leq 1 \end{cases} \tag{3.16}$$

Combining equations Eq. (3.15) and Eq. (3.16) gives:

$$\dot{\eta}_i = \begin{cases} -\phi_{1i} - \phi_{2i} \text{exp}^{\eta_i \varepsilon_i^\star - \varepsilon_i^\star}, & \text{if } \eta_i > 1 \\ -\varepsilon_i^\star \left(\phi_{1i} \eta_i + \phi_{2i}\right), & \text{if } 0 < \eta_i \leq 1 \end{cases} \tag{3.17}$$

Based on the above equation, the maximal convergence time can be calculated for each DoF as follows:

$$\begin{aligned} T_{i,max}^{slid} =& T_{i,max}^{reach} + \int_0^1 \frac{1}{\varepsilon_i^\star \left(\phi_{1i} \eta_i + \phi_{2i}\right)} d\eta_i + \lim_{\eta_{i0} \to \infty} \int_1^{\eta_{i0}} \frac{1}{\phi_{1i} + \phi_{2i} \text{exp}^{\eta_i \varepsilon_i^\star - \varepsilon_i^\star}} d\eta_i \\ =& T_{i,max}^{reach} + \frac{1}{\varepsilon_i^\star \phi_{1i}} \left[\ln \left(\eta_i + \frac{\phi_{2i}}{\phi_{1i}} \right) \right]_0^1 + \lim_{\eta_{i0} \to \infty} \int_1^{\eta_{i0}} \frac{1}{\phi_{1i} + \phi_{2i} \text{exp}^{\eta_i \varepsilon_i^\star - \varepsilon_i^\star}} d\eta_i \\ =& T_{i,max}^{reach} + \frac{1}{\varepsilon_i^\star \phi_{1i}} \ln \left(1 + \frac{\phi_{1i}}{\phi_{2i}} \right) + \lim_{\eta_{i0} \to \infty} \int_1^{\eta_{i0}} \frac{1}{\phi_{1i} + \phi_{2i} \text{exp}^{\eta_i \varepsilon_i^\star - \varepsilon_i^\star}} d\eta_i \end{aligned} \tag{3.18}$$

Introducing another variable $\chi_i = \text{exp} \eta_i \varepsilon_i^\star - \varepsilon_i^\star$ yields to:

$$\begin{aligned} T_{i,max}^{slid} =& T_{i,max}^{reach} + \frac{1}{\varepsilon_i^\star \phi_{1i}} \ln \left(1 + \frac{\phi_{1i}}{\phi_{2i}} \right) + \lim_{\chi_i \to \infty} \int_1^{\chi_i} \frac{1}{\phi_{1i} \varepsilon_i^\star \chi_i + \phi_{2i} \varepsilon_i^\star \chi_i^2} d\chi_i \\ =& T_{i,max}^{reach} + \frac{1}{\varepsilon_i^\star \phi_{1i}} \ln \left(1 + \frac{\phi_{1i}}{\phi_{2i}} \right) + \frac{1}{\varepsilon_i^\star \phi_{1i}} \lim_{\chi_i \to \infty} \left[\ln \left(\frac{\chi_i}{\phi_{2i} \chi_i + \phi_{1i}} \right) \right]_1^{\chi_i} \\ =& T_{i,max}^{reach} + \frac{1}{\varepsilon_i^\star \phi_{1i}} \ln \left(1 + \frac{\phi_{1i}}{\phi_{2i}} \right) + \frac{1}{\varepsilon_i^\star \phi_{1i}} \ln \left(1 + \frac{\phi_{1i}}{\phi_{2i}} \right) \\ =& T_{i,max}^{reach} + \frac{2}{\varepsilon_i^\star \phi_{1i}} \ln \left(1 + \frac{\phi_{1i}}{\phi_{2i}} \right) \end{aligned} \tag{3.19}$$

This completes the proof.

Now, to ensure that the proposed nonlinear manifold Eq. (3.8) converges to zero in a fixed time, the control law can be designed as follows:

$$\begin{aligned} \boldsymbol{u} &= -\boldsymbol{B}^{-1}(z_1)\left[F(z) + \hat{\boldsymbol{D}} - \boldsymbol{u}_0 + \Psi_1 \boldsymbol{S} + \Psi_2 \text{sign}^{\mu}(\boldsymbol{S}) + \text{sign}(\boldsymbol{S})\right] \\ \boldsymbol{u}_0 &= \dot{z}_{2d} - \Phi_1 \boldsymbol{e}_2 - \Phi_2 \boldsymbol{E}\, \boldsymbol{sat}\left(\lfloor \boldsymbol{e}_1 \rceil^{\varepsilon-1} \boldsymbol{e}_2, h\right) \end{aligned} \tag{3.20}$$

where:

- the matrices $\boldsymbol{\Psi}_1 = \text{diag}(\psi_{11}, \cdots, \psi_{16})$, $\boldsymbol{\Psi}_2 = \text{diag}(\psi_{21}, \cdots, \psi_{26})$ and $\boldsymbol{\Psi}_3 = \text{diag}(\psi_{31}, \cdots, \psi_{36})$ are diagonal positive-definite,
- $\boldsymbol{E} = \text{diag}(\varepsilon_1, \cdots, \varepsilon_6)$,
- $\lfloor \boldsymbol{e}_1 \rceil^{\boldsymbol{\varepsilon}-1} = \text{diag}(|e_{11}|^{\varepsilon_1-1}, \ldots, |e_{16}|^{\varepsilon_6-1})$,
- $\boldsymbol{sat}\left(\lfloor \boldsymbol{e}_1 \rceil^{\boldsymbol{\varepsilon}-1} \boldsymbol{e}_2, h\right) = \left[\text{sat}(|e_{11}|^{\varepsilon_1-1} e_{21}, h), \ldots \ldots, \text{sat}(|e_{16}|^{\varepsilon_6-1} e_{26}, h)\right]^T$ such as:

$$\text{sat}(\bullet, h) = \begin{cases} \bullet & \text{if} |\bullet| < h \\ h\text{sign}(\bullet) & \text{if} |\bullet| \geq h \end{cases}$$

  It uses the saturation function to replace the singularity term ($\lfloor \boldsymbol{e}_1 \rceil^{\varepsilon-1} \boldsymbol{e}_2$) in the control input, allowing the control approach to limit the amplitude of the singularity growth and keep it under control, which has been used in (Tian et al., 2020).
- $\text{sign}^{\boldsymbol{\mu}}(\boldsymbol{S}) = \left[|S_1|^{\mu_1}\text{sign}(S_1), \ldots, |S_6|^{\mu_6}\text{sign}(S_6)\right]^T$ with:

$$\mu_i = \begin{cases} 1 + \mu_i^{\star}, & \text{if } |S_i| > 1 \\ 1 - \mu_i^{\star}, & \text{if } |S_i| \leq 1 \end{cases} \quad 0 < \mu_i^{\star} < 0.5$$

- $\text{sign}(\boldsymbol{S}) = \left[\text{sign}(S_1), \ldots, \text{sign}(S_6)\right]^T$.

Theorem 3.2 Consider the legs dynamics Eq. (3.5), if the following condition is verified:

$$\boldsymbol{\psi}_{3i} \geq |\tilde{D}_i|, \;\; i = 1, \cdots, 6 \tag{3.21}$$

Then, the proposed NDO-based FTSM Eq. (3.20) ensures the convergence of the designed sliding surface Eq. (3.8) to zero in a fixed-time given by:

$$T_{i,max}^{reach} = \frac{2}{\mu_i^{\star}\psi_{1i}} \ln\left(1 + \frac{\psi_{1i}}{\psi_{2i}}\right) \tag{3.22}$$

Proof. Consider the fact that the derivative of the second Lyapunov function $\boldsymbol{V}_2 = 0.5\, \boldsymbol{S}^T \boldsymbol{S}$ is computed as follows:

$$\begin{aligned} \dot{\boldsymbol{V}}_2 =& \boldsymbol{S}^T \dot{\boldsymbol{S}} = \boldsymbol{S}^T \left[\dot{\boldsymbol{e}}_2 + \boldsymbol{\Phi}_1 \boldsymbol{e}_2 + \boldsymbol{\Phi}_2 E \lfloor \boldsymbol{e}_1 \rceil^{\varepsilon-1} \boldsymbol{e}_2\right] \\ =& \boldsymbol{S}^T \left[\boldsymbol{F}(z) + \boldsymbol{B}(z_1)\boldsymbol{u} + \boldsymbol{D} - \dot{z}_{2d} + \boldsymbol{\Phi}_1 \boldsymbol{e}_2 + \boldsymbol{\Phi}_2 \boldsymbol{E} \lfloor \boldsymbol{e}_1 \rceil^{\varepsilon-1} \boldsymbol{e}_2\right] \end{aligned} \tag{3.23}$$

Using (3.20), $\dot{\boldsymbol{V}}_2$ becomes:

$$\begin{aligned} \dot{\boldsymbol{V}}_2 =& \boldsymbol{S}^T \left[\tilde{\boldsymbol{D}} - \boldsymbol{\Psi}_1 \boldsymbol{S} - \boldsymbol{\Psi}_2 \mathrm{sign}^{\mu}(\boldsymbol{S}) - \boldsymbol{\Psi}_3 \mathrm{sign}(\boldsymbol{S})\right] \\ =& \sum_{i=1}^{6} S_i \tilde{D}_i - \psi_{1i} S_i^2 - \psi_{2i} |S_i|^{\mu_i+1} - \psi_{3i} |S_i| \\ \leq& \sum_{i=1}^{6} |S_i||\tilde{D}_i| - \psi_{1i} S_i^2 - \psi_{2i} |S_i|^{\mu_i+1} - \psi_{3i} |S_i| \end{aligned} \tag{3.24}$$

where $\tilde{D}_i$ is the i^{th} element of the estimation error vector $\tilde{\boldsymbol{D}} = \boldsymbol{D} - \hat{\boldsymbol{D}}$. The above $\dot{\boldsymbol{V}}_2$ is negative-definite if the switching gains Ψ_{3i} for $i = 1, \cdots, 6$ are chosen as in Eq. (3.21). Moreover, if the condition is respected, the following inequality holds:

$$\begin{aligned} \dot{\boldsymbol{V}}_2 \leq& \sum_{i=1}^{6} -\psi_{1i} S_i^2 - \psi_{2i} |S_i|^{\mu_i+1} \\ \leq& \sum_{i=1}^{6} -2\psi_{1i} V_{2i} - \psi_{2i} \left(2V_{2i}\right)^{0.5(\mu_i+1)} < 0 \\ \dot{V}_{2i} \leq& \begin{cases} -2\psi_{1i} V_{2i} - \psi_{2i} \left(2V_{2i}\right)^{1+0.5\mu_i^{\star}}, & \text{if } |S_i| > 1 \\ -2\psi_{1i} V_{2i} - \psi_{2i} \left(2V_{2i}\right)^{1-0.5\mu_i^{\star}}, & \text{if } |S_i| \leq 1 \end{cases} \end{aligned} \tag{3.25}$$

Once again, to prove the fixed-time convergence, let us introduce the following new variable ζ_i:

$$\zeta_i = \begin{cases} \ln(2V_{2i}) + 1, & \text{if } (2V_{2i}) > 1 \\ (2V_{2i})^{\mu_i^\star}, & \text{if } (2V_{2i}) \leq 1 \end{cases} \tag{3.26}$$

Combining Eq. (3.25) and Eq. (3.26) gives:

$$\dot{\zeta}_i \leq \begin{cases} -\psi_{1i} - \psi_{2i}\exp^{\zeta_i\mu_i^\star - \mu_i^\star}, & \text{if } \zeta_i > 1 \\ -\mu_i^\star\left(\psi_{1i}\zeta_i + \psi_{2i}\right), & \text{if } 0 < \zeta_i \leq 1 \end{cases} \tag{3.27}$$

Then, for each sliding surface, the convergence time can be computed as:

$$\begin{aligned} T_i^{reach} \leq & \int_0^1 \frac{1}{\mu_i^\star\left(\psi_{1i}\zeta_i + \psi_{2i}\right)} d\zeta_i + \int_1^\infty \frac{1}{\psi_{1i} + \psi_{2i}\exp^{\zeta_i\mu_i^\star - \mu_i^\star}} d\zeta_i \\ \leq & \frac{1}{\mu_i^\star\psi_{1i}}\left[\ln\left(\zeta_i + \frac{\psi_{2i}}{\psi_{1i}}\right)\right]_0^1 + \int_1^\infty \frac{1}{\psi_{1i} + \psi_{2i}\exp^{\zeta_i\mu_i^\star - \mu_i^\star}} d\zeta_i \\ \leq & \frac{1}{\mu_i^\star\psi_{1i}}\ln\left(1 + \frac{\psi_{1i}}{\psi_{2i}}\right) + \int_1^\infty \frac{1}{\psi_{1i} + \psi_{2i}\exp^{\zeta_i\mu_i^\star - \mu_i^\star}} d\zeta_i \end{aligned} \tag{3.28}$$

By choosing $\kappa_i = \exp^{\zeta_i\mu_i^\star - \mu_i^\star}$ yields to:

$$\begin{aligned} T_i^{reach} \leq & \frac{1}{\mu_i^\star\psi_{1i}}\ln\left(1 + \frac{\psi_{1i}}{\psi_{2i}}\right) + \int_1^\infty \frac{1}{\psi_{1i}\mu_i^\star\kappa_i + \psi_{2i}\mu_i^\star\kappa_i^2} d\kappa_i \\ \leq & \frac{1}{\mu_i^\star\psi_{1i}}\ln\left(1 + \frac{\psi_{1i}}{\psi_{2i}}\right) + \frac{1}{\mu_i^\star\psi_{1i}}\int_1^\infty \left(\frac{\psi_{2i}}{\psi_{2i}\kappa_i + \psi_{1i}} - \frac{1}{\kappa_i}\right) d\kappa_i \\ \leq & \frac{1}{\mu_i^\star\psi_{1i}}\ln\left(1 + \frac{\psi_{1i}}{\psi_{2i}}\right) + \frac{1}{\mu_i^\star\underline{\psi}_{1i}}\left[\ln\left(\frac{\kappa_i}{\psi_{2i}\kappa_i + \psi_{1i}}\right)\right]_1^\infty \\ \leq & \frac{1}{\mu_i^\star\psi_{1i}}\ln\left(1 + \frac{\psi_{1i}}{\psi_{2i}}\right) + \frac{1}{\mu_i^\star\psi_{1i}}\ln\left(1 + \frac{\psi_{1i}}{\psi_{2i}}\right) = \frac{2}{\mu_i^\star\psi_{1i}}\ln\left(1 + \frac{\psi_{1i}}{\psi_{2i}}\right) \end{aligned} \tag{3.29}$$

Hence, the maximal reaching time is fixed since it depends on the reaching law gains only. This completes the proof.

Remark 3.1 It is worth it to mention that the maximal reaching fixed-time given in Eq. (3.22) is independent of any initial state and is also independent of the observer convergence as long as the condition in Eq. (3.21) is met. Moreover, the estimated reaching fixed-time upper-bound in

Eq. (3.22) may be conservative, especially for small disturbance estimation error $\tilde{D}_i$ and high values for the switching gain ψ_{3i} in Eq. (3.21).

Remark 3.2 Performing a convergence within a fixed-time might lead to a peak phenomenon or a high control activity that can damage the system's actuators or lead to an undesirable high energy consumption. In some cases, due to the saturation, the control signal might have no physical meaning and can lead to undesirable behavior.

To control the NAO robot, the computed torques in Eq. (3.20) should be transformed into a

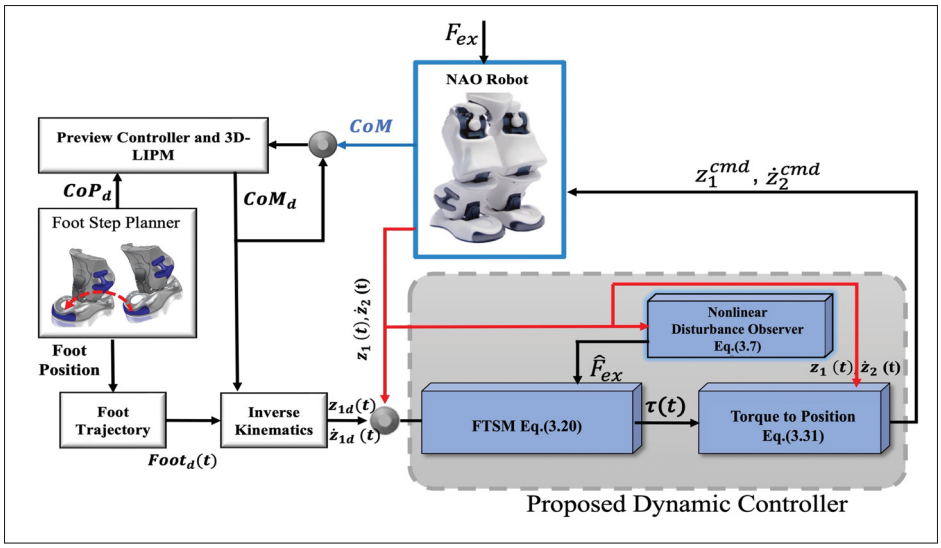

Figure 3.2 The structure of the proposed NDO-based FTSM control scheme

position command. Indeed, each DC motor of the NAO legs has the following PD controller:

$$\boldsymbol{u} = \boldsymbol{K}_p(z_1 - z_1^{cmd}) + \boldsymbol{K}_d z_2 \tag{3.30}$$

where $\boldsymbol{K}_p$ is the proportional gain and $\boldsymbol{K}_d$ is the derivative gain and z_1^{cmd} is the (6×1) reference position vector for the on-board joint PD controller. Hence, the NDO-based FTSM of the position commanded is generated as:

$$z_1^{cmd} = z_1 + \boldsymbol{K}_p^{-1}(\boldsymbol{K}_d z_2 - \boldsymbol{u}) \tag{3.31}$$

3.5 Experimental results

This section presents the experimental steps to validate the proposed controller that was involved in real-time on the lower body of the NAO robot (V6.0). Figure 3.2 describes the proposed structure of the NDO-based FTSM control. The desired joint angular trajectories are determined using the Zero-Moment Point (ZMP) (Farhat et al., 2021a) and the Center of Mass (CoM) trajectory motion that is an input to the inverse kinematics model as shown Figure 3.2. the Center of Pressure (CoP) is relative to the foot support polygon, related to the ZMP trajectory (Hof, 2008). On the other hand, the desired trajectory is derived from a predefined Zero Moment Point (ZMP) trajectory. The ZMP is a critical parameter that ensures the stability of the robot during walking. By maintaining the ZMP within the robot's support polygon (the region of ground contact for the feet), stability is guaranteed. Hence, the desired trajectory, including the joint angles for each joint, is determined based on the predefined ZMP trajectory (Wu et al.; Kashyap and Parhi, 2022a; 2023a). The proposed controller Eq. (3.20) is implemented using Microsoft Visual C++ with NAOqi 2.5 - Linux, which was developed by SoftBank Robotics. NAOqi will basically allow us to establish a connection to transmit instructions to the NAO robot in real-time. Hence, the left and right legs move cooperatively to maintain the balance of the robot's body by following a synchronized pattern. The stance leg supports the robot's weight and remains stable while the swing leg prepares for the next step. The NDO-based FTSM controller generates the joint torques and then the position commands of both legs, ensuring smooth coordination and preventing falls or loss of balance. This cooperative movement allows the robot to achieve balanced walking and body stability.

Table 3.2 Gains of the proposed controller

$\boldsymbol{\Phi}_1 = 20.05 I_{6\times6}$	$\boldsymbol{\Phi}]_2 = 1.75 I_{6\times6}$
$\boldsymbol{\Psi}_1 = 5.75 I_{6\times6}$	$\boldsymbol{\Psi}_2 = 0.75 I_{6\times6}$
$\boldsymbol{\Psi}_3 = 10.4 I_{6\times6}$	$h = 0.8$
$\boldsymbol{\mu}_i^{\star} = 0.5 I_{6\times6}$	$\boldsymbol{\varepsilon}_i^{\star} = 0.45 I_{6\times6}$
$\boldsymbol{K}_p = 0.5 I_{6\times6}$	$\boldsymbol{K}_d = 0.3 I_{6\times6}$

The parameters of the proposed method were selected experimentally trial and error technique to ensure the best balance between tracking accuracy and control effort. The selected gains of our controller in Eq. (3.20) are listed in Table 3.2. In the conducted experiments, the trajectory of each joint is measurable by utilizing the position sensors, specifically, Magnetic Rotary Encoders, which are integrated into the motors Robotics (Aldebaran Robotics, 2022). These position sensors provide accurate feedback information regarding the joint positions.

In this work, we performed two experimental tests and a comparison study to validate the effectiveness of the proposed approach. Figs.(3.3- 3.6) show the experimental results for the first adopted scenario where the NAO has to walk straight on a non perfect flat carpet. It is worth to mention that the considered walking speed is [44.7 cm/s] which is a bit above its maximum speed [44.44 cm/s]. The first experiment video for the NAO robot is available at the following URL: Walking at high speed on flat ground. According to Figure 3.5, it can be seen that the joint tracking errors are small for the right leg, demonstrating good tracking performance. The NAO robot's joint torque inputs during the non perfect flat-carpet walking are shown in Figure 3.6, it is obvious that the chattering is significantly reduced and the actuator efforts are acceptable for the NAO robot.

In order to consolidate the results obtained, a second scenario where the NAO robot has to walk on a sloping ground with 8.82 degrees from flat ground as shown in Figure 3.7. In this figure, we can see the progress of the robot on the slope over time. The video of this second scenario is available at the following URL: Walking on a sloped floor. The experimental results are depicted in Figs.(3.8- 3.11). It can be seen that the robot is able to achieve the control objective. According to Figs.(3.8- 3.9), the tracking is good even if the tracking errors for the right leg in Figure 3.10 are quite bigger than the one obtained in the first scenario Figure 3.5. This difference is caused by the nature of the surface which is slippery and non flat. Indeed, the NAO robot is designed to perform on a flat low-pile carpet with a firm surface as used for the first scenario on hardwood or laminate floor. Otherwise, the computed torques depicted in Figure 3.11 are chattering-free with still acceptable control effort. Figure 3.9 demonstrates the controller's effective ability to accurately track desired trajectories, even when walking on

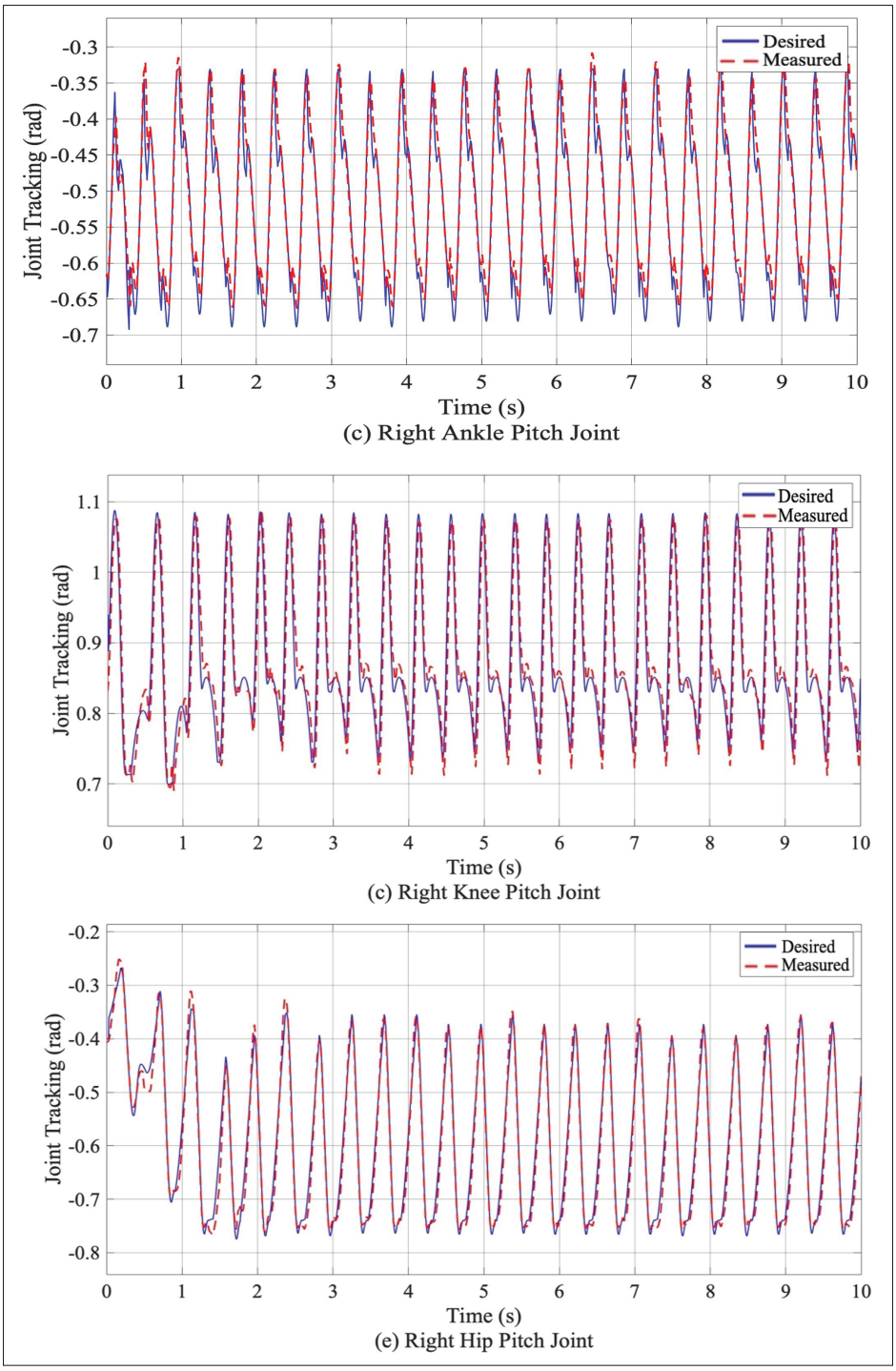

Figure 3.3 Right leg joint tracking during the 1^{st} scenario via the proposed controller

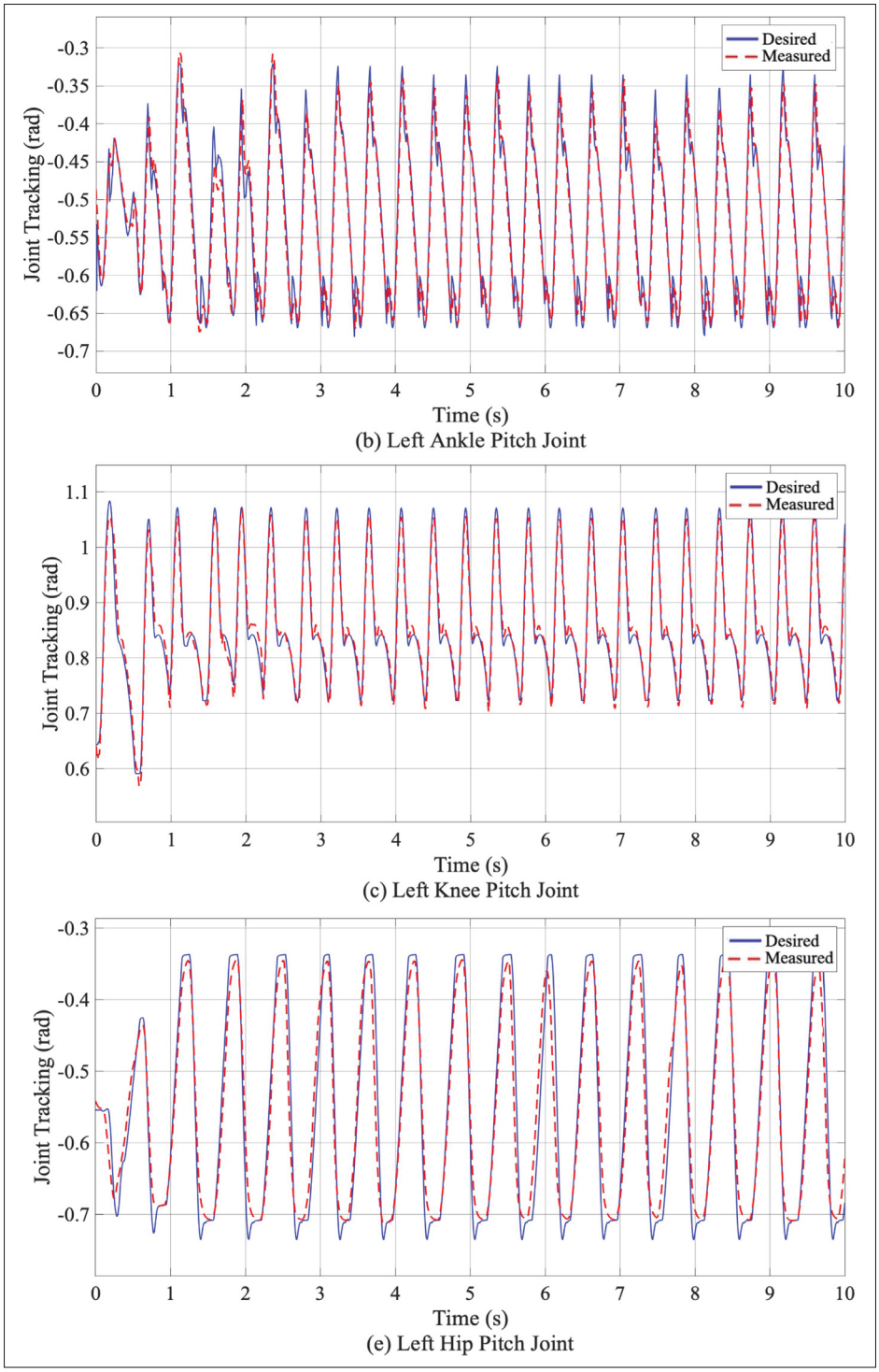

Figure 3.4 Left leg joint tracking during the 1^{st} scenario via the proposed controller

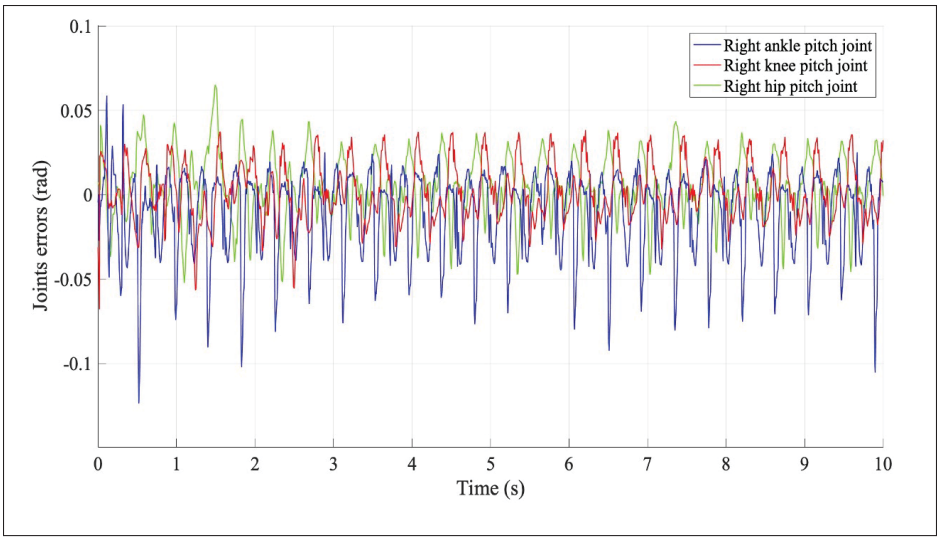

Figure 3.5 Right leg joint tracking error during the 1^{st} scenario via the proposed controller

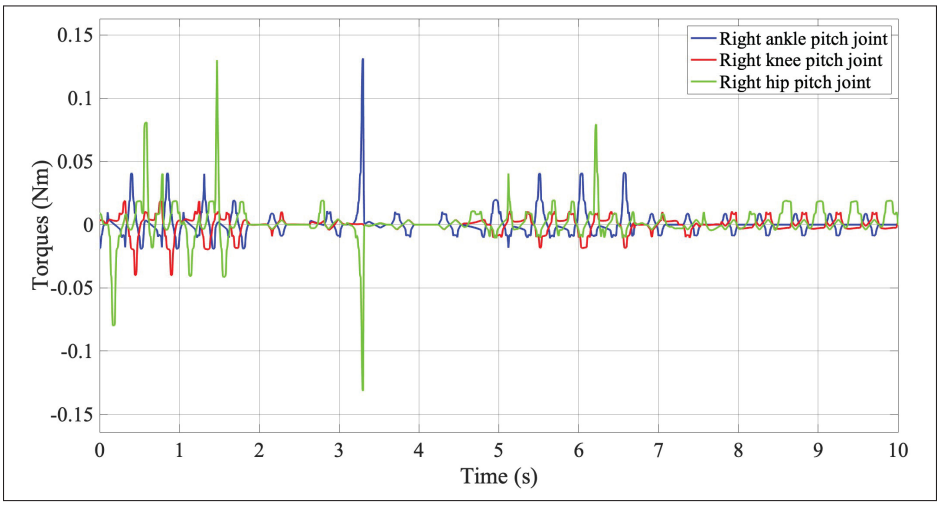

Figure 3.6 Right leg torque inputs during the 1^{st} scenario

sloping surfaces. Figure 3.10 presents the tracking errors of three joints of the right leg. This effective control mechanism mitigates leg slippage, even on a sloped surface inclined at an angle of 8.82°, as visualized in Figure 3.7.

In the third experiment, we compared with existing fixed-time control in (Qin et al., 2023b) with our proposed FTSM to validate its effectiveness. We selected the desired trajectory of the

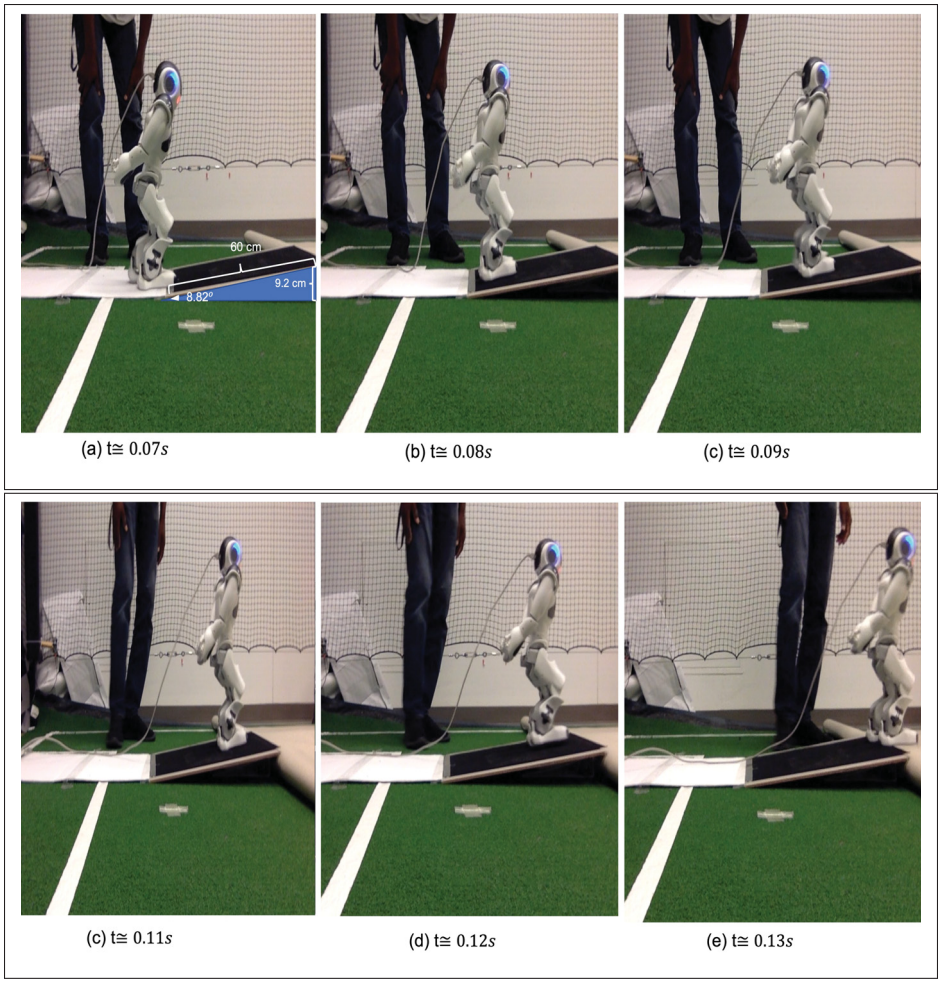

Figure 3.7 The NAO robot walks on an uphill sloped surface (second scenario)

right and left leg that includes ankle pitch, knee pitch, and hip pitch joints to show the tracking performance as shown in Figs. 3.12 and 3.13. The experimental results provide additional evidence that the proposed controller improves the tracking performance, as seen by rapid convergence and smaller tracking errors (in contrast to (Qin et al., 2023b) that are shown in Table 3.3.

In a comparable way, we evaluate the proposed FTSM control's higher efficiency in comparison to that of using integrated absolute error (IAE) and energy of control input (ECI) as specified by (Qin et al., 2023b) as shown in Eq. (3.32) and Eq. (3.33).

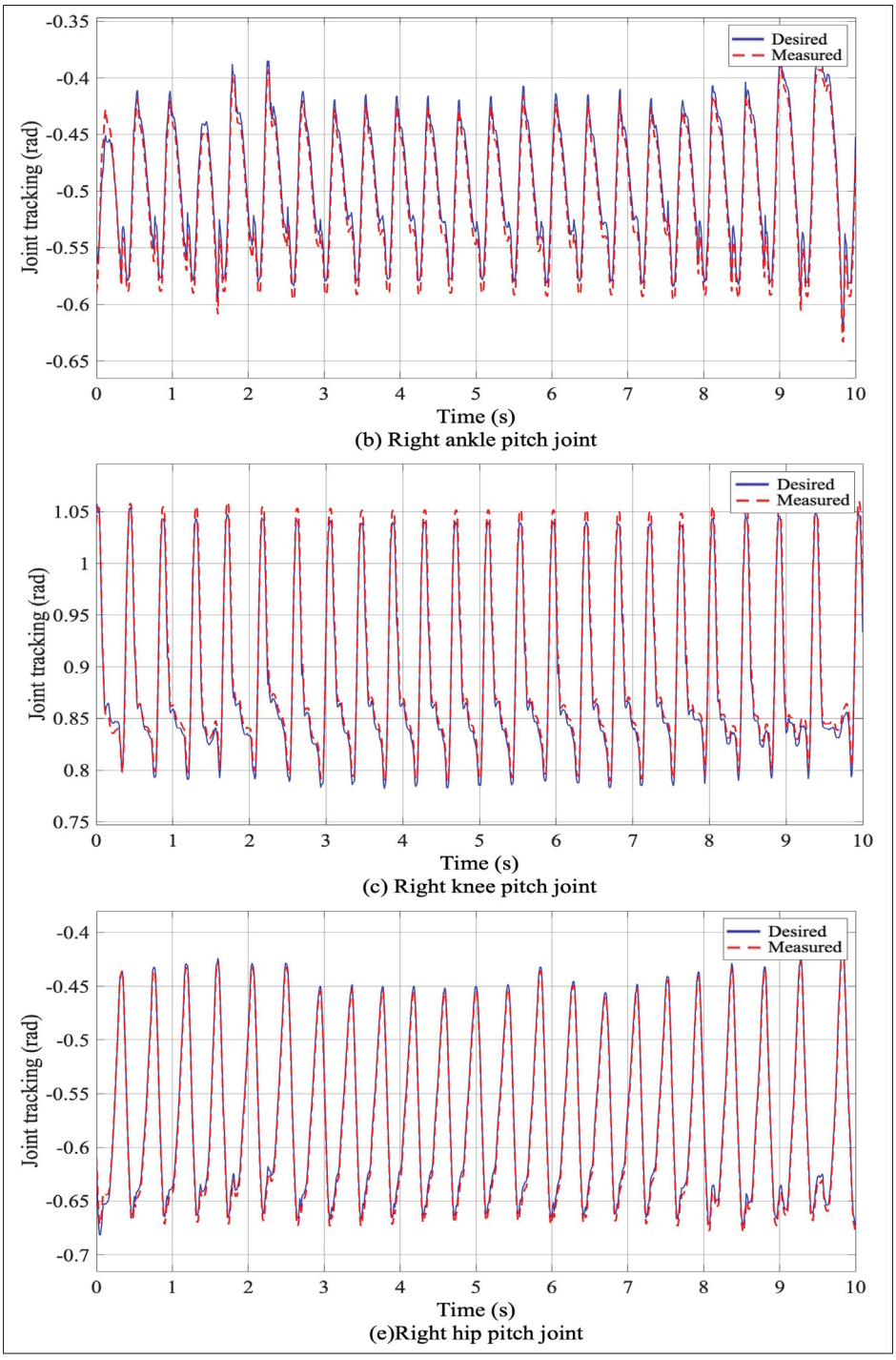

Figure 3.8 Right leg torque inputs during the 1st scenario via the proposed controller

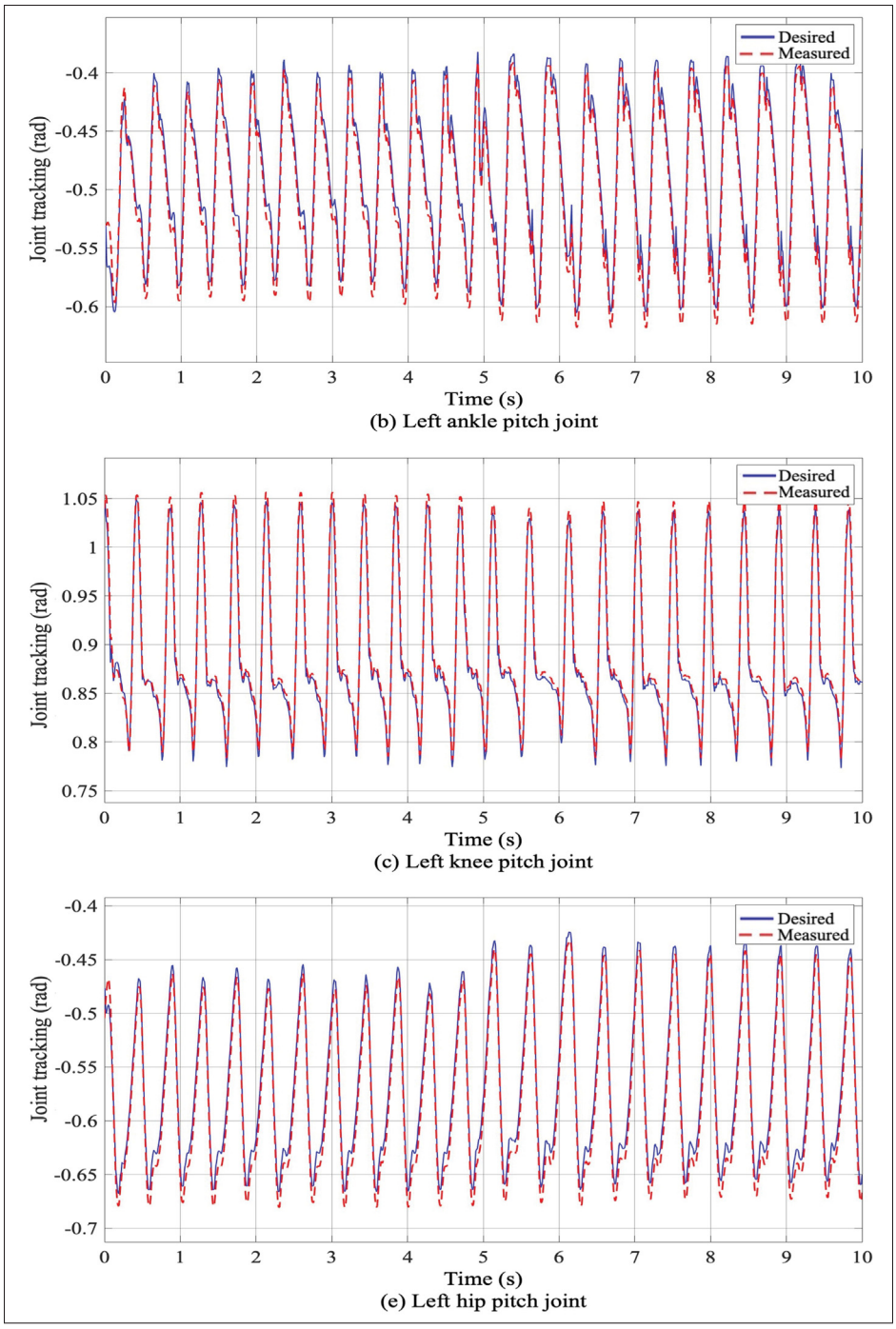

Figure 3.9 Right leg torque inputs during the 1^{st} scenario via the proposed controller

$$\|\boldsymbol{e}\|_{\mathrm{IAE}} = \sqrt{\frac{1}{N}\sum_{k=1}^{N}\|e(k)\|^2} \tag{3.32}$$

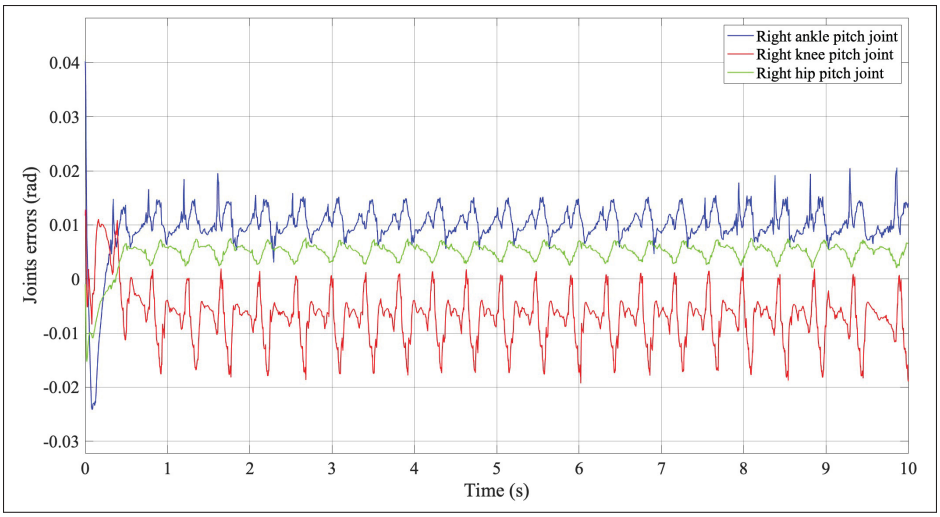

Figure 3.10 Right leg joint tracking error during the 2^{nd} scenario via the proposed controller

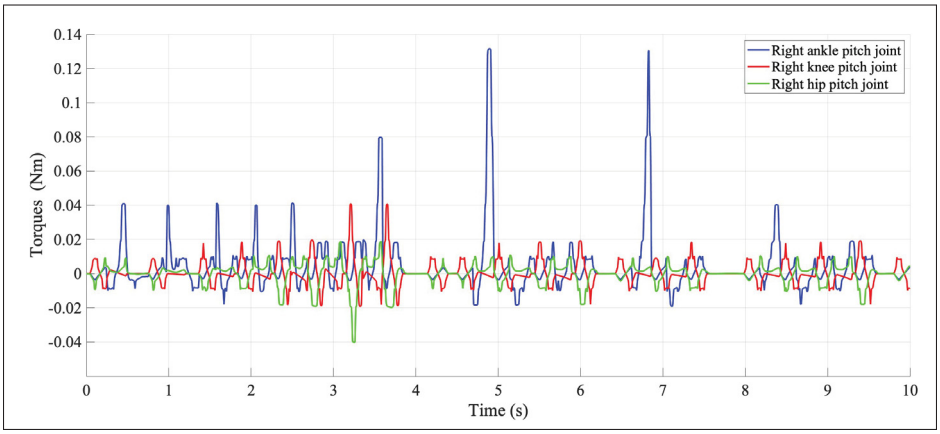

Figure 3.11 Right leg torque inputs during the 2^{nd} scenario via the proposed controller

$$\|\boldsymbol{\tau}\|_{\mathrm{ECI}} = \sqrt{\frac{1}{N}\sum_{k=1}^{N}\|\tau(k)\|^2} \tag{3.33}$$

where N represents the total number of samples. The position tracking error $e(k)$ and the control input of joint $\boldsymbol{\tau}(k)$ are values at samples (k). A summary of the comparisons of these two performance indices is shown in Table 3.3.

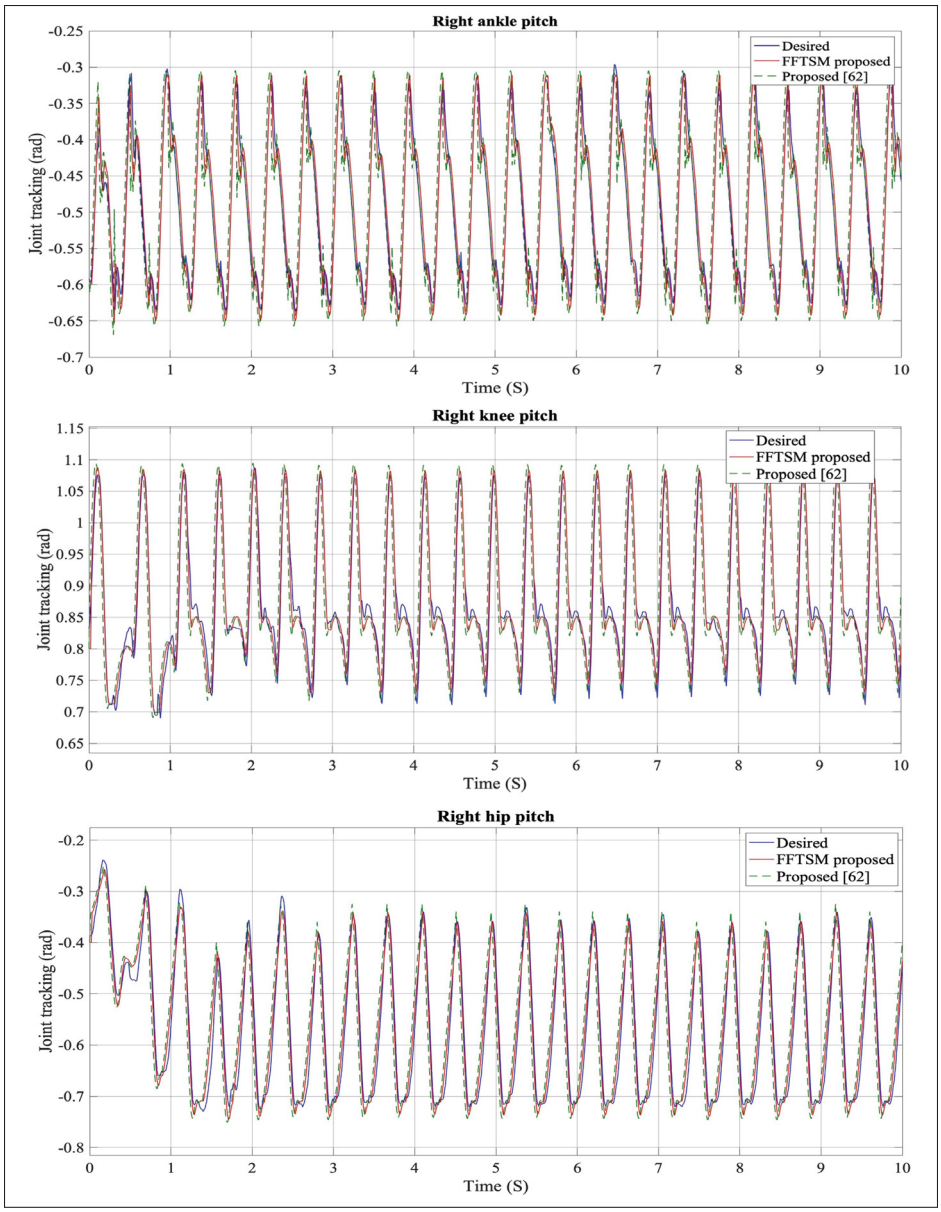

Figure 3.12 Comparative trajectory tracking experiment results of right leg

Figure 3.14 demonstrates uncertainties resulting from the inertia matrix, Coriolis, centrifugal matrix, gravitational forces, and external disturbances for both the left and right legs. These uncertainties were considered when designing the observer in Eq. (3.5). The experimental results revealed that the proposed FTSM control effectively works against system uncertainties and external disturbances.

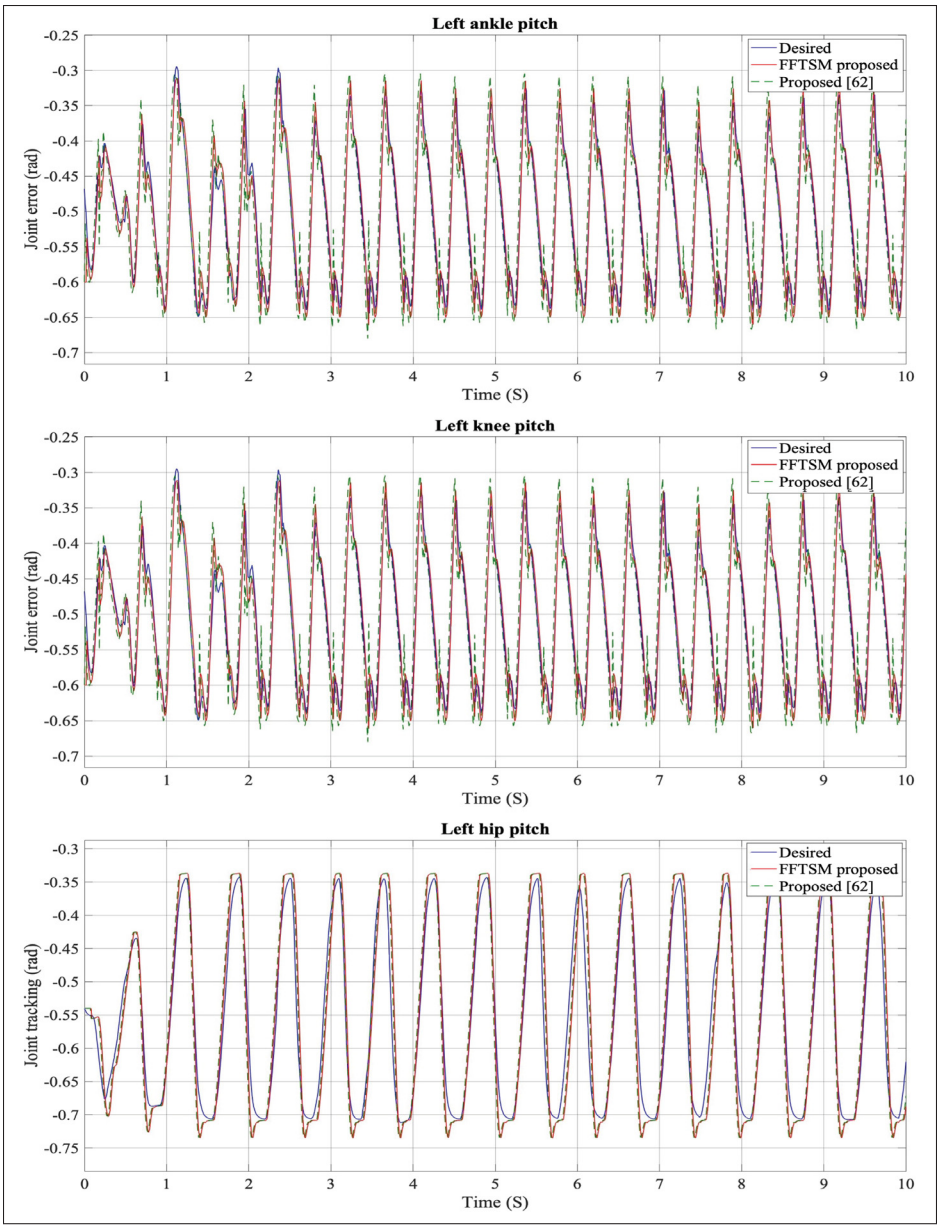

Figure 3.13 Comparative trajectory tracking experiment results of left leg

3.6 Conclusion

In this work, we derived a comprehensive model of the right and left legs for the NAO robot with 12 degrees of freedom. The proposed NDO-based FTSM of torque inputs was transformed into position commands for the NAO's servo-motors. On one hand, the designed FTSM surface

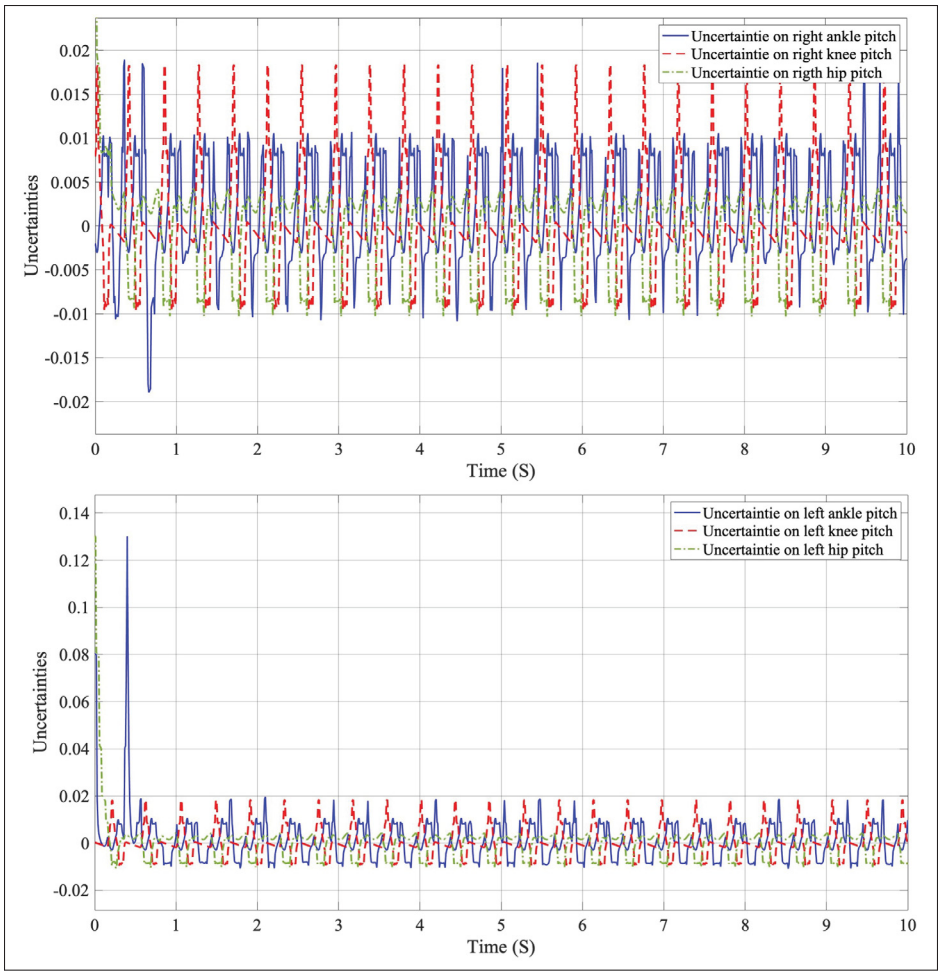

Figure 3.14 Uncertainties in experiment results of right and left legs

achieves fixed-time convergence of the tracking errors during the sliding phase. On the other hand, the chosen reaching law guarantees also the fixed-time convergence of the sliding surface to zero while exhibiting a robustness against the uncertainties. According to the experiments conducted on the NAO robot, it has been observed that using tuned control gains overcome the dynamic constraint, whereas the torque control approach coped with a variety of conditions to ensure the balance of the NAO robot's feet. The experimental results demonstrate the effectiveness of the suggested controller design. In future work, interesting ideas can be explored in order to enhance the performance of proposed method. The first idea consists of combining the used fixed-time controller with intelligent algorithms such as fuzzy logic or radial basis function

Table 3.3 Comparison of control performance

Controllers	**Right leg**		**Left leg**	
FTSM Proposed	$\|\boldsymbol{e}\|_{\text{IAE}}$	$\|\boldsymbol{\tau}\|_{ECI}$	$\|\boldsymbol{e}\|_{\text{IAE}}$	$\|\boldsymbol{\tau}\|_{ECI}$
Ankle pitch	0.0146	0.0113	0.0146	0.0064
Knee pitch	0.0143	0.0081	0.0160	0.0025
Hip pitch	0.0317	0.0051	0.0317	0.0083
Proposed (Qin et al., 2023b)	$\|\boldsymbol{e}\|_{\text{IAE}}$	$\|\boldsymbol{\tau}\|_{ECI}$	$\|\boldsymbol{e}\|_{\text{IAE}}$	$\|\boldsymbol{\tau}\|_{ECI}$
Ankle pitch	0.0343	0.0147	0.0343	0.0098
Knee pitch	0.473	0.0059	0.0492	0.0049
Hip pitch	0.0310	0.0059	0.0310	0.0041

neural network. Implementing and testing this integrated approach can overcome the challenges of dynamic environments. These intelligent techniques allow high accurate estimation of the uncertainties. This first idea will be applied to another robotic system since the NAO robot uses an on-board processor with very limited computational power. In case of unavailable system states for measurement, the same observer used in this paper can be adopted. The second idea consists of modifying the fixed-time convergent sliding surface by incorporating both prescribed desired transient and desired steady-state performances. This idea is interesting since it can be an effective method to satisfy the output and states constraints. Finally, further works will concentrate on the chattering reduction by proposing new reaching laws.

CHAPTER 4

NEW FIXED-TIME OBSERVER-BASED MODEL-FREE FIXED-TIME SLIDING MODE OF JOINT ANGLE COMMANDED NAO HUMANOID ROBOT

Mahmoud Farhat, Yassine Kali, *Member, IEEE,* Maarouf Saad, *Senior Member, IEEE,*
Mohammad H. Rahman, *Senior Member, IEEE,* and Roberto E. Lopez-Herrejon,

"IEEE Transactions on Control Systems Technology", 2024 Oct 4

4.1 Abstract

In this article, a new fixed-time observer with time delay estimation-based model-free fixed-time sliding mode for the problem of robust walking of the NAO robot. The proposed technique ensures convergence in fixed-time, regardless of initial conditions, thereby enhancing both convergence speed and robustness. This method allows for precise tracking of the joint angles' positions without depending on the robot's dynamic models while reducing the chattering via a modified exponential reaching law. To address the complexities of stabilizing the walking dynamics of the NAO robot, which include highly nonlinear dynamics and limited computational process, the proposed strategy utilizes the time delay estimation technique for system model estimation. To mitigate estimation errors, a novel observer with guaranteed fixed-time stability is proposed. This last helps to enhance the tracking performance. Using Lyapunov theory and experimental validation, within the proposed composite control method, the proposed non-singular terminal sliding surface's fixed-time stability along with the system state's stability is verified. Significantly improved stability and accuracy in the robot's joint movements are demonstrated through experimental results, validating the efficacy of the tracking trajectory for robotic systems such as the NAO humanoid robot.

keyword: humanoid robot, stable walking, fixed-time convergence, time delay estimation, uncertainties, NAO robot.

4.2 Introduction

A sliding humanoid robot, stable walking, fixed-time convergence, time delay estimation, uncertainties, NAO robot. (Slotine et al.; Wang et al.; Arteaga-Peréz et al.; Zhang et al., 1991b; 2019; 2020; 2020)) For instance, SMC has been used to control robot manipulators to improve trajectory tracking, accuracy, and stability (Rahmani et al., 2020). This technique is utilized in (Cherfouh et al., 2022) to tackle uncertain system models and external disturbances. Furthermore, simulations carried out on biped humanoid robot systems with uncertainties have demonstrated the robustness of the sliding mode approach (Rincon et al., 2019). In (Olvera-Pons et al., 2019), the results show that precise trajectory tracking can be accomplished by implementing the discrete-time sliding mode algorithm on the yaw and pitch joint angles using SMC.

In recent years, NAO robots have received significant attention as a platform for developing humanoid robots capable of performing various tasks such as walking, dancing, and playing soccer (Kulk et al., 2008). SMC has been explored in several research to control the joint angle of the walking NAO robot, with promising results. In (Ali et al., 2017), researchers propose using a sliding mode controller instead of a traditional PID controller to improve tracking performance for the ankle joint of the NAO robot. The introduction of SMC technique by (Chen et al., 2019) aimed to improve the stability and resilience of the NAO robot during walking by controlling joint angles. Nevertheless, conventional sliding mode control techniques suffer from the well-known chattering phenomenon, leading to high-frequency oscillations and undesired wear and tear of mechanical components in the system. Therefore, an improved SMC strategy is needed to overcome this limitation and to offer better performance for robotic systems.

Adaptive SMC has garnered considerable interest as a nonlinear control technique due to its efficacy in handling uncertain systems (Xiao et al.; Zhang and Xu, 2012; 2017). It is a modification of the sliding mode control approach incorporating adaptation laws to compensate for system uncertainties (Boukas et al.; Aydi et al., 2019; 2016). This method has been implemented in a range of domains, including cable-driven manipulators (Li and Xu, 2019) and

biped robots (Wang et al., 2019), to enhance their performance in uncertain conditions. In the context of NAO robots, adaptive sliding mode observers have been used for various applications, such as obstacle avoidance (Song et al., 2018) and force control (Li and Wang, 2018). While adaptive sliding mode observers have been developed to mitigate the chattering effect commonly associated with SMC, they still face challenges related to robustness and the speed at which they converge, which can affect the overall performance of these observers.

Fixed-time SMC has gained popularity due to its robustness and fast convergence properties, making it a promising approach to sliding mode control. Regardless of initial conditions and disturbances. By using this technique, the system's equilibrium point is ensured to be reached within a fixed-time (Zhang et al., 2019a). As a result, this approach has been implemented in various fields, including robotics, to improve control system performance. An example of its application is in promoting control performance against uncertain disturbances (Anjum et al., 2023). Additionally, the convergence of tracking error trajectories can be improved by controlling biped robots (Rincon et al., 2019). The encouraging outcomes observed with FTSMC underscore its significance in the realm of control theory. By ensuring fixed-time convergence, FTSMC can enhance the robustness and performance of robotic systems. However, the design and tuning of FSMC can be complex, owing to the numerous parameters involved. These complexities may not align well with the processing capabilities of the NAO robot to effectively implement this approach in real-time (Mattamala et al., 2018).

Time Delay Estimation (TDE) is acknowledged and extensively utilized for controlling multi-Degrees of Freedom (DoF) robot manipulators due to its capability in model estimation and handling nonlinearities (Setchi et al.; Wang et al., 2020; 2022). To effectively approximate system dynamics, the TDE approach uses previous system data, such as input and state values, to estimate current uncertain models and perturbations (Wang et al., 2017c). Although the TDE approach can reduce unknown dynamics, the resulting estimation errors could lead to stability issues. Therefore, a robust controller is crucial for stability maintenance (Lu et al., 2014). To address the instability issues in these controllers, TDE is integrated with different control laws, such as adaptive robust control (Lee et al.; Xia et al., 2017; 2010), Super-twisting algorithm

((Kali et al., 2018)), fuzzy control (Zhang et al., 2019c). However, theoretical analysis of the system often requires certain assumptions about system properties like boundedness, which may not always hold in practical scenarios.

This study presents a new fixed-time observer-based a model-free fixed-time nonsingular terminal SMC in order to overcome these limitations. The time delay method has been introduced to estimate the system's dynamics, facilitating adjustments of the robot's joint angles for improved movement accuracy. This technique, which is designed to provide stability to the closed-loop system, aims to ensure the convergence of joint angles to their target values within a fixed-time, regardless of beginning conditions and disturbances. The proposed strategy enables real-time estimation of the model dynamics, thereby enhancing the controller's robustness.

The main contributions of the proposed control strategy are outlined as follows:

1. Designing a new Fixed-Time Observer (FTO) to approximate the TDE error. The rationale behind employing TDE is to estimate the entire dynamics, allowing for the design of a model-free controller while minimizing computations, as since the on-board processor has limited computation power,
2. Designing a Fixed-time Nonsingular Terminal SMC (FNTSMC) to guarantee accurate tracking of joints movements of the NAO during walking, while ensuring robustness and achieving new fixed-time convergence,
3. Proposing a Modified Exponential Reaching Law (MERL) to further reduce the chattering phenomenon during the sliding phase.

This article delineates its contents starting with Section 4.3, which lays the groundwork by introducing essential preliminaries such as a the dynamics of the NAO's legs and an outline of the problem being addressed. Section 4.4 delves into the control strategy formulation, which includes an assessment of dynamics and disturbances estimation, the development of a Fixed-Time TDE Error Observer, and the implementing of a fixed-time controller. Section 4.5 showcases the control strategy's success through experimental findings. The article concluded in Section 4.6 with a summary of findings and potential directions for future research.

4.3 Preliminaries

4.3.1 Modeling the Lower Body of the NAO Robot

As illustrated in Figure 4.1, the lowest body of the NAO robot contains a maximum of 12 degrees of freedom (DoF), which are equally distributed over its legs, each of which has 6 DoF. Beginning from the lower part, the first two joints are tasked with controlling the movements for ankle flexion-extension and pronation-supination. In contrast, the third joint is dedicated to knee flexion extension. The activities of hip flexion-extension, external-internal rotation, along with abduction-adduction, are managed by the last three joints (Fierro et al.; Bayraktaroğlu et al.; Khajepour and Hashemi; Niku, 2017b; 2018; 2017; 2020). The movement principles of the robot are established on a revised version of the Denavit-Hartenberg standard, with its four essential parameters presented in Table 4.1.

Table 4.1 Modified DH Parameters
Taken from (Hashemi and Jadidi, 2012a)

	Left leg				Right leg			
link i	α_{i-1}	a_{i-1}	d_i	θ_i	α_{i-1}	a_{i-1}	d_i	θ_i
1	90^o	0	0	θ_{1l}	-90^o	0	d_7	θ_{1r}
2	90^o	0	0	θ_{2l}	90^o	0	0	θ_{2r}
3	0	l_3	0	θ_{3l}	0	l_2	0	θ_{3r}
4	0	l_4	0	θ_{4l}	0	l_1	0	θ_{4r}
5	-90^o	0	0	θ_{5l}	90^o	0	0	θ_{5r}
6	90^o	0	d_6	θ_{6l}	90^o	0	0	θ_{6r}

The NAO bipedal robot's left and right leg dynamic modeling shows an extensive amount of similarities. Therefore, the motions of these limbs can be explained based on the details provided in (Craig; Mokhtari et al.; González-Mejía et al., 2018b; 2021b; 2020b):

$$\begin{aligned} \ddot{\theta}_j(t) &= M(\theta_j(t))^{-1}\left[\Gamma_j(t) - F(\theta_j(t), \dot{\theta}_j(t)) - d(t)\right] \\ F(\theta_j(t), \dot{\theta}_j(t)) &= C(\theta_j(t), \dot{\theta}_j(t))\dot{\theta}_j(t) + G(\theta_j(t)) \end{aligned} \tag{4.1}$$

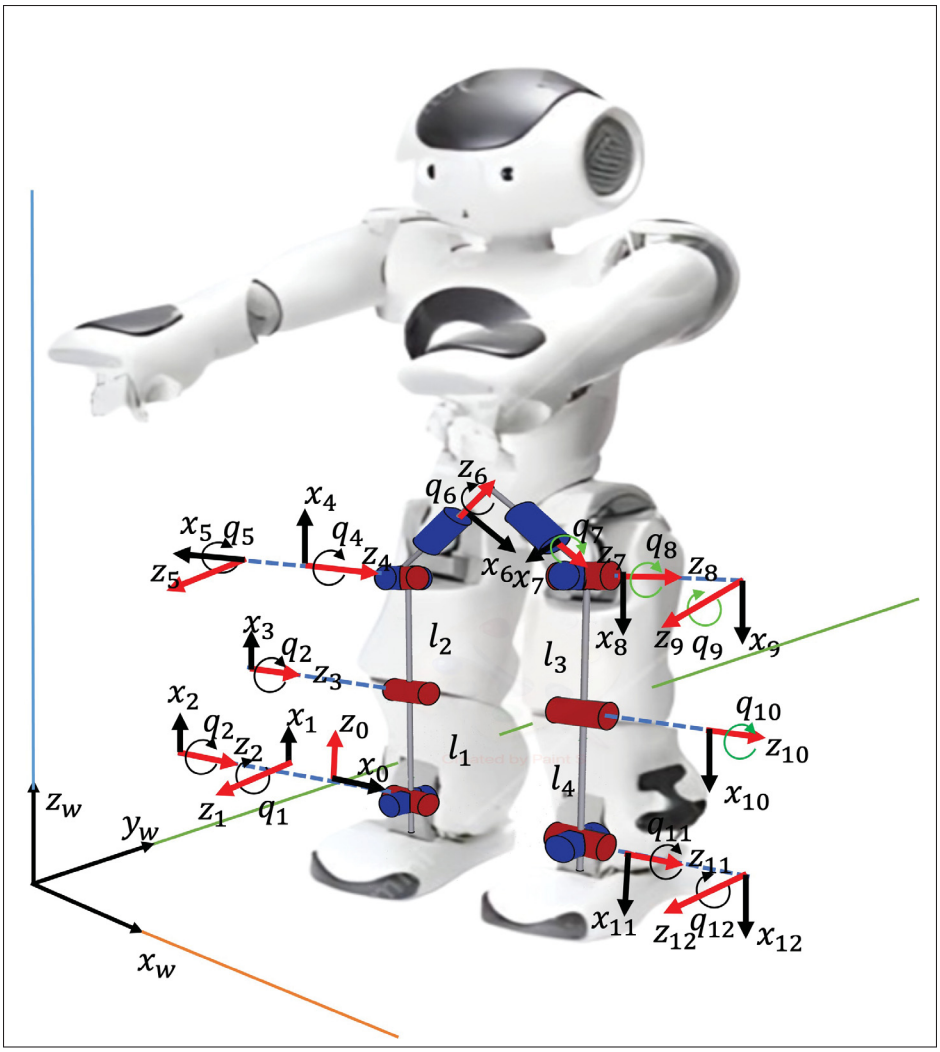

Figure 4.1 The coordinate frames and joints of the NAO humanoid robot kinematic model

For $j = \{r, l\}$, representing the right and left leg respectively, the dynamic model incorporates the rotation angle, velocity, and acceleration vectors $\theta_j(t), \dot{\theta}_j(t), \ddot{\theta}_j(t)$, each belonging to $\mathbb{R}^6$. The model also includes $M(\theta_j(t))$, the positive-definite inertia matrix within $\mathbb{R}^{6\times6}$. The Coriolis and centrifugal forces are represented by $C(\theta_j(t), \dot{\theta}_j(t))$ within $\mathbb{R}^{6\times6}$, whereas $G(\theta_j(t))$ in $\mathbb{R}^6$ symbolizes the gravitational force vectors. Additionally, $d(t)$ in $\mathbb{R}^6$ denotes the disturbance vector, originating from the foot's contact pressure, and $\Gamma_j(t)$ in $\mathbb{R}^6$ describes the control torque vector.

The Nao robot, a fully actuated humanoid, features joints powered by DC servo motors, with the dynamics for each leg described as follows:

$$\ddot{\theta}_m(t) = J_m^{-1}\left[\Gamma_m(t) - \Gamma_l(t) - B_m\dot{\theta}_m(t)\right] \tag{4.2}$$

The angular accelerations, velocities and positions of the motor shaft, denoted respectively $\ddot{\theta}_m(t)$, $\dot{\theta}_m(t)$, and $\theta_m(t) = R\theta_j(t)$, incorporate a relationship where $R = \text{diag}\left(\frac{1}{r_1}, \cdots, \frac{1}{r_6}\right)$. Here, r_i represents the gear reduction ratio, constrained by $0 < r_i < 1$, and is a fixed value. The matrices $J_m = \text{diag}(J_{m1}, \cdots, J_{m6})$ and $B_m = \text{diag}(B_{m1}, \cdots, B_{m6})$ respectively symbolize the moment of inertia and the viscous friction encountered by the motors. In addition, the motor torque vector is represented by $\Gamma_m(t) \in \mathbb{R}^6$, and the vector of the load torque experienced at the motor shaft is indicated by $\Gamma_l(t) = R\Gamma_j(t) \in \mathbb{R}^6$. Equations (4.1) and (4.2) combined result in:

$$\ddot{\theta}_j(t) = A^{-1}(\theta_j(t))R^{-1}\Gamma_m(t) - D(\theta_j(t), \dot{\theta_j}(t)) \tag{4.3}$$

where:

$$\begin{aligned} A^{-1}(\theta_j(t)) &= \left(M(\theta_j(t)) + J_m\right)^{-1} \\ D(\theta_j(t), \dot{\theta_j}(t)) &= A^{-1}((\theta_j(t))\left(F(\theta_j(t), \dot{\theta_j}(t)) + B_m\dot{\theta}_j(t) + d(t)\right) \end{aligned}$$

Subsequently, selecting a diagonal positive-definite matrix $\overline{A}$ ensures the fulfillment of the condition outlined in (Song et al., 2022b):

$$\|I - A^{-1}(\theta_j(t))\overline{A}\| < 1 \tag{4.4}$$

By reformulating the combined equation (4) to describe motor dynamics, as follows:

$$\ddot{\theta}_j(t) = \overline{A}^{-1}\left[R^{-1}\Gamma_m(t) - \overline{D}(t)\right] \tag{4.5}$$

where $\overline{D}(t) = \left[A(\theta_j(t)) - \overline{A}\right]\ddot{\theta}_j(t) + D(\theta_j(t), \dot{\theta}_j(t))$. Therefore, $\overline{D}(t)$ is disturbance compensation terms involving the joint positions $\theta_j(t)$, and velocities $\dot{\theta}_j(t)$.

4.3.2 Problem Formulation

Let define the vector of tracking error as $\tilde{\theta}_j(t) = \theta_j(t) - \theta_j^d(t) \in \mathbb{R}^6$, where $\theta_j^d(t) \in \mathbb{R}^6$ denotes the vector of desired joint angles. The aim is to use a nonlinear control strategy, specifically the proposed FTO-based model-free FNTSMC method, to address uncertainties and convert torque into a position command through a PD compensator integrated in the studied robot's framework. The approaching sections will elaborate on the control design and affirm fixed-time stability, premised on the subsequent assumption:

Assumption 5.1.: The derivative of the functions $\overline{D}_i(t)$ for $i = 1, \cdots, 6$ are bounded such as:

$$\left| \frac{d}{dt} \overline{D}_i(t) \right| \leq \delta_i$$

where $\delta_i > 0$ is a known positive constant.

4.4 Control Design

4.4.1 Dynamics and Disturbances Estimation

The proposed control technique is model-free since it uses the time delay estimation method to approximate the robot dynamics. This technique will avoid the burden of computations due to the complex mathematical model that is not supported by the processor on-board. Based on the **Assumption 5.1**, the approximation is obtained as:

$$\hat{\overline{D}}(t) \cong \overline{D}(t - T_s) = R^{-1}\Gamma_m(t - T_s) - \overline{A}\ddot{\theta}_j(t - T_s) \tag{4.6}$$

where $\Gamma_M(t - T_s)$ and $\ddot{\theta}_j(t - T_s)$ represent respectively the delayed value of $\Gamma_M(t)$ and $\ddot{\theta}_j(t)$ with T_s is the sampling time period and presents the TDE. Notice that the approximation is more accurate when the sampling period is small. However, often we only have access to position and velocity measurements. Then, the joint acceleration can be obtained using the following

approximation:

$$\ddot{\theta}_j(t) = \begin{cases} 0, & \text{if } t \leq T_s \\ \dfrac{1}{T_s^2}\left(\theta_j(t) - 2\theta_j(t-T_s) + \theta_j(t-2T_s)\right), & \text{if } t > T_s \end{cases} \tag{4.7}$$

With the previous approximation above, the integrated dynamics of the NAO robot and its motors, as outlined in (4.5), can be reformulated in the subsequent form:

$$\ddot{\theta}_j(t) = \overline{A}^{-1}\left[R^{-1}\Gamma_m(t) - \hat{\overline{D}}(t) - \varepsilon(t)\right] \tag{4.8}$$

where $\varepsilon(t) = \overline{D}(t) - \hat{\overline{D}}(t)$ denotes the bounded TDE error such as:

$$\begin{aligned} |\varepsilon_i(t)| \leq & \varepsilon_i^{max} \\ |\dot{\varepsilon}_i(t)| \leq & \delta\varepsilon_i^{max} \end{aligned} \tag{4.9}$$

where ε_i^{max} is a positive constant. The above equation is true if the matrix $\overline{A}$ is well selected according to the condition in (4.5) (Wang et al., 2022), (Boudjedir et al., 2023). Considering the TDE error as a disturbance in the model dynamics (4.8), a fixed-time observer will be designed to approximate it.

4.4.2 Fixed-Time TDE Error Observer

The idea here is to approximate the time delay estimation error to better compensate for the uncertainties. To that end, let us introduce the following auxiliary function:

$$\dot{x}(t) + \hat{\overline{D}}(t) + \hat{\varepsilon}(t) + \mu(t) = \Gamma_m(t) \tag{4.10}$$

where $x(t) \in \mathbb{R}^6$ represents the auxiliary state variable with $x(0) = [0,0,0,0,0,0]^T$, $\hat{\varepsilon}(t)$ is the estimate of the TDE error $\varepsilon(t)$ and $\mu(t)$ is selected as:

$$\mu(t) = \Lambda_1 s(t) + \Lambda_2 \text{sig}^{\alpha}(s(t)) + \Lambda_3 \text{sign}(s(t)) \tag{4.11}$$

where Λ_1, Λ_2 and Λ_3 are (6×6) diagonal positive-definite matrices, s is defined as:

$$s(t) = x(t) - \overline{A}\dot{\theta}_j(t) \tag{4.12}$$

and $\text{sig}^{\alpha}(s(t)) = \left[|s_1|^{\alpha_1}\text{sign}(s_1), \ldots, |s_6|^{\alpha_6}\text{sign}(s_6)\right]^T$ with:

$$\alpha_i = \begin{cases} 1 + \alpha_{0i}, & \text{if } |s_i(t)| > 1 \\ 1 - \alpha_{0i}, & \text{if } |s_i(t)| \leq 1 \end{cases} \quad 0 < \alpha_{0i} < 0.5 \tag{4.13}$$

and $\text{sign}(s(t)) = \left[\text{sign}(s_1), \ldots, \text{sign}(s_6)\right]^T$ with:

$$\text{sign}(s_i(t)) = \begin{cases} -1, & \text{if } \quad s_i(t) < 0 \\ 0, & \text{if } \quad s_i(t) = 0 \\ 1, & \text{if } \quad s_i(t) > 0 \end{cases} \tag{4.14}$$

It's important to note that the specified sliding mode variable $s(t)$ is designed to converge to zero in a fixed-time. To substantiate this, consider selecting the ensuing Lyapunov function and calculating its derivative

$$\begin{aligned} V_1 =& \frac{1}{2}s^T(t)s(t) \\ \dot{V}_1 =& s^T(t)\dot{s}(t) \end{aligned} \tag{4.15}$$

Utilizing the auxiliary function outlined in (4.10) alongside the NAO-motor dynamics specified in (4.8), the derivative of $s(t)$ is computed as follows:

$$\begin{aligned} \dot{s}(t) =& \dot{x}(t) - \overline{A}\ddot{\theta}_j(t) \\ =& \tilde{\varepsilon}(t) - \mu(t) \end{aligned} \tag{4.16}$$

where $\tilde{\varepsilon}(t) = \varepsilon(t) - \hat{\varepsilon}(t)$ is the approximation error. Substituting the above equation in $\dot{V}_1$ gives:

$$\begin{aligned}
\dot{V}_1 =& s^T(t)\left(\tilde{\varepsilon}(t) - \mu(t)\right) \\
=& s^T(t)\left(\tilde{\varepsilon}(t) - \Lambda_1 s(t) - \Lambda_2 \text{sig}^{\alpha}(s(t)) - \Lambda_3 \text{sign}(s(t))\right) \\
=& \sum_{i=1}^{6} s_i(t)\tilde{\varepsilon}_i(t) - \lambda_{1i} s_i^2(t) - \lambda_{2i}|s_i(t)|^{\alpha_i+1} - \lambda_{3i}|s_i(t)| \\
\leq& \sum_{i=1}^{6} -\lambda_{1i} s_i^2(t) - \lambda_{2i}|s_i(t)|^{\alpha_i+1} - (\lambda_{3i} - |\tilde{\varepsilon}_i(t)|)|s_i(t)|
\end{aligned} \tag{4.17}$$

It becomes evident that $\dot{V}1$ exhibits negative definiteness provided that $\lambda 3i > |\tilde{\varepsilon}_i(t)|$ for $i = 1, \ldots, 6$. Furthermore, upon satisfying this condition, the ensuing inequality is maintained:

$$\begin{aligned}
\dot{V}_1 \leq& \sum_{i=1}^{6} -\lambda_{1i} s_i^2(t) - \lambda_{2i}|s_i(t)|^{\alpha_i+1} \\
\leq& \sum_{i=1}^{6} -2\lambda_{1i} V_{1i} - \lambda_{2i}\left(2V_{1i}\right)^{0.5(\alpha_i+1)} < 0 \\
\dot{V}_{1i} \leq& \begin{cases} -2\lambda_{1i} V_{1i} - \lambda_{2i}\left(2V_{1i}\right)^{1+0.5\alpha_{0i}}, & \text{if } |s_i(t)| > 1 \\ -2\lambda_{1i} V_{1i} - \lambda_{2i}\left(2V_{1i}\right)^{1-0.5\alpha_{0i}}, & \text{if } |s_i(t)| \leq 1 \end{cases}
\end{aligned} \tag{4.18}$$

Otherwise, introducing a new variable z_i such as:

$$z_i = \begin{cases} 1 + \ln(2V_{1i}), & \text{if } (2V_{1i}) > 1 \\ (2V_{1i})^{0.5\alpha_{0i}}, & \text{if } (2V_{1i}) \leq 1 \end{cases} \tag{4.19}$$

and

$$\dot{z}_i \leq \begin{cases} -2\lambda_{1i} - 2\lambda_{2i}\text{exp}^{(z_i-1)0.5\alpha_{0i}}, & \text{if } z_i > 1 \\ -\alpha_{0i}\left(\lambda_{1i} z_i + \lambda_{2i}\right), & \text{if } 0 < z_i \leq 1 \end{cases} \tag{4.20}$$

Using the above information, the maximal convergence time has two components such as:

$$T_{0i}^{\max} \leq T_{01i} + T_{02i} \tag{4.21}$$

where T_{01i} and T_{02i} are obtained by solving the following integrals:

$$\begin{aligned} T_{01i} =& \int_0^1 \frac{1}{\alpha_{0i}\left(\lambda_{1i} z_i + \lambda_{2i}\right)} dz_i \\ =& \frac{1}{\alpha_{0i}\lambda_{1i}} \left[\ln\left(z_i + \frac{\lambda_{2i}}{\lambda_{1i}} \right) \right]_0^1 \\ =& \frac{1}{\alpha_{0i}\lambda_{1i}} \ln\left(1 + \frac{\lambda_{1i}}{\lambda_{2i}} \right) \end{aligned} \tag{4.22}$$

and

$$\begin{aligned} T_{02i} =& \int_1^\infty \frac{1}{2\lambda_{1i} + 2\lambda_{2i} \exp^{(z_i - 1)0.5\alpha_{0i}}} dz_i \\ =& \int_1^\infty \frac{1}{\lambda_{1i}\alpha_{0i}\kappa_i + \lambda_{2i}\alpha_{0i}\kappa_i^2} d\kappa_i \\ =& \frac{1}{\alpha_{0i}\lambda_{1i}} \int_1^\infty \left(\frac{\lambda_{2i}}{\lambda_{2i}\kappa_i + \lambda_{1i}} - \frac{1}{\kappa_i} \right) d\kappa_i \\ =& \frac{1}{\alpha_{0i}\lambda_{1i}} \left[\ln\left(\frac{\kappa_i}{\lambda_{2i}\kappa_i + \lambda_{1i}} \right) \right]_1^\infty \\ =& \frac{1}{\alpha_{0i}\lambda_{1i}} \ln\left(1 + \frac{\lambda_{1i}}{\lambda_{2i}} \right) \end{aligned} \tag{4.23}$$

where $\kappa_i = \exp^{(z_i - 1)0.5\alpha_{0i}}$. Then:

$$T_{0i}^{\max} = \frac{2}{\alpha_{0i}\lambda_{1i}} \ln\left(1 + \frac{\lambda_{1i}}{\lambda_{2i}} \right) \tag{4.24}$$

After establishing the convergence time of $s(t)$ to zero, the subsequent phase involves formulating the fixed-time TDE error observer as delineated below:

$$\hat{\varepsilon}(t) = \zeta(t) - L\overline{A}\dot{\theta}_j(t) \tag{4.25}$$

where $L \in \mathbb{R}^{6\times 6}$ is a diagonal positive-definite matrix and $\zeta(t) \in \mathbb{R}^6$ with $\zeta(0) = [0, 0, 0, 0, 0, 0]^T$ is another auxiliary state variable defined as:

$$\begin{aligned} \dot{\zeta}(t) =& L\left(\Gamma_m(t) - \hat{\overline{D}}(t) - \hat{\varepsilon}(t) \right) + K_1\mu(t) \\ &+ K_2 \mathrm{sig}^\alpha(\mu(t)) + K_3 \mathrm{sign}(\mu(t)) \end{aligned} \tag{4.26}$$

To prove that the TDE error converges to zero, let us choose the following Lyapunov function and compute its derivative:

$$\begin{aligned} V_2 =& \frac{1}{2}\tilde{\varepsilon}^T(t)\tilde{\varepsilon}(t) \\ \dot{V}_2 =& \tilde{\varepsilon}^T(t)\dot{\tilde{\varepsilon}}(t) = \tilde{\varepsilon}^T(t)\left(\dot{\varepsilon}(t) - \dot{\hat{\varepsilon}}(t)\right) \end{aligned} \tag{4.27}$$

using (4.25), (4.26) and (4.8) yields to:

$$\begin{aligned} \dot{V}_2 =& \tilde{\varepsilon}^T(t)\left(\dot{\varepsilon}(t) - \dot{\zeta}(t) + L\overline{A}\ddot{\theta}_j(t)\right) \\ =& \tilde{\varepsilon}^T(t)\dot{\varepsilon}(t) - \tilde{\varepsilon}^T(t)L\left(\Gamma_m(t) - \hat{\overline{D}}(t) - \hat{\varepsilon}(t) - \overline{A}\ddot{\theta}_j(t)\right) \\ & - \tilde{\varepsilon}^T(t)L\left(K_1\mu(t) + K_2\text{sig}^{\alpha}(\mu(t)) + K_3\text{sign}(\mu(t))\right) \\ =& \tilde{\varepsilon}^T(t)\dot{\varepsilon}(t) - \tilde{\varepsilon}^T(t)L\tilde{\varepsilon}(t) \\ & - \tilde{\varepsilon}^T(t)L\left(K_1\mu(t) + K_2\text{sig}^{\alpha}(\mu(t)) + K_3\text{sign}(\mu(t))\right) \end{aligned} \tag{4.28}$$

When a sliding mode occurs, we have:

$$\tilde{\varepsilon}(t) = \mu(t) \tag{4.29}$$

Hence:

$$\begin{aligned} \dot{V}_2 =& \tilde{\varepsilon}^T(t)\dot{\varepsilon}(t) - \tilde{\varepsilon}^T(t)\left(L + LK_1\right)\tilde{\varepsilon}(t) \\ & - \tilde{\varepsilon}^T(t)L\left(K_2\text{sig}^{\alpha}(\tilde{\varepsilon}(t)) + K_3\text{sign}(\tilde{\varepsilon}(t))\right) \end{aligned} \tag{4.30}$$

Notice that $\dot{V}_2$ is negative-definite if $k_{3i} > |\dot{\varepsilon}_i(t)|$ for $i = 1, \ldots, 6$. Then, the following inequality holds:

$$\begin{aligned} \dot{V}_2 \leq& -\tilde{\varepsilon}^T(t)\left(L + LK_1\right)\tilde{\varepsilon}(t) - \tilde{\varepsilon}^T(t)LK_2\text{sig}^{\alpha}(\tilde{\varepsilon}(t)) \\ \dot{V}_{2i} \leq& -(l_i + l_i k_{1i})\tilde{\varepsilon}_i^2(t) - (l_i k_{2i})|\tilde{\varepsilon}_i(t)|^{\alpha_i+1} \end{aligned} \tag{4.31}$$

The above inequality is similar to the one in (4.18). Then, based on the results obtained in (4.24), the maximal require time for $\tilde{\varepsilon}_i(t)$ to converge to zero is given by:

$$T_{1i}^{\max} = \frac{2}{\alpha_{0i} l_i (1 + k_{1i})}\ln\left(1 + \frac{1 + k_{1i}}{k_{2i}}\right) \tag{4.32}$$

where α_{0i} is defined in (4.13).

4.4.3 Fixed-time controller

To commence, the proposal for a fixed-time nonlinear sliding manifold is as follows:

$$\sigma(t) = \dot{\tilde{\theta}}_j(t) + C_1 \text{sig}^{\nu_1}(\tilde{\theta}_j(t)) + C_2 \text{sig}^{\nu_2}(\tilde{\theta}_j(t)) \tag{4.33}$$

where $\tilde{\theta}_j(t) = \theta_j(t) - \theta_j^d(t) \in \mathbb{R}^6$ denotes the joint angle tracking error vector such $\theta_j^d(t)$ is the desired joint angle vector, C_1 and $C_2 \in \mathbb{R}^{6\times 6}$ are diagonal positive-definite matrices, ν_{1i} and ν_{2i} are defined for $i = 1, \cdots, 6$ by:

$$\nu_{1i} = \begin{cases} \nu_{01i}, & \text{if } |\tilde{\theta}_{ji}| > 1 \\ 1, & \text{if } |\tilde{\theta}_{ji}| \leq 1 \end{cases} \tag{4.34}$$

$$\nu_{2i} = \begin{cases} 1, & \text{if } |\tilde{\theta}_{ji}| > 1 \\ \nu_{02i}, & \text{if } |\tilde{\theta}_{ji}| \leq 1 \end{cases} \tag{4.35}$$

such as $1 < \nu_{01i}$, $0.5 < \nu_{02i} < 1$. The proposed nonlinear surface (4.33) can be rewritten for $i = 1, \cdots, 6$ as:

$$\sigma_i(t) = \begin{cases} \dot{\tilde{\theta}}_{ji}(t) + c_{1i}|\tilde{\theta}_{ji}(t)|^{\nu_{01i}} \text{sign}(\tilde{\theta}_{ji}) + c_{2i}\tilde{\theta}_{ji}(t), & \text{if } |\tilde{\theta}_{ji}(t)| > 1 \\ \dot{\tilde{\theta}}_{ji}(t) + c_{2i}|\tilde{\theta}_{ji}(t)|^{\nu_{02i}} \text{sign}(\tilde{\theta}_{ji}) + c_{1i}\tilde{\theta}_{ji}(t), & \text{if } |\tilde{\theta}_{ji}(t)| \leq 1 \end{cases} \tag{4.36}$$

To avoid the singularity that might occur because of the time derivative of $|\tilde{\theta}_{ji}(t)|^{\nu_{02i}} \text{sign}(\tilde{\theta}_{ji})$, the above surface is modified as follows:

$$\sigma_i(t) = \begin{cases} \tilde{\theta}_{ji}(t) + \psi_{1i}|\dot{\tilde{\theta}}_{ji}(t)|^{\beta_{1i}} \text{sign}(\dot{\tilde{\theta}}_{ji}) + \psi_{2i}|\tilde{\theta}_{ji}(t)|^{\beta_{1i}} \text{sign}(\tilde{\theta}_{ji}), & \text{if } |\tilde{\theta}_{ji}(t)| > 1 \\ \tilde{\theta}_{ji}(t) + \psi_{3i}|\dot{\tilde{\theta}}_{ji}(t)|^{\beta_{2i}} \text{sign}(\dot{\tilde{\theta}}_{ji}) + \psi_{4i}|\tilde{\theta}_{ji}(t)|^{\beta_{2i}} \text{sign}(\tilde{\theta}_{ji}), & \text{if } |\tilde{\theta}_{ji}(t)| \leq 1 \end{cases} \tag{4.37}$$

where $\psi_{1i} = \frac{1}{c_{1i}}$, $\psi_{2i} = \frac{c_{2i}}{c_{1i}}$, $\psi_{3i} = \frac{1}{c_{2i}}$, $\psi_{4i} = \frac{c_{1i}}{c_{2i}}$, $\beta_{1i} = \frac{1}{\nu_{01i}}$ and $\beta_{2i} = \frac{1}{\nu_{02i}}$.

Theorem 5.1 *Taking into account the proposed sliding manifold in* (4.37)*, it is observed that each tracking error* $\tilde{\theta}_{ji}(t)$ *tends to zero within a maximal fixed-time given by:*

$$\begin{aligned} T_{2i}^{max} =& T_{3i}^{max} + \frac{1}{(1-\nu_{02i})c_{1i}} \ln\left(1+\frac{c_{1i}}{c_{2i}}\right) \\ &- \frac{1}{(1-\nu_{01i})c_{2i}} \ln\left(1+\frac{c_{2i}}{c_{1i}}\right) \end{aligned} \tag{4.38}$$

where T_{3i}^{max} *is the maximal time required for each robot's trajectory to reach the proposed sliding variable* $\sigma_i(t)$*.*

Proof. The derivative of the positive-definite Lyapunov function $V_3 = \frac{1}{2}\tilde{\theta}_j^T(t)\tilde{\theta}_j(t)$ may be calculated as follows:

$$\dot{V}_3 = \tilde{\theta}_j^T(t)\dot{\tilde{\theta}}_j(t) = \sum_{i=1}^{6} \tilde{\theta}_{ji}(t)\dot{\tilde{\theta}}_{ji}(t) \tag{4.39}$$

During the sliding phase ($\sigma(t) = 0$), we have:

$$\dot{\tilde{\theta}}_j(t) = \begin{cases} -c_{1i}|\tilde{\theta}_{ji}(t)|^{\nu_{01i}}\text{sign}(\tilde{\theta}_{ji}) - c_{2i}\tilde{\theta}_{ji}(t), & \text{if } |\tilde{\theta}_{ji}(t)| > 1 \\ -c_{2i}|\tilde{\theta}_{ji}(t)|^{\nu_{02i}}\text{sign}(\tilde{\theta}_{ji}) - c_{1i}\tilde{\theta}_{ji}(t), & \text{if } |\tilde{\theta}_{ji}(t)| \leq 1 \end{cases} \tag{4.40}$$

Substituting the above equation into (4.39) yields to:

$$\begin{aligned} \dot{V}_3 &= \sum_{i=1}^{6} \begin{cases} -c_{1i}|\tilde{\theta}_{ji}(t)|^{\nu_{01i}+1} - c_{2i}\tilde{\theta}_{ji}^2(t), & \text{if } |\tilde{\theta}_{ji}(t)| > 1 \\ -c_{2i}|\tilde{\theta}_{ji}(t)|^{\nu_{02i}+1} - c_{1i}\tilde{\theta}_{ji}^2(t), & \text{if } |\tilde{\theta}_{ji}(t)| \leq 1 \end{cases} \\ \dot{V}_{3i} &= \begin{cases} -c_{1i}(2V_{3i})^{0.5(\nu_{01i}+1)} - c_{2i}2V_{3i}, & \text{if } 2V_{3i} > 1 \\ -c_{2i}(2V_{3i})^{0.5(\nu_{02i}+1)} - c_{1i}2V_{3i}, & \text{if } 2V_{3i} \leq 1 \end{cases} \end{aligned} \tag{4.41}$$

Therefore, the origin is a globally stable equilibrium point since $\dot{V}_3 \leq 0$. Moreover, (4.40) can be rewritten as follows:

$$\dot{\eta}_i = \begin{cases} -2c_{1i}\exp^{0.5(\eta_i-1)(\nu_{01i}-1)} - 2c_{2i}, & \text{if } \eta_i > 1 \\ -0.5(1-\nu_{02i})\left(c_{1i}\eta_i + c_{2i}\right), & \text{if } 0 < \eta_i \leq 1 \end{cases} \tag{4.42}$$

where $\eta_i = 1 + \ln(2V_{3i})$ when $(2V_{3i}) > 1$ and $\eta_i = (2V_{3i})^{0.5(1-\nu_{02i})}$ when $(2V_{3i}) \leq 1$. Using the same methodology to compute $T_{0i}^{\max}$, the maximal sliding time for each DoF is obtained as:

$$\begin{aligned} T_{2i}^{\max} =& T_{3i}^{\max} + \int_0^1 \frac{1}{(1-\nu_{02i})\,(c_{1i}\eta_i + c_{2i})} d\eta_i + \int_1^{\infty} \frac{1}{2c_{1i}\exp^{0.5(\eta_i-1)(\nu_{01i}-1)} + 2c_{2i}} d\eta_i \\ =& T_{3i}^{\max} + \frac{1}{(1-\nu_{02i})c_{1i}} \ln\left(1 + \frac{c_{1i}}{c_{2i}}\right) - \frac{1}{(1-\nu_{01i})c_{2i}} \ln\left(1 + \frac{c_{2i}}{c_{1i}}\right) \end{aligned}$$

The proof is completed.

Now, to ensure the occurrence of the reaching phase within a fixed-time, The design of the proposed control law is as follows:

$$\begin{aligned} \Gamma_m(t) =& \Gamma_{m0}(t) + \Gamma_{m1}(t) + \Gamma_{m2}(t) \\ \Gamma_{m0}(t) =& \hat{\overline{D}}(t) + \hat{\varepsilon}(t) + \overline{A}\ddot{\theta}_j^d(t) - \overline{A}\,\overline{C}_1 \mathrm{sig}^{2-\beta^*}\left(\dot{\tilde{\theta}}_j(t)\right) \\ & - \overline{A}\,\overline{C}_2 \lfloor \tilde{\theta}_j(t) \rfloor^{\beta^*-1} \lfloor \dot{\tilde{\theta}}_j(t) \rfloor^{2-\beta^*} \mathrm{sign}\left(\dot{\tilde{\theta}}_j(t)\right) \\ \Gamma_{m1}(t) =& -\overline{A}\,\overline{C}_1 \lfloor \dot{\tilde{\theta}}_j(t) \rfloor^{1-\beta^*} \left(M_1\sigma(t) + M_2 \mathrm{sig}^{\rho_1}(\sigma(t))\right) \\ & - \overline{A}\,\overline{C}_1 \lfloor \dot{\tilde{\theta}}_j(t) \rfloor^{1-\beta^*} M_3 \mathrm{sig}^{\rho_2}(\sigma(t)) \\ \Gamma_{m2}(t) =& -E(\sigma)\mathrm{sign}(\sigma) \end{aligned} \tag{4.43}$$

where $\Gamma_{m0}(t)$ is the solution of $\dot{\sigma}(t) = 0$ using the non-singular surface (4.36) and:

- $\overline{C}_1 = \mathrm{diag}(\overline{c}_{11}, \cdots, \overline{c}_{16})$
  with:
  $\overline{c}_{1i} = \left(\frac{c_{1i}\nu_{01i} + c_{2i}\nu_{02i}}{2}\right) + \left(\frac{c_{1i}\nu_{01i} - c_{2i}\nu_{02i}}{2}\right) \mathrm{sign}(|\tilde{\theta}_{ji}(t)| - 1)$
- $\overline{C}_2 = \mathrm{diag}(\overline{c}_{21}, \cdots, \overline{c}_{26})$
  with:
  $$\overline{c}_{2i} = \left(\frac{c_{1i} + c_{2i}}{2}\right) + \left(\frac{c_{2i} - c_{1i}}{2}\right) \mathrm{sign}(|\tilde{\theta}_{ji}(t)| - 1)$$
- $\mathrm{sig}^{2-\beta^*}\left(\dot{\tilde{\theta}}_j(t)\right) = \left[|\dot{\tilde{\theta}}_{j1}(t)|^{2-\beta_1^*}\mathrm{sign}(\dot{\tilde{\theta}}_{j1}), \cdots, |\dot{\tilde{\theta}}_{j6}(t)|^{2-\beta_6^*}\mathrm{sign}(\dot{\tilde{\theta}}_{j6})\right]^T$ with:

$$\beta_i^* = \left(\frac{\beta_{1i} + \beta_{2i}}{2}\right) + \left(\frac{\beta_{1i} - \beta_{2i}}{2}\right) \mathrm{sign}(|\tilde{\theta}_{ji}(t)| - 1)$$

- $\lfloor\tilde{\theta}_j(t)\rfloor^{\beta^*-1} = \text{diag}\left(|\tilde{\theta}_{j1}(t)|^{\beta_1^*-1}, \cdots, |\tilde{\theta}_{j6}(t)|^{\beta_6^*-1}\right)$
- $\lfloor\dot{\tilde{\theta}}_j(t)\rfloor^{2-\beta^*} = \text{diag}\left(|\dot{\tilde{\theta}}_{j1}(t)|^{2-\beta_1^*}, \cdots, |\tilde{\theta}_{j6}(t)|^{2-\beta_6^*}\right)$
- $\text{sign}\left(\dot{\tilde{\theta}}_j(t)\right) = \left[\text{sign}\left(\dot{\tilde{\theta}}_{j1}(t)\right), \cdots, \text{sign}\left(\dot{\tilde{\theta}}_{j6}(t)\right)\right]^T$
- M_1, M_2 and $M_3 \in \mathbb{R}^{6\times 6}$ are diagonal positive-definite matrices
- ρ_{1i} and ρ_{2i} are defined for $i = 1, \cdots, 6$ by:

$$\rho_{1i} = \begin{cases} \rho_{01i}, & \text{if } |\sigma_i| > 1 \\ 1, & \text{if } |\sigma_i| \leq 1 \end{cases}$$

$$\rho_{2i} = \begin{cases} 1, & \text{if } |\sigma_i| > 1 \\ \rho_{02i}, & \text{if } |\sigma_i| \leq 1 \end{cases}$$

  such as $1 < \rho_{01i}$, $0.5 < \rho_{02i} < 1$
- $E(\sigma) = \text{diag}\left(\dfrac{E_i}{e_{0i} + (\varrho_i - e_{0i})\exp^{(p_i|\sigma_i|_i^q)}}\right)$ with $E_i > 0$, $0 < e_{0i} < 1$, $\varrho_i > 1$, $p_i < 0$ and $q_i > 0$.

Remark 5.1 *The adaptive gain matrix $E(\sigma)$ is a modified exponential reaching law (Fallaha et al., 2011). The only difference is the gain $\varrho_i > 1$ that will reduce the effect of the chattering caused by the gain E_i during the sliding phase such as $E_i(\sigma)$ converges to $(E_i/\varrho_i) < E_i$ when $\sigma_i(t) = 0$. Hence, the main action responsible of the chattering will have a small gain.*

Theorem 5.2 *Consider the NAO's leg model* (4.5) *and the designed controller* (4.43) *based on the fixed-time sliding variable* (4.36)*, when the following inequality holds for $i = 1, \cdots, 6$:*

$$E_i \geq |\tilde{\varepsilon}_i(t)|, \tag{4.44}$$

Then, each $\sigma_i(t)$ tends to zero in a maximal time that does not depend on any initial condition:

$$\begin{aligned} T_{3i}^{max} =& \frac{1}{(1-\rho_{02i})(m_{1i}+m_{2i})}\ln\left(\frac{m_{1i}+m_{2i}+m_{3i}}{m_{3i}}\right) \\ &- \frac{1}{(1-\rho_{01i})(m_{1i}+m_{3i})}\ln\left(\frac{m_{1i}+m_{2i}+m_{3i}}{m_{1i}+m_{3i}}\right) \end{aligned} \tag{4.45}$$

Proof. Consider the closed-loop error dynamics resulting from substitution of the designed controller (4.43) in the dynamics (4.5) and consider the 4$^{\text{th}}$ positive-definite Lyapunov function $V_4 = 0.5\,\sigma^T(t)\sigma(t)$ and its derivative:

$$\begin{aligned}
\dot{V}_4 =& \sigma^T(t)\dot{\sigma}(t) \\
=& \sigma^T(t)\chi\left(-\tilde{\varepsilon}(t) - E(\sigma)\text{sign}(\sigma)\right) \\
&+ \sigma^T(t)\left(-M_1\sigma(t) - M_2\text{sig}^{\rho_1}(\sigma(t)) - M_3\text{sig}^{\rho_2}(\sigma(t))\right) \\
=& \sum_{i=1}^{6} \frac{-\chi_i E_i|\sigma_i(t)|}{e_{0i} + (\varrho_i - e_{0i})\exp^{(p_i|\sigma_i|_i^q)}} - \sigma_i(t)\chi_i\tilde{\varepsilon}_i(t) \\
&+ \sum_{i=1}^{6} -m_{1i}\sigma_i^2(t) - m_{2i}|\sigma_i(t)|^{\rho_{1i}+1} - m_{3i}|\sigma_i(t)|^{\rho_{2i}+1} \\
\leq& \sum_{i=1}^{6} \chi_i|\sigma_i(t)|\left(|\tilde{\varepsilon}_i(t)| - E_i\right) \\
&+ \sum_{i=1}^{6} -m_{1i}\sigma_i^2(t) - m_{2i}|\sigma_i(t)|^{\rho_{1i}+1} - m_{3i}|\sigma_i(t)|^{\rho_{2i}+1}
\end{aligned} \tag{4.46}$$

where $\chi = \overline{C}_1^{-1}\lfloor\dot{\tilde{\theta}}_j(t)\rfloor^{\beta^*-1}\overline{A}^{-1}$ is a diagonal matrix where all the elements are positive-definite. The closed-loop stability is ensured if (4.44) is met (i.e., $\dot{V}_4$ is negative-definite). Then, one can establish:

$$\begin{aligned}
\dot{V}_4 \leq& \sum_{i=1}^{6} -m_{1i}\sigma_i^2(t) - m_{2i}|\sigma_i(t)|^{\rho_1+1} - m_{3i}|\sigma_i(t)|^{\rho_2+1} \\
\leq& \sum_{i=1}^{6} \begin{cases} -(m_{1i}+m_{3i})\sigma_i^2(t) - m_{2i}|\sigma_i(t)|^{\rho_{01i}+1}, & \text{if } |\sigma_i(t)| > 1 \\ -(m_{1i}+m_{2i})\sigma_i^2(t) - m_{3i}|\sigma_i(t)|^{\rho_{02i}+1}, & \text{if } |\sigma_i(t)| \leq 1 \end{cases} \\
\dot{V}_{4i} \leq& \sum_{i=1}^{6} \begin{cases} -(m_{1i}+m_{3i})2V_{4i} - m_{2i}(2V_{4i})^{0.5(\rho_{01i}+1)}, & \text{if } 2V_{4i} > 1 \\ -(m_{1i}+m_{2i})2V_{4i} - m_{3i}(2V_{4i})^{0.5(\rho_{02i}+1)}, & \text{if } 2V_{4i} \leq 1 \end{cases}
\end{aligned} \tag{4.47}$$

Taking after the same steps as within the demonstration for Theorem 1, the maximal reaching time in (4.45) is obtained. This completes the proof.

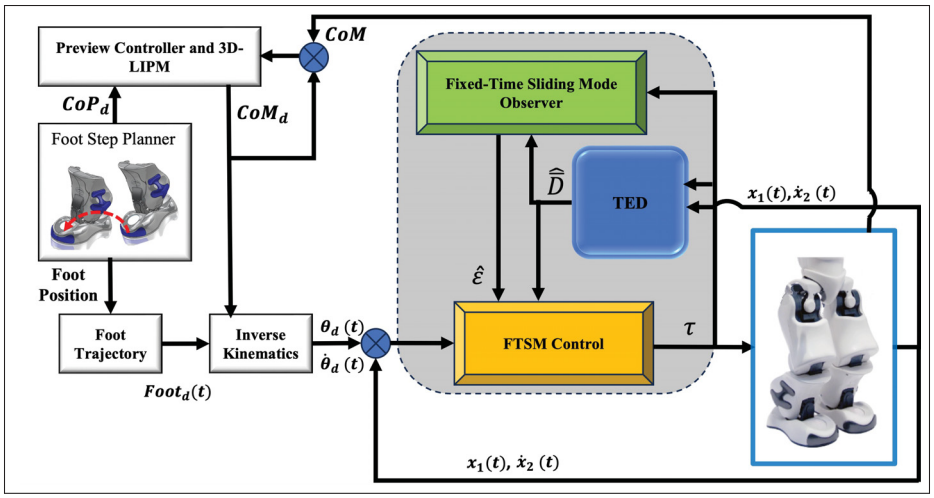

Figure 4.2 Control scheme diagram

Remark 5.2 *It is well known that the switching control action* $\Gamma_{m2}(t)$ *contributes to the reaching speed. Indeed, the higher the value of* $E_i(\sigma_i)$*, the faster the reaching is especially when the estimation error* $\tilde{\varepsilon}_i(t)$ *has a very small value. Hence, the upper-bound of the maximal reaching time* T_{3i}^{max} *in* (4.45) *might be conservative. However, the gains choice should respect the physical limits of the controlled system.* Now, the calculated torques (4.43) will be transformed into the following position command:

$$\theta_j^{cmd}(t) = \theta_j(t) + K_p^{-1}(K_d\dot{\theta}_j(t) - \Gamma_m(t)) \tag{4.48}$$

where K_p and K_d denote respectively the proportional and derivative gains of the on-board motor compensator.

4.5 Experimental results

This section focuses on validating the developed controller by employing all twelve joints of the NAO robot, whose dynamics are presented in Figure 4.1. The proposed approach is outlined in Figure 4.2, featuring a systematically organized design. The target joint angular trajectories are determined via the inverse kinematics that take as inputs the Center of Mass (CoM) direction movement and the zero-moment point as depicted in Figure 4.2. The positioning of the Center

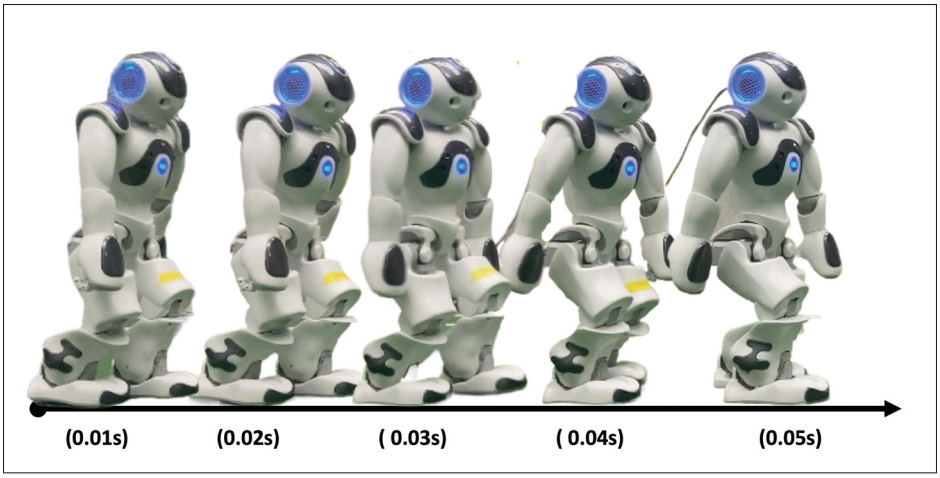

Figure 4.3 Experiment of walking using the developed controller

of Pressure (CoP) in relation to the foot support polygon correlates with the zero-moment point trajectory (Vukobratović and Borovac, 2004). The target trajectory derivation stems from a predefined zero-moment point trajectory, a critical factor for maintaining the robot's stability during movement. Hence, the formulation of the desired trajectory, which includes each joint angle, relies on a pre-established zero-moment point trajectory (Cao et al.; Wu et al.; Kashyap and Parhi, 2017; 2022b; 2023b). Real-time testing of the proposed controller was conducted on the NAO robot (V6.0) using Microsoft Visual C++ integrated with the NAOqi 2.5 - Linux of SoftBank Robotics, enabling real-time interaction with the robot.

The proposed controller's parameters are selected as in Table 4.2. Given that the controller gains are positive constants, the process of their adjustment and fine-tuning is straightforward. The selection of parameters was conducted manually, aiming to meet stability criteria and enhance the performance of the proposed control, utilizing a trial-and-error approach. Experimental tests for the proposed control were executed on both the right and left joints, specifically targeting the ankle pitch, knee pitch, and hip pitch. Figure 4.3 displays the experimental outcomes for the initial scenario in which the NAO is required to execute a straight walk in one step on a flat carpet, from 0.01s to 0.05s. Notably, the walking speed set for this experiment is [44.7 cm/s]. For those interested in visual evidence of the controller's efficacy, the experimental validation

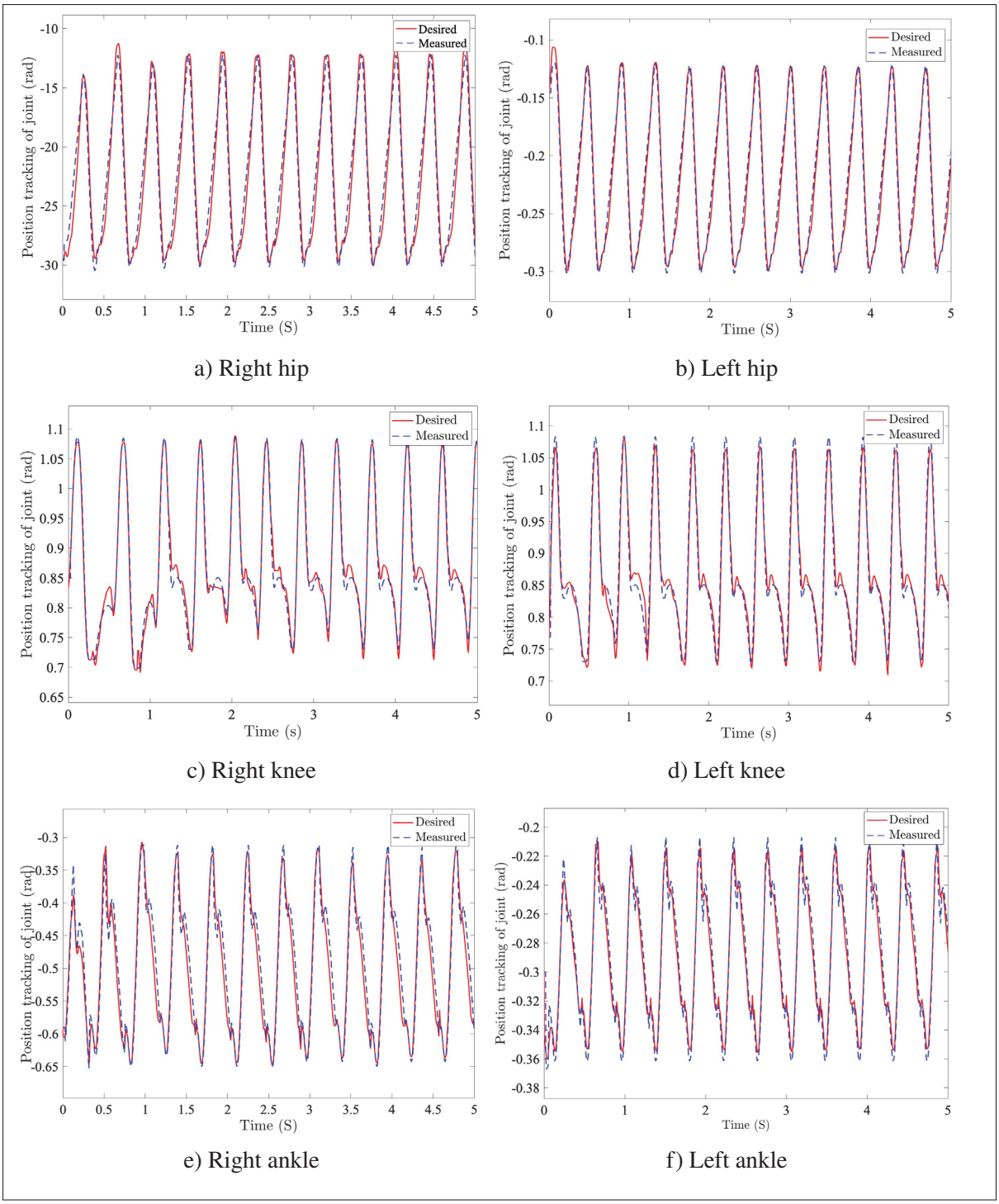

Figure 4.4 Experiment: trajectory tracking the performance of the proposed controller on right and left legs

Table 4.2 Parameters of the Proposed Controller

Parameter	Value	Parameter	Value
$\bar{C}_1$	$0.8I_{6\times6}$	M_2	$5.0I_{6\times6}$
$\bar{C}_2$	$3.0I_{6\times6}$	M_3	$5.0I_{6\times6}$
K_p	$0.5I_{6\times6}$	ρ_{01}	$3I_{6\times6}$
K_d	$0.3I_{6\times6}$	ρ_{02}	$0.25I_{6\times6}$
Λ_1	$10.0I_{6\times6}$	ψ_{1i}	$0.5I_{6\times6}$
Λ_2	0.5	ψ_{2i}	$0.3I_{6\times6}$
Λ_3	5.0	ψ_{3i}	$0.5I_{6\times6}$
M_1	$5.0I_{6\times6}$	ν_{01i}	$0.02I_{6\times6}$
		ν_{02i}	$0.05I_{6\times6}$

Table 4.3 Numerical comparison in terms of the IAE

Joint	Proposed	Reference (Farhat et al., 2024)
RHipPitch	0.0263	0.0317
RKneePitch	0.0137	0.0143
RAnklePitch	0.0127	0.0146
LHipPitch	0.0280	0.0317
LKneePitch	0.0149	0.0081
LAnklePitch	0.0135	0.0146

video is accessible at the following URL: [https://youtu.be/Cs5Jyubik9s]. The time responses, depicted in Figure 4.4, demonstrate the successful convergence of the measured joint position states to their desired trajectories. Furthermore, as demonstrated in Figure 4.5, the controller ensures that the tracking errors reach zero in a fixed time, indicating rapid convergence and consistently reduced error values.

The effectiveness of the proposed scheme, as described in Figure4.2, was verified through an experiment demonstrating the robustness of the control law even in the presence of uncertainties.

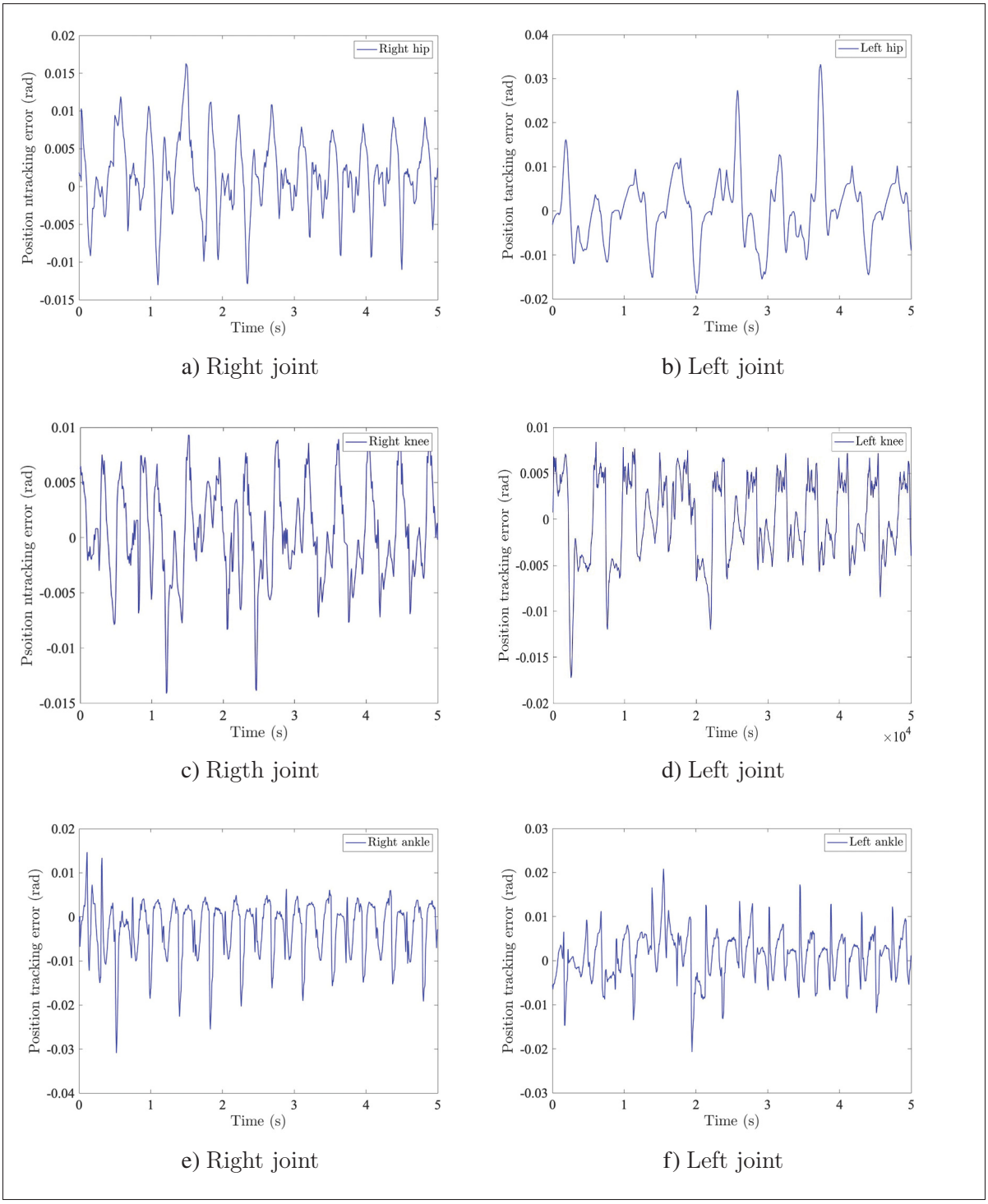

Figure 4.5 Experiment: trajectory tracking error signals using a proposed controller on right and left legs

Additionally, a conventional sliding mode control was implemented with the sliding mode consistent with (4.33).

The proposed method's effectiveness was verified through experiments demonstrating its robustness, even in the presence of uncertainties, and its ability to eliminate chattering in the time derivatives of control inputs for the 12 Degrees of Freedom (DoF) of the robot's legs. The torque profiles for the right ankle, knee, and hip pitch joints demonstrate smooth transitions, indicating an absence of chattering as shown in Figure 4.7. Such behavior suggests that the system operates with efficient control effort, potentially contributing to reduced energy consumption.

Figure 4.6 presents the experimental findings for the second scenario, showcasing the NAO robot's stability during locomotion. In this particular setup, the NAO robot accelerated to a high speed in a straight direction momentarily before performing a sit-down action twice, each lasting several seconds. The experimental demonstration, validating the efficacy of the proposed controller, is available for viewing at the following URL: [https://youtu.be/NWI_NSPuS3g]

In the third scenario, the effectiveness of the proposed control strategy is assessed against the Integrated Absolute Error (IAE) criterion $\|\boldsymbol{e}\|_{\text{IAE}}$ (Farhat et al., 2024). Additionally, the Energy of Control Input (ECI) criterion $\|\boldsymbol{\tau}\|_{\text{ECI}}$ (Farhat et al., 2024) serves as a basis for comparative analysis between the proposed approach, and the method detailed in (Farhat et al., 2024). Tables(4.3 and 4.4) provide a comparative overview between the proposed method, and the approach introduced in (Farhat et al., 2024).

Table 4.4 Numerical comparison in terms of the ECI

Joint	Proposed	Reference (Farhat et al., 2024)
RHipPitch	0.0036	0.0051
RKneePitch	0.0078	0.0081
RAnklePitch	0.0114	0.0113
LHipPitch	0.0077	0.0083
LKneePitch	0.0023	0.0025
LAnklePitch	0.0068	0.0064

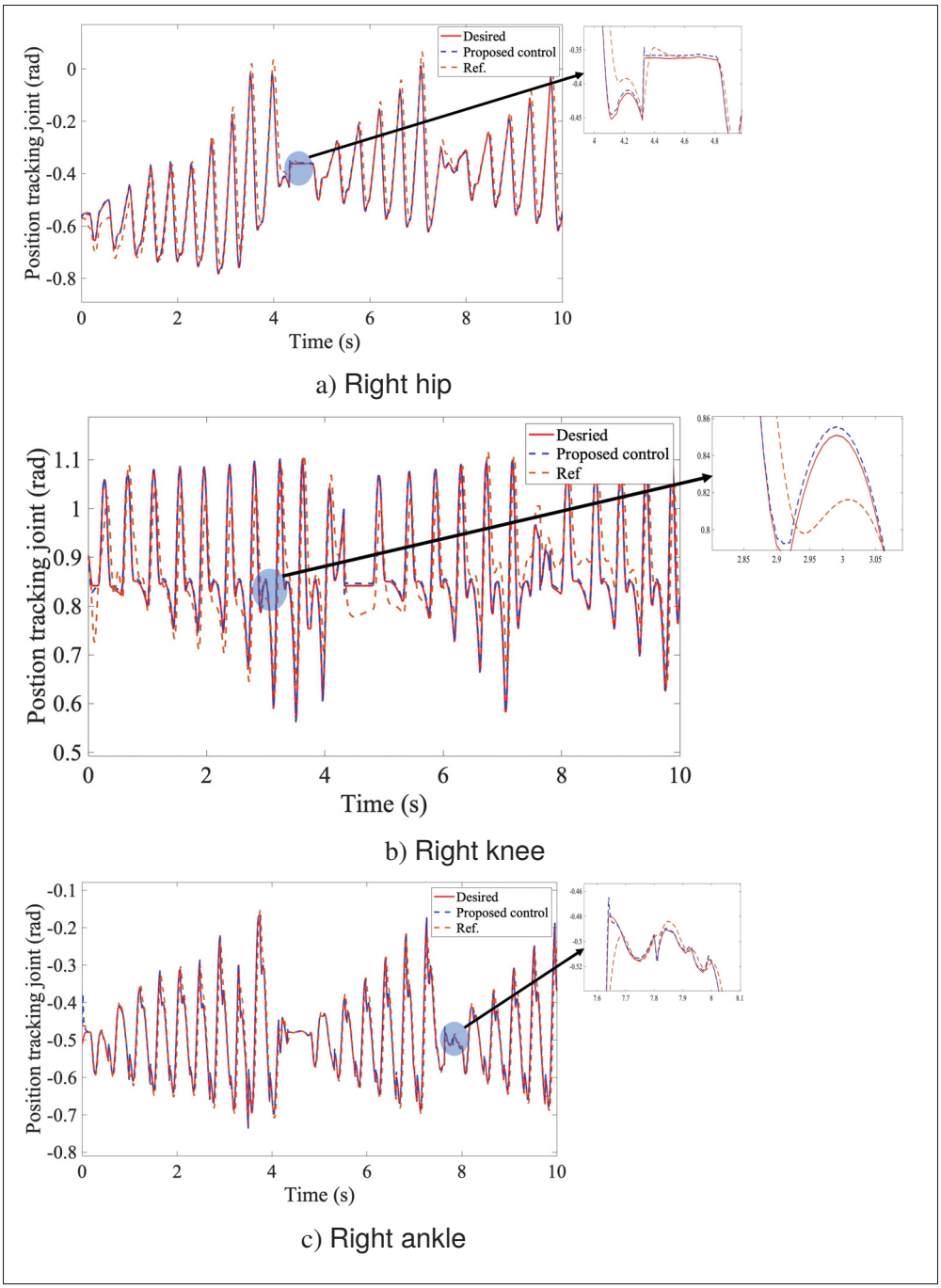

Figure 4.6 Experiment: Comparison of the tracking performance of joints under the proposed control and the reference
Taken from (Farhat et al., 2024)

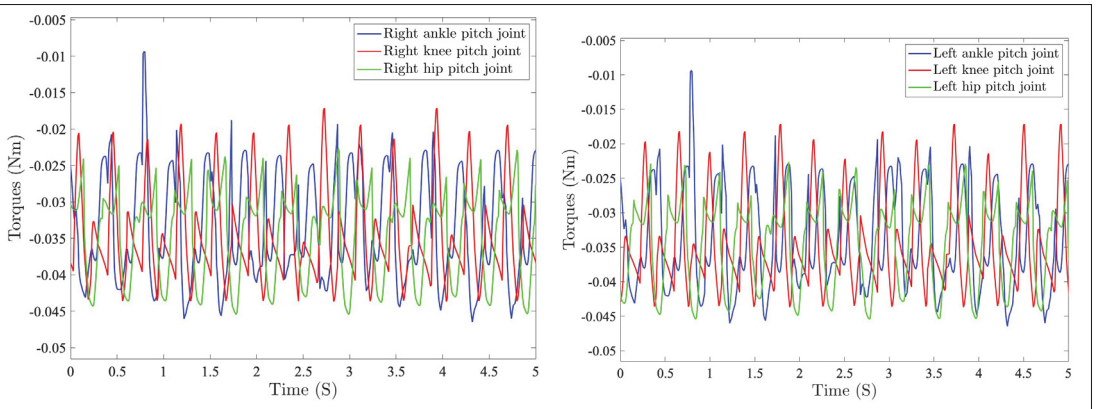

a) Right joint b) Left joint

Figure 4.7 Experiment: right and left legs torque inputs via the proposed controller

4.6 Conclusion

This research introduces a new FTO combined with fixed-time non-singular terminal sliding mode control, that aims to improve the NAO robot's walking stability amidst disturbances and uncertainties. The FTO is deployed to estimate the error induced by TDE, facilitating the development of a fixed-time non-singular terminal sliding mode surface and its corresponding controller. Transforming the calculated torques from the controller into position commands plays a crucial role in the adept management of the NAO robot. Such a conversion guarantees that the controller's outputs harmonize with the robot's actuation potential, thereby enabling accurate and stable regulation of its motions, particularly when confronting uncertainties. By employing this approach, the chattering in control inputs for the robot's legs with 12 DoF is successfully eliminated. Compared to the existing controller, the proposed control exhibits superior performance, highlighted by smaller tracking errors and quick convergence in a variety of scenarios. Experiments demonstrate that the proposed composite control method works effectively in terms of robustness, high control accuracy, and rapid finite time convergence. Future endeavors will explore the application of this control strategy across various robotic platforms, aiming to further validate its versatility and effectiveness in diverse operational scenarios.

CONCLUSION AND RECOMMENDATIONS

This thesis represents a significant advancement in the field of humanoid robotics, specifically in enhancing the walking system of the NAO humanoid robot. Through the integration of novel control strategies and sophisticated methodologies, we have effectively addressed several critical issues that previously hindered the robot's performance. These issues included limited flexibility, stability, and adaptability in NAO's walking mechanism. Our innovations have led to marked enhancements, enabling more stable, dynamic, and efficient locomotion across diverse environments. All strategies of controllers were implemented on the NAO robot in the GREPCI robotics laboratory at ÉTS Montreal: École de technologie supérieure - Montréal. The results of the work are summarized as follows:

Chapter 2 introduces a significant advancement in control strategies for the NAO robot by employing the Modified Function Approximation Technique (MFAT) combined with sliding mode control. The key innovation of MFAT lies in its ability to approximate the unknown dynamic model of the robot without relying on predefined basis functions, which are commonly used in traditional function approximation techniques. This approach significantly reduces the complexity and computational overhead, making the control system more efficient and adaptable to real-time changes in the robot's dynamics. The Lyapunov stability analysis presented confirms that all system errors remain bounded, ensuring reliable operation under various conditions. Simulations and comparative studies highlight MFAT's effectiveness in enhancing the NAO's locomotion, showcasing improved trajectory tracking and stability compared to conventional model-based controllers.

A significant advancement in adaptive control strategies for humanoid robotics has been achieved through the development of the Modified Function Approximation Technique (MFAT) integrated with sliding mode control for the NAO robot. This innovative approach overcomes the limitations of traditional Function Approximation Techniques (FAT) by eliminating the need for predefined

base functions in the dynamic model estimation law. This simplification not only reduces the computational load but also enhances the flexibility and responsiveness of the control system.

The MFAT, in combination with adaptive sliding mode control, has been meticulously designed to finely tune the dynamics of the NAO robot, facilitating precise motor control and trajectory tracking. The effectiveness of this approach has been rigorously validated through a series of simulations using ROS and MATLAB, demonstrating its superior performance in accurately guiding the robot's movements according to the desired trajectories. This has shown to be particularly effective in handling the inherent uncertainties and nonlinearities in the robot's dynamics, which are typical challenges in humanoid robotics.

Moreover, the comparative analysis between the traditional model-based controllers and the proposed sliding mode-based adaptive MFAT controller has highlighted the distinct advantages and potential limitations of each approach. This comparison not only provides a clear indication of the progress made but also outlines the areas for potential improvement and further research. The findings from this study underscore the importance of continued innovation in control strategies to enhance the functionality and adaptability of humanoid robots in various applications.

This work lays a robust foundation for future work in the field, suggesting avenues for further enhancing the MFAT approach, such as integrating machine learning techniques to enable real-time learning and adaptation. Additionally, exploring the applicability of this control strategy in different robotic platforms could extend its benefits beyond humanoid robots, potentially transforming a broader range of robotic systems with enhanced control capabilities.

Chapter 3 has successfully developed a new control system for the NAO humanoid robot, making its movement more stable through advanced control techniques. We created a detailed model of the robot's legs, which have 12 degrees of freedom, forming the basis for our control strategies. The Nonlinear Disturbance Observer-based Fixed-Time Terminal Sliding Mode

(NDO-FTSM) approach was used to manage the robot's torque inputs effectively, translating these into precise commands for the robot's motors. This method not only quickly corrected errors during movement but also remained reliable under various uncertain conditions.

Our experiments showed that the adjustments we made to the control settings helped the robot maintain its balance under different situations. These results confirm that the NDO-FTSM approach significantly improves the robot's ability to walk stably.

Future directions, looking forward, there are several promising paths to further improve the control system introduced in this thesis. Integrating the fixed-time controller with intelligent algorithms like fuzzy logic or radial basis function neural networks could make the control system more adaptive and capable of handling unpredictable changes more accurately. Combines different control strategies to exploit the advantages of each. For example, a hybrid system might use PID control for basic task execution while integrating adaptive control for handling dynamic environmental changes. These approaches could be particularly beneficial in environments that are dynamic and challenging.

Another potential improvement is to adjust the control method to better manage both quick changes and stable conditions. This could make the robot's movements even smoother and more controlled. Additionally, future work could focus on minimizing the abruptness in the robot's movements, known as chattering, by developing new control techniques that ensure smoother operation.

These future research directions aim to expand upon the achievements of this thesis, exploring ways to apply these advanced control systems to different types of robots, potentially transforming how humanoid robots operate.

Chapter 4 introduces an innovative control strategy combining Fixed-Time Observer (FTO) with fixed-time non-singular terminal sliding mode control, aimed at improving the walking stability

of the NAO robot amidst various disturbances and uncertainties. The FTO plays a pivotal role in estimating errors caused by Time Delay Estimation (TDE), which is crucial for developing an effective fixed-time non-singular terminal sliding mode surface and its corresponding controller. This approach ensures that the torques calculated by the controller are accurately converted into position commands, which is essential for the precise and efficient operation of the NAO robot. This conversion ensures that the outputs from the controller are well-aligned with the robot's capabilities, thereby allowing for precise and stable movement control, especially in the face of uncertainties.

The implementation of this new control strategy significantly reduces the chattering in the control inputs of the robot's legs, which have 12 degrees of freedom. When compared to existing controllers, this proposed system shows superior performance, characterized by reduced tracking errors and faster response times across various scenarios. The effectiveness of this composite control method is further demonstrated through rigorous experiments, which confirm its robustness, high accuracy, and quick convergence.

Looking forward, this thesis lays the groundwork for future studies to explore the application of this advanced control strategy across different robotic platforms. Such research will help to further establish the adaptability and effectiveness of this method in various operational environments, potentially leading to broader applications in the field of robotics. This conclusion not only highlights the successes of the current research but also opens avenues for further exploration and development in robotic control systems.

Recommendations

- **Advanced Energy Management:** Future research should focus on optimizing the energy consumption of control systems to enhance operational efficiency and extend the robot's active time. Reducing energy usage also decreases the likelihood of overheating and mechanical wear, which can lead to falls or system failures.

- **Cross-Platform Implementation:** The methodologies and strategies developed in this thesis should be tested and adapted for use with other humanoid robots. This could facilitate broader applications in robotics, including industrial automation, personal assistance, and educational purposes.
- **Innovative Control Techniques:** There is significant potential for breakthroughs in control technology by exploring machine learning algorithms and real-time adaptive control systems. These advancements could push the boundaries of what humanoid robots can achieve, enabling more complex and naturalistic movements.
- **User-Centric Design:** It is crucial to consider the end-users in the design and functionality of humanoid robots. Future projects should aim to tailor robot interactions for specific applications such as assistance for the elderly, therapeutic uses in mental health, and educational tools for children. Understanding and integrating user feedback into design iterations will be key to creating robots that are both functional and user-friendly.
- **Safety and Ethics:** As humanoid robotics continue to evolve, it is imperative to continuously evaluate and update safety protocols and ethical guidelines to ensure the well-being of humans interacting with robots. This includes regular safety audits, risk assessments, and the development of failsafe mechanisms to prevent accidents.

These recommendations are designed to guide future developments in humanoid robotics, aiming to enhance their practicality, reliability, and acceptance in various societal sectors. Implementing these suggestions will require a meticulous approach to research and development, focusing on innovation, user safety, and ethical considerations.

Published Work

Ultimately, this thesis has resulted in three journal papers already published. These publications are detailed below:

1. Farhat M, Brahmi B, Saad M, Rahman MH. Novel adaptive balanced control of humanoid robot type NAO robot. International Journal of Modelling, Identification and Control. 2021;39(3):211-20.
2. Farhat M, Kali Y, Saad M, Rahman MH, Lopez-Herrejon RE. Walking position commanded NAO robot using nonlinear disturbance observer-based fixed-time terminal sliding mode. ISA transactions. 2023 Dec 23.
3. Farhat M, Kali Y, Saad M, Rahman MH, Lopez-Herrejon RE. New Fixed-Time Observer-Based Model-Free Fixed-Time Sliding Mode of Joint Angle Commanded NAO Humanoid Robot. IEEE Transactions on Control Systems Technology. 2024 Oct 4.

BIBLIOGRAPHY

Added, E., Gritli, H., and Belghith, S. (2021). Additional complex behaviors, bifurcations and chaos, in the passive walk of the compass-type bipedal robot. *IFAC-PapersOnLine*, 54(17):111–116. 6th IFAC Conference on Analysis and Control of Chaotic Systems CHAOS 2021.

Ai, Y. and Wang, H. (2023). Fixed-time integral fast nonsingular terminal sliding mode control and its application to chaos suppression in gyros system. *International Journal of Control*, 0(0):1–8.

Al-Shuka, H. F., Corves, B. J., and Zhu, W.-H. (2014). Dynamic modeling of biped robot using lagrangian and recursive newton-euler formulations. *International Journal of Computer Applications*, 101(3).

Al-Shuka, H. F. and Song, R. (2018). Hybrid regressor and approximation-based adaptive control of robotic manipulators with contact-free motion. In *2018 2nd IEEE Advanced Information Management, Communicates, Electronic and Automation Control Conference (IMCEC)*, pages 325–329. IEEE.

Al-Shuka, H. F. N., Corves, B., and Zhu, W.-H. (2019). Dynamics of biped robots during a complete gait cycle: Euler-Lagrange vs. Newton-Euler formulations.

Aldebaran Robotics (2022). Joint position sensors.

Aldebaran Robotics (2024). NAO. Retrieved January 21, 2024.

Ali, M., Hoque, M. A., and Saha, S. (2017). Ankle joint control of nao robot using sliding mode control. In *2017 IEEE International Conference on Robotics and Biomimetics (ROBIO)*, pages 117–122. IEEE.

Amirkhani, S., Mobayen, S., Iliaee, N., Boubaker, O., and Hosseinnia, S. H. (2019). Fast terminal sliding mode tracking control of nonlinear uncertain mass–spring system with experimental verifications. *International Journal of Advanced Robotic Systems*, 16(1):1729881419828176.

Anjum, Z., Zhou, H., Ahmed, S., and Guo, Y. (2023). Fixed time sliding mode control for disturbed robotic manipulator. *Journal of Vibration and Control*, page 10775463231165094.

Araujo, H., Mousavi, M. R., and Varshosaz, M. (2023). Testing, validation, and verification of robotic and autonomous systems: a systematic review. *ACM Transactions on Software Engineering and Methodology*, 32(2):1–61.

Arteaga-Peréz, M. A., Pliego-Jiménez, J., and Romero, J. G. (2020). Experimental results on the robust and adaptive control of robot manipulators without velocity measurements. *IEEE Transactions on Control Systems Technology*, 28(6):2770–2773.

Aydi, A., Djemel, M., and Chtourou, M. (2016). Robust sliding mode control for nonlinear uncertain discrete-time systems. In *2016 17th International Conference on Sciences and Techniques of Automatic Control and Computer Engineering (STA)*, pages 657–662.

Bayraktaroğlu, Z. Y., Acar, M., Gerçek, A., and Tan, N. M. (2018). Design and development of the i.t.u. biped robot. *Gazi University Journal of Science*, 31(1):251 – 271.

Boudjedir, C. E., Bouri, M., and Boukhetala, D. (2023). An enhanced adaptive time delay control-based integral sliding mode for trajectory tracking of robot manipulators. *IEEE Transactions on Control Systems Technology*, 31(3):1042–1050.

Boukas, E., Kaczorek, T., and Zhang, H. (2019). Adaptive sliding mode observer design for a class of uncertain systems. *Applied Mathematics and Computation*, 347:25–35.

Bououden, S. and Abdessemed, F. (2011). 0-flat canonical form control scheme for rabbit's dynamic walking control. In *2011 15th International Conference on Advanced Robotics (ICAR)*, pages 645–652. IEEE.

Bououden, S., Abdessemed, F., and Abderraouf, B. (2009). Control of a bipedal walking robot using a fuzzy precompensator. In *KES International Symposium on Agent and Multi-Agent Systems: Technologies and Applications*, pages 853–862. Springer.

Bouzaouache, H. and Braiek, N. B. (2008). On the stability analysis of nonlinear systems using polynomial lyapunov functions. *Mathematics and Computers in Simulation*, 76(5-6):316–329.

Brahmi, B., Laraki, M. H., Rahman, M. H., Rasedul, I. M., and Uz-Zaman, M. A. (2019a). Combined model predictive controller technique for enhancing nao gait stabilization. *International Journal of Electrical and Computer Engineering*, 13(8):577–584.

Brahmi, B., Laraki, M. H., Rahman, M. H., Rasedul, I. M., and Uz-Zaman, M. A. (2019b). Combined model predictive controller technique for enhancing nao gait stabilization. *International Journal of Electrical and Computer Engineering*, 13(8):577–584.

Bu, X.-W., Wu, X.-Y., Chen, Y.-X., and Bai, R.-Y. (2015). Design of a class of new nonlinear disturbance observers based on tracking differentiators for uncertain dynamic systems. *International Journal of Control, Automation and Systems*, 13(3):595–602.

Buschmann, T., Lohmeier, S., and Ulbrich, H. (2009). Humanoid robot lola: Design and walking control. *Journal of Physiology-Paris*, 103(3):141–148. Neurorobotics.

Cao, X., Gu, L., Qiu, H., Lai, C., and Qin, Y. (2017). Continuous nonsingular terminal sliding mode contouring control of manipulator based on time delay estimation. *Proceedings of the Institution of Mechanical Engineers, Part I: Journal of Systems and Control Engineering*, 231(10):836–848.

Castano, J. A., Li, Z., Zhou, C., Tsagarakis, N., and Caldwell, D. (2016a). Dynamic and reactive walking for humanoid robots based on foot placement control. *International Journal of Humanoid Robotics*, 13(02):1550041.

Castano, J. A., Li, Z., Zhou, C., Tsagarakis, N., and Caldwell, D. (2016b). Dynamic and reactive walking for humanoid robots based on foot placement control. *International Journal of Humanoid Robotics*, 13(02):1550041.

Castillo, G. A., Weng, B., Stewart, T. C., Zhang, W., and Hereid, A. (2020). Velocity regulation of 3d bipedal walking robots with uncertain dynamics through adaptive neural network controller. In *2020 IEEE/RSJ International Conference on Intelligent Robots and Systems (IROS)*, pages 7703–7709. IEEE.

Cerón, J. C., Sunny, M. S. H., Brahmi, B., Mendez, L. M., Fareh, R., Ahmed, H. U., and Rahman, M. H. (2023). A novel multi-modal teleoperation of a humanoid assistive robot with real-time motion mimic. *Micromachines*, 14(2):461.

Chang, I., Baca, J., Moreno, H. A., Carrera, I. G., and Cardona, M. N. (2017). *Advances in Automation and Robotics Research in Latin America: Proceedings of the 1st Latin American Congress on Automation and Robotics, Panama City, Panama 2017*, volume 13. Springer.

Chen, H., Li, J., Li, W., and Wang, J. (2019). Sliding mode control for joint angle control of humanoid robot. In *2019 3rd IEEE International Conference on Robotics and Automation Engineering (ICRAE)*, pages 458–463. IEEE.

Chen, H.-Y., Dong, X.-C., Yang, Y., and Liu, J.-T. (2021). Fixed-time tracking control for flexible joint manipulator with prescribed performance constraint. *IEEE Access*, 9:99388–99397.

Chen, J., Wang, G., Hu, X., and Shen, J. (2018). Lower-body control of humanoid robot nao via kinect. *Multimedia Tools and Applications*, 77:10883–10898.

Chen, W.-H., Yang, J., and Zhao, Z. (2016). Robust control of uncertain nonlinear systems: a nonlinear dobc approach. *Journal of Dynamic Systems, Measurement, and Control*, 138(7):071002.

Chen, Y., Li, F., and Zhang, L. (2024). Fixed-time nonsingular terminal sliding mode control for trajectory tracking of uncertain robot manipulators. *Transactions of the Institute of Measurement and Control*, page 01423312241230032.

Cherfouh, K., Gu, J., Farooq, U., Asad, M. U., Dey, R., Adhikary, N., and Chang, C. (2022). Performance comparison between higher-order sliding mode and fixed boundary layer sliding mode controller for a 10-dof bipedal robot. *Communication and Control for Robotic Systems*, pages 45–62.

Chien, M.-C. and Huang, A.-C. (2004). Adaptive impedance control of robot manipulators based on function approximation technique. *Robotica*, 22(4):395–403.

Chien, S.-Y., Lin, Y.-L., and Chang, B.-F. (2024). The effects of intimacy and proactivity on trust in human-humanoid robot interaction. *Information Systems Frontiers*, 26(1):75–90.

Coron, J.-M., Praly, L., and Teel, A. (1995). Feedback stabilization of nonlinear systems: Sufficient conditions and lyapunov and input-output techniques. *Trends in Control: A European Perspective*, pages 293–348.

Craig, J. J. (2005). *Introduction to robotics: mechanics and control*, volume 3. Pearson/Prentice Hall Upper Saddle River, NJ, USA:, 3 edition.

Craig, J. J. (2018a). *Introduction to Robotics: Mechanics and Control. 4th*. Upper Saddle River, New Jersey: Pearson Education, Inc.

Craig, J. J. (2018b). Introduction to robotics: Mechanics and control. 4th.

Dalibard, S., El Khoury, A., Lamiraux, F., Nakhaei, A., Taïx, M., and Laumond, J.-P. (2013). Dynamic walking and whole-body motion planning for humanoid robots: an integrated approach. *The International Journal of Robotics Research*, 32(9-10):1089–1103.

Ding, B., Plummer, A., and Iravani, P. (2016). Investigating balancing control of a standing bipedal robot with point foot contact. *IFAC-PapersOnLine*, 49(21):403–408.

Donca, O. A., Beokhaimook, C., and Hereid, A. (2022). Real-time navigation for bipedal robots in dynamic environments. *arXiv preprint arXiv:2210.03280*.

Dong, E. Z., Wang, D. D., Tong, J. G., Chen, C., and Wang, Z. H. (2018). A stable gait planning method of biped robot based on ankle motion smooth fitting. *International Journal of Control, Automation and Systems*, 16(1):284–294.

ExtremeTech (2013). Meet darpa's real-world terminator, atlas, https://www.extremetech.com/defense/161193-meet-darpas-real-world-terminator-atlas.

Fallaha, C. J., Saad, M., Kanaan, H. Y., and Al-Haddad, K. (2011). Sliding-mode robot control with exponential reaching law. *IEEE Transactions on Industrial Electronics*, 58(2):600–610.

Faraji, S., Razavi, H., and Ijspeert, A. J. (2019). Bipedal walking and push recovery with a stepping strategy based on time-projection control. *The International Journal of Robotics Research*, 38(5):587–611.

Farhat, M., Brahmi, B., Saad, M., and Rahman, M. H. (2021a). Novel adaptive balanced control of humanoid robot type nao robot. *International Journal of Modelling, Identification and Control*, 39(3):211–220.

Farhat, M., Brahmi, B., Saad, M., and Rahman, M. H. (2021b). Novel adaptive balanced control of humanoid robot type nao robot. *International Journal of Modelling, Identification and Control*, 39(3):211–220.

Farhat, M., Kali, Y., Saad, M., Rahman, M. H., and Lopez-Herrejon, R. E. (2024). Walking position commanded nao robot using nonlinear disturbance observer-based fixed-time terminal sliding mode. *ISA Transactions*, 146:592–602.

Farid, Y. and Ruggiero, F. (2021). Finite-time disturbance reconstruction and robust fractional-order controller design for hybrid port-hamiltonian dynamics of biped robots. *Robotics and Autonomous Systems*, 144:103836.

Fesharaki, S. J., Kamali, M., Sheikholeslam, F., and Talebi, H. A. (2020). Robust model predictive control with sliding mode for constrained non-linear systems. *IET Control Theory & Applications*, 14(17):2592–2599.

Fierro, J. E., Pamanes, J. A., Moreno, H. A., and Nunez, V. (2017a). On the constrained walking of the nao humanoid robot. In *Advances in Automation and Robotics Research in Latin America*, pages 13–29. Springer.

Fierro, J. E., Pamanes, J. A., Moreno, H. A., and Nunez, V. (2017b). On the constrained walking of the nao humanoid robot. In *Advances in Automation and Robotics Research in Latin America*, pages 13–29. Springer.

Freese, M., Singh, S., Ozaki, F., and Matsuhira, N. (2010). Virtual robot experimentation platform v-rep: A versatile 3d robot simulator. In *International Conference on Simulation, Modeling, and Programming for Autonomous Robots*, pages 51–62. Springer.

Fridman, L. (2014). *Introduction to Time-Delay Systems: Analysis and Control*. Springer.

Gao, L. and Wu, W. (2018). Kinetic energy attenuation method for posture balance control of humanoid biped robot under impact disturbance. In *IECON 2018-44th Annual Conference of the IEEE Industrial Electronics Society*, pages 2564–2569. IEEE.

González-Mejía, S., Ramírez-Scarpetta, J. M., Moreno, J. C., and Pons, J. L. (2020a). Simulation platform for dynamic modeling of lower limb rehabilitation exoskeletons: Exo-h3 case study. pages 425–428. Springer.

González-Mejía, S., Ramírez-Scarpetta, J. M., Moreno, J. C., and Pons, J. L. (2020b). Simulation platform for dynamic modeling of lower limb rehabilitation exoskeletons: Exo-h3 case study. In *International Symposium on Wearable Robotics*, pages 425–428. Springer.

Goswami, A. and Vadakkepat, P. (2019). *Humanoid robotics: a reference*. Springer.

Graf, B. and Eckstein, J. (2023). Service robots and automation for the disabled and nursing home care. In *Springer Handbook of Automation*, pages 1331–1347. Springer.

Grizzle, J. W., Abba, G., and Plestan, F. (2001a). Asymptotically stable walking for biped robots: Analysis via systems with impulse effects. *IEEE Transactions on automatic control*, 46(1):51–64.

Grizzle, J. W., Abba, G., and Plestan, F. (2001b). Asymptotically stable walking for biped robots: Analysis via systems with impulse effects. *IEEE Transactions on automatic control*, 46(1):51–64.

Grizzle, J. W., Chevallereau, C., Ames, A. D., and Sinnet, R. W. (2010). 3d bipedal robotic walking: models, feedback control, and open problems. *IFAC Proceedings Volumes*, 43(14):505–532.

Gu, Y. and Yuan, C. (2021). Adaptive robust tracking control for hybrid models of three-dimensional bipedal robotic walking under uncertainties. *Journal of Dynamic Systems, Measurement, and Control*, 143(8):081007.

Guoyuan, Q., Zengqiang, C., and Zhuzhi, Y. (2004). New tracking-differentiator design and analysis of its stability and convergence. *Journal of Systems Engineering and Electronics*, 15(4):780–787.

Han, S., Wang, H., and Tian, Y. (2018). Model-free based adaptive nonsingular fast terminal sliding mode control with time-delay estimation for a 12 dof multi-functional lower limb exoskeleton. *Advances in Engineering Software*, 119:38–47.

Hashemi, E. and Jadidi, M. G. (2012a). Dynamic modeling and control study of the nao biped robot with improved trajectory planning. In *Materials with Complex Behaviour II*, pages 671–688. Springer.

Hashemi, E. and Jadidi, M. G. (2012b). Dynamic modeling and control study of the nao biped robot with improved trajectory planning. In *Materials with Complex Behaviour II*, pages 671–688. Springer.

Hashemi, E. and Khajepour, A. (2017). Kinematic and three-dimensional dynamic modeling of a biped robot. *Proceedings of the Institution of Mechanical Engineers, Part K: Journal of Multi-body Dynamics*, 231(1):57–73.

Hauser, H., Neumann, G., Ijspeert, A. J., and Maass, W. (2011). Biologically inspired kinematic synergies enable linear balance control of a humanoid robot. *Biological cybernetics*, 104(4-5):235–249.

He, W., Li, Z., Dong, Y., and Zhao, T. (2018). Design and adaptive control for an upper limb robotic exoskeleton in presence of input saturation. *IEEE transactions on neural networks and learning systems*, 30(1):97–108.

He, Z., Liu, C., Zhan, Y., Li, H., Huang, X., and Zhang, Z. (2014). Nonsingular fast terminal sliding mode control with extended state observer and tracking differentiator for uncertain nonlinear systems. *Mathematical Problems in Engineering*, 2014.

Herdt, A., Diedam, H., Wieber, P.-B., Dimitrov, D., Mombaur, K., and Diehl, M. (2010a). Online walking motion generation with automatic footstep placement. *Advanced Robotics*, 24(5-6):719–737.

Herdt, A., Diedam, H., Wieber, P.-B., Dimitrov, D., Mombaur, K., and Diehl, M. (2010b). Online walking motion generation with automatic footstep placement. *Advanced Robotics*, 24(5-6):719–737.

Herzog, A., Righetti, L., Grimminger, F., Pastor, P., and Schaal, S. (2014). Balancing experiments on a torque-controlled humanoid with hierarchical inverse dynamics. In *2014 IEEE/RSJ International Conference on Intelligent Robots and Systems*, pages 981–988.

Hof, A. L. (2008). The 'extrapolated center of mass' concept suggests a simple control of balance in walking. *Human movement science*, 27(1):112–125.

Hosseinmemar, A., Baltes, J., Anderson, J., Lau, M. C., Lun, C. F., and Wang, Z. (2019). Closed-loop push recovery for inexpensive humanoid robots. *Applied Intelligence*, 49:3801–3814.

Hou, Y. T.-Y., Cheon, E., and Jung, M. F. (2024). Power in human-robot interaction. In *Proceedings of the 2024 ACM/IEEE International Conference on Human-Robot Interaction*, pages 269–282.

Huang, A.-C. and Chien, M.-C. (2010). *Adaptive control of robot manipulators: a unified regressor-free approach*. World Scientific.

Huang, A.-C., Wu, S.-C., and Ting, W.-F. (2006). A fat-based adaptive controller for robot manipulators without regressor matrix: theory and experiments. *Robotica*, 24(2):205.

Janardhan, V. and Kumar, R. P. (2019). Generating real-time trajectories for a planar biped robot crossing a wide ditch with landing uncertainties. *Robotica*, 37(1):109–140.

Jia, Z., Liu, X., and Fang, Y. (2019). An adaptive nonsingular fast terminal sliding mode controller for dynamic walking of a 5-link planar biped robot in both single and double support phases. *Journal of Dynamic Systems, Measurement, and Control*, 141(1):011006–1–011006–8.

Kaddar, B., Aoustin, Y., and Chevallereau, C. (2015). Arm swing effects on walking bipedal gaits composed of impact, single and double support phases. *Robotics and Autonomous Systems*, 66:104–115.

Kali, Y., Saad, M., and Benjelloun, K. (2018). Optimal super-twisting algorithm with time delay estimation for robot manipulators based on feedback linearization. *Robotics & Autonomous Systems*, 108:87–99.

Kali, Y., Saad, M., Boland, J.-F., Fortin, J., and Girardeau, V. (2021). Walking task space control using time delay estimation based sliding mode of position controlled nao biped robot. *International Journal of Dynamics and Control*, 9(2):679–688.

Kashyap, A. K. and Parhi, D. R. (2021a). Optimization of stability of humanoid robot nao using ant colony optimization tuned mpc controller for uneven path. *Soft Computing*, pages 1–20.

Kashyap, A. K. and Parhi, D. R. (2021b). Optimization of stability of humanoid robot nao using ant colony optimization tuned mpc controller for uneven path. *Soft Computing*, 25(7):5131–5150.

Kashyap, A. K. and Parhi, D. R. (2021c). Particle swarm optimization aided pid gait controller design for a humanoid robot. *ISA Transactions*, 114:306–330.

Kashyap, A. K. and Parhi, D. R. (2023a). Dynamic walking of multi-humanoid robots using bfgs quasi-newton method aided artificial potential field approach for uneven terrain. *Soft Computing*, 27(9):5893–5910.

Kashyap, A. K. and Parhi, D. R. (2023b). Dynamic walking of multi-humanoid robots using bfgs quasi-newton method aided artificial potential field approach for uneven terrain. *Soft Computing*, 27(9):5893–5910.

Kashyap, A. K., Parhi, D. R., Muni, M. K., and Pandey, K. K. (2020a). A hybrid technique for path planning of humanoid robot nao in static and dynamic terrains. *Applied Soft Computing*, 96:106581.

Kashyap, A. K., Parhi, D. R., Muni, M. K., and Pandey, K. K. (2020b). A hybrid technique for path planning of humanoid robot nao in static and dynamic terrains. *Applied Soft Computing*, 96:106581.

Kashyap, D. R. and Kumar, S. (2020). Dynamic stabilization of nao humanoid robot based on whole-body control with simulated annealing. *International Journal of Humanoid Robotics*, pages 1–20.

Kellett, C. M. and Braun, P. (2023). *Introduction to Nonlinear Control: Stability, Control Design, and Estimation*. Princeton University Press.

Kemp, C. C., Fitzpatrick, P., Hirukawa, H., Yokoi, K., Harada, K., and Matsumoto, Y. (2008). *Humanoids*. Springer Berlin Heidelberg, Berlin, Heidelberg.

Khajepour, A. and Hashemi, E. (2017). Kinematic and three-dimensional dynamic modeling of a biped robot.

Khalil, H. K. (2009). Lyapunov stability. *Control systems, robotics and automation*, 12:115.

Khoi, P. B. and Nguyen Xuan, H. (2021). Fuzzy logic-based controller for bipedal robot. *Applied Sciences*, 11(24).

Kim, I.-S., Han, Y.-J., and Hong, Y.-D. (2019). Stability control for dynamic walking of bipedal robot with real-time capture point trajectory optimization. *Journal of Intelligent & Robotic Systems*, 96(3):345–361.

Kim, M. and Collins, S. H. (2017). Once-per-step control of ankle push-off work improves balance in a three-dimensional simulation of bipedal walking. *IEEE Transactions on Robotics*, 33(2):406–418.

Komurcugil, H., Biricik, S., Bayhan, S., and Zhang, Z. (2020). Sliding mode control: Overview of its applications in power converters. *IEEE Industrial Electronics Magazine*, 15(1):40–49.

Koptev, M., Figueroa, N., and Billard, A. (2021). Real-time self-collision avoidance in joint space for humanoid robots. *IEEE Robotics and Automation Letters*, 6(2):1240–1247.

Kulk, J., Welsh, J., et al. (2008). A low power walk for the nao robot. In *Proceedings of the Australasian Conference on Robotics & Automation (ACRA)*, pages 1–7.

Kuniyoshi, Y., Inaba, M., and Inoue, H. (2000). Motion imitation for humanoid robot. *Robotics and Autonomous Systems*, 31(1-2):123–132.

Lee, J., Chang, P. H., and Jin, M. (2017). Adaptive integral sliding mode control with time-delay estimation for robot manipulators. *IEEE Transactions on Industrial Electronics*, 64(8):6796–6804.

Lee, S.-H. and Goswami, A. (2012). A momentum-based balance controller for humanoid robots on non-level and non-stationary ground. *Autonomous Robots*, 33(4):399–414.

Li, D.-P., Liu, Y.-J., Tong, S., Chen, C. L. P., and Li, D.-J. (2019). Neural networks-based adaptive control for nonlinear state constrained systems with input delay. *IEEE Transactions on Cybernetics*, 49(4):1249–1258.

Li, G., Huang, Q., Tang, Y., Li, G., and Li, M. (2008). Kinematic analysis and motion planning of a biped robot with 7-dof and double spherical hip joint. In *2008 7th World Congress on Intelligent Control and Automation*, pages 2982–2987.

Li, Y. and Wang, D. (2018). Adaptive sliding mode observer-based force control for the compliant humanoid robot. *Journal of Intelligent and Robotic Systems*, 92(2):205–215.

Li, Y. and Xu, L. (2019). Model-free continuous nonsingular fast terminal sliding mode control for cable-driven manipulators. *IEEE Transactions on Industrial Electronics*, 66(6):4684–4695.

Li, Z., Wang, F., Ke, D., Li, J., and Zhang, W. (2021). Robust continuous model predictive speed and current control for pmsm with adaptive integral sliding-mode approach. *IEEE Transactions on Power Electronics*, 36(12):14398–14408.

Li, Z., Yang, C., and Fan, L. (2012). *Advanced control of wheeled inverted pendulum systems*. Springer Science & Business Media.

Liu, C., Ning, J., and Chen, Q. (2018a). Dynamic walking control of humanoid robots combining linear inverted pendulum mode with parameter optimization. *International Journal of Advanced Robotic Systems*, 15(1):1729881417749672.

Liu, C., Ning, J., and Chen, Q. (2018b). Dynamic walking control of humanoid robots combining linear inverted pendulum mode with parameter optimization. *International Journal of Advanced Robotic Systems*, 15(1):1729881417749672.

Liu, C., Ning, J., and Chen, Q. (2018c). Dynamic walking control of humanoid robots combining linear inverted pendulum mode with parameter optimization. *International Journal of Advanced Robotic Systems*, 15(1):1729881417749672.

Liu, Y., Zang, X., Heng, S., Lin, Z., and Zhao, J. (2017). Human-like walking with heel off and toe support for biped robot. *Applied Sciences*, 7(5):499.

Lu, K., Xia, Y., Yu, C., and Chen, R. (2015). Finite-time intercept-angle guidance. *International Journal of Control*, 88(2):264–275.

Lu, R., Wu, H., and Bai, J. (2014). New delay-dependent robust stability criteria for uncertain neutral systems with mixed delays. *Journal of the Franklin Institute*, 351(3):1386–1399.

Mahyuddin, M., Khan, S., and Herrmann, G. (2014). A novel robust adaptive control algorithm with finite-time online parameter estimation of a humanoid robot arm. *Robotics and Autonomous Systems*, 62(3):294–305. Advances in Autonomous Robotics — Selected extended papers of the joint 2012 TAROS Conference and the FIRA RoboWorld Congress, Bristol, UK.

Mattamala, M., Olave, G., González, C., Hasbún, N., and Ruiz-del Solar, J. (2018). The nao backpack: An open-hardware add-on for fast software development with the nao robot. In Akiyama, H., Obst, O., Sammut, C., and Tonidandel, F., editors, *RoboCup 2017: Robot World Cup XXI*, pages 302–311, Cham. Springer International Publishing.

McBride, C. and Del Vecchio, D. (2020). The number of equilibrium points of perturbed nonlinear positive dynamical systems. *Automatica*, 112:108732.

Mechali, O., Xu, L., Huang, Y., Shi, M., and Xie, X. (2021). Observer-based fixed-time continuous nonsingular terminal sliding mode control of quadrotor aircraft under uncertainties and disturbances for robust trajectory tracking: Theory and experiment. *Control Engineering Practice*, 111:104806.

Mendez-Monroy, P. (2017). Walking motion generation and neuro-fuzzy control with push recovery for humanoid robot. *Int. J. Comput. Commun.*, 12(3):330–346.

Meng, C., Sun, L., Meng, X., and Hu, J. (2020). Fixed-time sliding mode control for humanoid robot position tracking. *IEEE Transactions on Industrial Informatics*, 16(6):3713–3723.

Meng, L., Macleod, C., Porr, B., et al. (2018). Bipedal robotic walking control derived from analysis of human locomotion. *Biological Cybernetics*, 112:277–290.

Mikolajczyk, T. and Czarnowski, J. (2019). A review of gait, drive, sensors, and control systems for bipedal walking robots. *Journal of Intelligent & Robotic Systems*, 94(1):1–22.

Mokhtari, M., Taghizadeh, M., and Mazare, M. (2021a). Hybrid adaptive robust control based on cpg and zmp for a lower limb exoskeleton. *Robotica*, 39(2):181–199.

Mokhtari, M., Taghizadeh, M., and Mazare, M. (2021b). Hybrid adaptive robust control based on cpg and zmp for a lower limb exoskeleton. *Robotica*, 39(2):181–199.

Mu, X. and Wu, Q. (2006). On impact dynamics and contact events for biped robots via impact effects. *IEEE Transactions on Systems, Man, and Cybernetics, Part B (Cybernetics)*, 36(6):1364–1372.

Nair, R. R., Behera, L., and Kumar, S. (2019). Event-triggered finite-time integral sliding mode controller for consensus-based formation of multirobot systems with disturbances. *IEEE Transactions on Control Systems Technology*, 27(1):39–47.

Nguyen, X. T., Tran, T. D., Nguyen, H. H., Tong, N. P., Nguyen, T. P., and Nguyen, T. T. (2020). Controlling center of mass in humanoid robot using sliding mode control. pages 17–22.

Niku, S. B. (2020). *Introduction to robotics: analysis, control, applications*. John Wiley & Sons.

Olvera-Pons, M., Castañeda, C. E., Chiul, R., and Petrilli-Barceló, A. (2019). Nao's head modelling and control using discrete-time sliding mode algorith. In *2019 IEEE International Autumn Meeting on Power, Electronics and Computing (ROPEC)*, pages 1–6. IEEE.

Park, I.-G. and Kim, J.-G. (2001). Robust control for dynamic walking of a biped robot with ground contacting condition. 3:2067–2072 vol.3.

Parra-Moreno, J., Yanguas-Rojas, D., and Mojica-Nava, E. (2023). Imitation methods for bipedal locomotion of humanoid robots: A survey. In *2023 IEEE 6th Colombian Conference on Automatic Control (CCAC)*, pages 1–6.

Piperakis, S., Koskinopoulou, M., and Trahanias, P. (2018). Nonlinear state estimation for humanoid robot walking. *IEEE Robotics and Automation Letters*, 3(4):3347–3354.

Pournazhdi, A. B., Mirzaei, M., and Ghiasi, A. R. (2011). Dynamic modeling and sliding mode control for fast walking of seven-link biped robot. In *The 2nd International Conference on Control, Instrumentation and Automation*, pages 1012–1017. IEEE.

Qi, R., Tao, G., and Jiang, B. (2019). *Adaptive Control: A Tutorial Introduction*, pages 55–74. Springer International Publishing, Cham.

Qin, H., Si, J., Wang, N., and Gao, L. (2023a). Fast fixed-time nonsingular terminal sliding-mode formation control for autonomous underwater vehicles based on a disturbance observer. *Ocean Engineering*, 270:113423.

Qin, H., Si, J., Wang, N., and Gao, L. (2023b). Fast fixed-time nonsingular terminal sliding-mode formation control for autonomous underwater vehicles based on a disturbance observer. *Ocean Engineering*, 270:113423.

Rahmani, M., Ghanbari, A., and Ettefagh, M. M. (2018). A novel adaptive neural network integral sliding-mode control of a biped robot using bat algorithm. *Journal of Vibration and Control*, 24(10):2045–2060.

Rahmani, M., Komijani, H., and Rahman, M. (2020). New sliding mode control of 2-dof robot manipulator based on extended grey wolf optimizer. *International Journal of Control, Automation and Systems*, 18:1572–1580.

Reher, J., Cousineau, E. A., Hereid, A., Hubicki, C. M., and Ames, A. D. (2016). Realizing dynamic and efficient bipedal locomotion on the humanoid robot durus. In *2016 IEEE International Conference on Robotics and Automation (ICRA)*, pages 1794–1801. IEEE.

Ren, B., Wang, Y., and Chen, J. (2019). A novel robust finite-time trajectory control with the high-order sliding mode for human–robot cooperation. *IEEE Access*, 7:130874–130882.

Rezoug, A., Iqbal, J., and Tadjine, M. (2022). Extended grey wolf optimization–based adaptive fast nonsingular terminal sliding mode control of a robotic manipulator. *Proceedings of the Institution of Mechanical Engineers, Part I: Journal of Systems and Control Engineering*, 236(9):1738–1754.

Rincon, K., Chairez, I., and Yu, W. (2019). Fixed-time robust output feedback control of a restricted state biped robot based on a tangent barrier lyapunov function. pages 1–6.

Ryoo, Y.-J. (2016). Walking engine using zmp criterion and feedback control for child-sized humanoid robot. *International Journal of Humanoid Robotics*, 13(04):1650021.

Sadeque, M. and Balachandran, S. K. (2020). Overview of medical device processing. *Trends in Development of Medical Devices*, pages 177–188.

Said, A., Rodriguez-Leal, E., Soto, R., Gordillo, J., and Garrido, L. (2015a). Decoupled closed-form solution for humanoid lower limb kinematics. *Mathematical Problems in Engineering*, 2015.

Said, A., Rodriguez-Leal, E., Soto, R., Gordillo, J., and Garrido, L. (2015b). Decoupled closed-form solution for humanoid lower limb kinematics. *Mathematical Problems in Engineering*, 2015.

Said, A., Rodriguez-Leal, E., Soto, R., Gordillo, J., and Garrido, L. (2015c). Decoupled closed-form solution for humanoid lower limb kinematics. *Mathematical Problems in Engineering*, 2015.

Said, A., Rodriguez-Leal, E., Soto, R., Gordillo, J., Garrido, L., et al. (2015d). Decoupled closed-form solution for humanoid lower limb kinematics. *Mathematical Problems in Engineering*, 2015.

Sanchez-Magos, M., Ballesteros, M., Cruz-Ortiz, D., Salgado, I., and Chairez, I. (2020). Terminal sliding-mode control of virtual humanoid robot with joint restrictions walking on stepping objects. *Cybernetics and Systems*, 51(4):402–425.

Seleem, I. A. and Assal, S. F. (2017). Sliding mode control of underactuated five-link biped robot for climbing stairs based on real human data. In *2017 IEEE International Conference on Industrial Technology (ICIT)*, pages 878–883. IEEE.

Setchi, R., Dehkordi, M. B., and Khan, J. S. (2020). Explainable robotics in human-robot interactions. *Procedia Computer Science*, 176:3057–3066.

Shi, Y.-L. and Hou, C.-Z. (2008). Design of improved nonlinear tracking differentiator. *Control and Decision*, 23(6):647–650.

Shimkin, N. (2009). *Nonlinear Control Systems*, pages 2886–2889. Springer Berlin Heidelberg, Berlin, Heidelberg.

Siciliano, B., Sciavicco, L., Villani, L., and Oriolo, G. (2009a). Kinematics. *Robotics: Modelling, Planning and Control*, pages 39–103.

Siciliano, B., Sciavicco, L., Villani, L., and Oriolo, G. (2009b). Kinematics. *Robotics: Modelling, Planning and Control*, pages 39–103.

Slotine, J.-J. E., Li, W., et al. (1991a). *Applied nonlinear control*, volume 199. Prentice hall Englewood Cliffs, NJ.

Slotine, J.-J. E., Li, W., et al. (1991b). *Applied nonlinear control*, volume 199. Prentice hall Englewood Cliffs, NJ.

Song, E., Li, J., and Liao, Y. (2022a). Kinematic analysis and motion planning simulation of cooperative robot. *Cobot*, 1(8):8.

Song, J. P., Kim, C. Y., and Lee, J. K. (2018). Adaptive sliding mode observer for obstacle avoidance control of humanoid robot. *Journal of Mechanical Science and Technology*, 32(5):2255–2264.

Song, T., Fang, L., and Wang, H. (2022b). Model-free finite-time terminal sliding mode control with a novel adaptive sliding mode observer of uncertain robot systems. *Asian Journal of Control*, 24(3):1437–1451.

Source, N. R. I. (Accessed 2024). Nao robot png image.

Stephens, B. J. and Atkeson, C. G. (2010). Push recovery by stepping for humanoid robots with force controlled joints. In *2010 10th IEEE-RAS International Conference on Humanoid Robots*, pages 52–59.

Su, H., Qi, W., Schmirander, Y., Ovur, S. E., Cai, S., and Xiong, X. (2022). A human activity-aware shared control solution for medical human–robot interaction. *Assembly Automation*, 42(3):388–394.

Technical University of Munich (Accessed 2024). Humanoid robot lola.

Tian, Y., Cai, Y., and Deng, Y. (2020). A fast nonsingular terminal sliding mode control method for nonlinear systems with fixed-time stability guarantees. *IEEE Access*, 8:60444–60454.

Vadakkepat, P. and Walker, I. D. (2002). Biped locomotion: stability, control and application. *Robotica*, 20(3):313–322.

Vidyasagar, M. (2002). *Nonlinear systems analysis*. SIAM.

Vo, A. T., Kang, H.-J., and Truong, T. N. (2020). A fast terminal sliding mode control strategy for trajectory tracking control of robotic manipulators. In Huang, D.-S. and Premaratne, P., editors, *Intelligent Computing Methodologies*, pages 177–189, Cham. Springer International Publishing.

Vukobratović, M. and Borovac, B. (2004). Zero-moment point—thirty five years of its life. *International journal of humanoid robotics*, 1(01):157–173.

Wan, L., Chen, G., Sheng, M., Zhang, Y., and Zhang, Z. (2020). Adaptive chattering-free terminal sliding-mode control for full-order nonlinear system with unknown disturbances and model uncertainties. *International Journal of Advanced Robotic Systems*, 17(3):1729881420925295.

Wang, F., Wang, Y., Wen, S., and Zhao, S. (2012). Nao humanoid robot gait planning based on the linear inverted pendulum. In *2012 24th Chinese Control and Decision Conference (CCDC)*, pages 986–990.

Wang, H., Pan, Y., Li, S., and Yu, H. (2019). Robust sliding mode control for robots driven by compliant actuators. *IEEE Transactions on Control Systems Technology*, 27(3):1259–1266.

Wang, H., Zhang, H., Wang, Z., and Chen, Q. (2020a). Finite-time stabilization of periodic orbits for under-actuated biped walking with hybrid zero dynamics. *Communications in Nonlinear Science and Numerical Simulation*, 80:104949.

Wang, J., Lee, M. C., Kim, J. H., and Kim, H. H. (2020b). Fast fractional-order terminal sliding mode control for seven-axis robot manipulator. *Applied Sciences*, 10(21).

Wang, L., Ge, Y., Chen, M., and Fan, Y. (2017a). Dynamical balance optimization and control of biped robots in double-support phase under perturbing external forces. *Neural Computing and Applications*, 28(12):4123–4137.

Wang, L., Ge, Y., Chen, M., and Fan, Y. (2017b). Dynamical balance optimization and control of biped robots in double-support phase under perturbing external forces. *Neural Computing and Applications*, 28(12):4123–4137.

Wang, Y., Feng, Y., Yu, X., and Zhang, N. (2003). Terminal sliding mode control of mimo linear systems with unmatched uncertainties. In *IECON'03. 29th Annual Conference of the IEEE Industrial Electronics Society (IEEE Cat. No.03CH37468)*, volume 2, pages 1146–1151 Vol.2.

Wang, Y., Gu, L., Chen, B., and Wu, H. (2017c). A new discrete time delay control of hydraulic manipulators. *Proceedings of the Institution of Mechanical Engineers, Part I: Journal of Systems and Control Engineering*, 231(3):168–177.

Wang, Y., Gu, L., Xu, Y., and Cao, X. (2016). Practical tracking control of robot manipulators with continuous fractional-order nonsingular terminal sliding mode. *IEEE Transactions on Industrial Electronics*, 63(10):6194–6204.

Wang, Y., Leibold, M., Lee, J., Ye, W., Xie, J., and Buss, M. (2022). Incremental model predictive control exploiting time-delay estimation for a robot manipulator. *IEEE Transactions on Control Systems Technology*, 30(6):2285–2300.

Wang, Y., Yan, F., Chen, J., Ju, F., and Chen, B. (2018). A new adaptive time-delay control scheme for cable-driven manipulators. *IEEE Transactions on Industrial Informatics*, 15(6):3469–3481.

Wang, Y., Zhu, Q., Xiong, R., and Chu, J. (2013). Standing balance control for position control-based humanoid robot. *IFAC Proceedings Volumes*, 46(20):429–436.

Wei, B. (2023). Stability analysis of equilibrium point and limit cycle of two-dimensional nonlinear dynamical systems and mdash; a tutorial. *Applied Sciences*, 13(2).

Wen, S., Hu, X., Li, Z., Lam, H. K., Sun, F., and Fang, B. (2019a). Nao robot obstacle avoidance based on fuzzy q-learning. *Industrial Robot: the international journal of robotics research and application*.

Wen, S., Hu, X., Li, Z., Lam, H. K., Sun, F., and Fang, B. (2019b). Nao robot obstacle avoidance based on fuzzy q-learning. *Industrial Robot: the international journal of robotics research and application*.

Westervelt, E. R., Grizzle, J. W., Chevallereau, C., Choi, J. H., and Morris, B. (2018). *Feedback control of dynamic bipedal robot locomotion*. CRC press.

Winkler, A. W., Farshidian, F., Pardo, D., Neunert, M., and Buchli, J. (2017). Fast trajectory optimization for legged robots using vertex-based zmp constraints. *IEEE Robotics and Automation Letters*, 2(4):2201–2208.

Wu, S., Wang, C., Ye, L., Wang, X., Liu, H., and Liang, B. (2022a). Quasi-static walking for biped robots with a sinusoidal gait. In *2022 IEEE 18th International Conference on Automation Science and Engineering (CASE)*, pages 849–856.

Wu, S., Wang, C., Ye, L., Wang, X., Liu, H., and Liang, B. (2022b). Quasi-static walking for biped robots with a sinusoidal gait. In *2022 IEEE 18th International Conference on Automation Science and Engineering (CASE)*, pages 849–856.

Wu, X., Chen, W., Ji, F., and Ye, J. (2018). Implementation of robot nao on sprint. *Journal of Computers*, 29(2):268–275.

Xia, Y. and Jia, Y. (2003). Robust sliding-mode control for uncertain time-delay systems: an lmi approach. *IEEE transactions on automatic control*, 48(6):1086–1091.

Xia, Y., Zhu, Z., Li, C., Yang, H., and Zhu, Q. (2010). Robust adaptive sliding mode control for uncertain discrete-time systems with time delay. *Journal of the Franklin Institute*, 347(1):339–357. Dynamics and Control.

Xiao, B., Hu, Q., and Zhang, Y. (2012). Adaptive sliding mode fault tolerant attitude tracking control for flexible spacecraft under actuator saturation. *IEEE Transactions on Control Systems Technology*, 20(6):1605–1612.

Xie, X.-J., Park, J. H., Mukaidani, H., Zhang, W., et al. (2019). Mathematical theories and applications for nonlinear control systems.

Xiong, X., Reher, J., and Ames, A. D. (2021). Global position control on underactuated bipedal robots: Step-to-step dynamics approximation for step planning. In *2021 IEEE International Conference on Robotics and Automation (ICRA)*, pages 2825–2831. IEEE.

Yao, J. and Deng, W. (2017). Active disturbance rejection adaptive control of uncertain nonlinear systems: Theory and application. *Nonlinear Dynamics*, 89:1611–1624.

Yazdani, M., Salarieh, H., and Foumani, M. S. (2018). Bio-inspired decentralized architecture for walking of a 5-link biped robot with compliant knee joints. *International Journal of Control, Automation and Systems*, 16(6):2935–2947.

Ye, H., Wang, D., Wu, J., Yue, Y., and Zhou, Y. (2020). Forward and inverse kinematics of a 5-dof hybrid robot for composite material machining. *Robotics and Computer-Integrated Manufacturing*, 65:101961.

Yedavalli, R. K. (2014). Robust control of uncertain dynamic systems. *AMC*, 10:12.

Yi, S. and Zhai, J. (2019). Adaptive second-order fast nonsingular terminal sliding mode control for robotic manipulators. *ISA transactions*, 90:41–51.

Yu, S., Yu, X., Shirinzadeh, B., and Man, Z. (2005). Continuous finite-time control for robotic manipulators with terminal sliding mode. *Automatica*, 41(11):1957–1964.

Yu, X. and Zhihong, M. (2002). Fast terminal sliding-mode control design for nonlinear dynamical systems. *IEEE Transactions on Circuits and Systems I: Fundamental Theory and Applications*, 49(2):261–264.

Zhang, B., Pi, Y., and Luo, Y. (2012). Fractional order sliding-mode control based on parameters auto-tuning for velocity control of permanent magnet synchronous motor. *ISA Transactions*, 51(5):649–656.

Zhang, L., Wang, Y., Hou, Y., and Li, H. (2019a). Fixed-time sliding mode control for uncertain robot manipulators. *IEEE Access*, 7:149750–149763.

Zhang, L., Wang, Y., Hou, Y., and Li, H. (2019b). Fixed-time sliding mode control for uncertain robot manipulators. *IEEE Access*, 7:149750–149763.

Zhang, L. and Yang, J. (2013). Continuous nonsingular terminal sliding mode control for systems with mismatched disturbances. *Automatica*, 49(7):2287–2291.

Zhang, Y. and Xu, Q. (2017). Adaptive sliding mode control with parameter estimation and kalman filter for precision motion control of a piezo-driven microgripper. *IEEE Transactions on Control Systems Technology*, 25(2):728–735.

Zhang, Y., Zhang, Q., Zhang, J., and Wang, Y. (2019c). Sliding mode control for fuzzy singular systems with time delay based on vector integral sliding mode surface. *IEEE Transactions on Fuzzy Systems*, 28(4):768–782.

Zhang, Z., Leibold, M., and Wollherr, D. (2020). Integral sliding-mode observer-based disturbance estimation for euler–lagrangian systems. *IEEE Transactions on Control Systems Technology*, 28(6):2377–2389.

Zhao, Y. and Gu, Y. (2020). A non-periodic planning and control framework of dynamic legged locomotion. *International Journal of Intelligent Robotics and Applications*, 4(1):95–108.

Zheng, J., Wang, H., Man, Z., Jin, J., and Fu, M. (2015). Robust motion control of a linear motor positioner using fast nonsingular terminal sliding mode. *IEEE/ASME Transactions on Mechatronics*, 20(4):1743–1752.

Zhong, Q.-b. and Chen, F. (2016). Trajectory planning for biped robot walking on uneven terrain–taking stepping as an example. *CAAI Transactions on intelligence technology*, 1(3):197–209.